1994

SEAWATER pH AND THE OCEANIC CARBON CYCLE

BELLERBY, RICHARD GARTH JAMES

COPYRIGHT

Signed: R. Bellerby.....

SEAWATER pH AND THE OCEANIC CARBON CYCLE

by

RICHARD GARTH JAMES BELLERBY
B.Sc. (Hons.)

A thesis submitted to the University of Plymouth
in partial fulfilment for the degree of

DOCTOR OF PHILOSOPHY

Department of Environmental Sciences
Faculty of Science

In collaboration with the
Plymouth Marine Laboratory

July 1994

SEAWATER pH AND THE OCEANIC CARBON CYCLE

RICHARD Garth James BELLERBY

Abstract

The buffering of carbon dioxide in seawater and the intimate relationship between the carbonate system, air-sea gas exchange and biological productivity in the oceans is described. Characterisation of the carbonate system is enabled through the concurrent measurement of any two of the variables pH, alkalinity, TCO_2 and pCO_2. It is identified that to obtain the high density, high precision measurements necessary to better constrain carbon cycle models, with respect to estimating the effect of anthropogenic carbon release to the atmosphere, it will be necessary to develop *in situ* techniques for the measurement of pH and pCO_2. The theory of pH scales and both potentiometric and spectrophotometric pH measurement is presented as well as a chronology of pH measurements at sea. The development of automated potentiometric and spectrophotometric techniques for the simultaneous, continuous, shipboard determination of seawater pH is documented and the performance of the instrumentation on a cruise to the Southern Ocean is reported. The potentiometric system was optimised for electrode response and incorporated increased temperature control and a novel flow cell to help reduce bubble effects and maintain the integrity of the liquid junction. Nevertheless, the technique illustrated very erratic potential and the data was of unacceptable quality. The spectrophotometric technique used a flow injection technique and phenol red indicator and showed a precision of ± 0.005 pH unit with a sampling frequency of about 25 h^{-1}. A comparison of calculated alkalinity from the combinations pH and pCO_2 and pCO_2 and TCO_2 had a residual of 1.3 ± 7.3 $\mu equiv.kg^{-1}$ (n = 79) or about 0.32 %. The theoretical precision of the comparison calculated from the precisions of the methods used is 0.34 %. A comparison of *in situ* pH and that calculated from alkalinity and TCO_2 showed a standard deviation of ± 0.016 with a standard error dependent on the choice of sulphate formation constant used to convert from the free to the total hydrogen ion concentration scale. Surface pH(SWS) at 25°C has been shown to vary significantly in the Southern Ocean from 7.65 in the Bransfield Strait to 7.85 in a area of intense biological activity associated with the South Polar Front (SPF). Throughout the majority of the cruise the surface waters were undersaturated with respect to carbon dioxide and the main control on pH was from the hydrography, although in areas of high chlorophyll concentrations, associated predominantly with the SPF, there existed considerable correspondence with biological activity. A previously unknown sink for atmospheric CO_2 has been identified in the Bellingshausen Sea which has significant implications for our understanding of the global carbon budget. The spectrophotometric method is put forward as the method of choice for future measurements of seawater pH.

Contents

ACKNOWLEDGEMENTS

I would like to thank my supervisors: Dr. Geoff Millward for his faith and encouragement throughout; Prof. David Turner for sharing his intimate knowledge of carbon dioxide chemistry and expertise on instrument automation; and Prof. Paul Worsfold for advice on flow injection techniques.

Help from Phil Goy and John Woods in *talking* to the instrumentation was indispensable. The patience of NCS is also appreciated. Thanks to Polly Machin and Roy Lowry from BODC for help with data processing.

Detailed discussion with Drs. Bob Byrne and Andrew Dickson on spectrophotometric seawater pH measurements during this work has been helpful.

A research student grant from the Natural Environmental Research Council is gratefully acknowledged. The Royal Society is thanked for the award of the *John Murray Travelling Studentship.* Awards from the Plymouth Marine Fund, the Nansen Centennial Symposium, NERC Special Topics and the UK Associates of the Bermuda Biological Station for Research permitted my participation on courses and conferences.

The master and crew of R.R.S. *Discovery* eased the collection of the data, whilst the scientific officers tried their hardest to complicate matters with their numerous social events, especially Phil, Jane, Sean, Wendy, Howard, John, Anne, Mikey, Colin and Colin.

I would like to thank the Plymouth Marine Laboratory for allowing full access to their facilities and for providing an excellent environment for both work and play. I thank all my friends at PML - you know who you are.

AUTHOR'S DECLARATION

At no time during the registration for the degree of Doctor of Philosophy has the author been registered for any other University award.

This study was financed with the aid of a studentship from the Natural Environmental Research Council, and carried out in collaboration with the Plymouth Marine Laboratory.

Relevant scientific seminars and conferences were attended at which work was often presented; external institutions were visited for consultation purposes, a paper published and two papers prepared for publication.

Publications;

Bellerby R.G.J., Millward G.E., Turner D.R. and Worsfold P.J., 1993. Approaches to the continuous monitoring of seawater pH and its rôle in the oceanic carbon cycle. *Trends in Analytical Chemistry*, 12(9), 382-86.

Bellerby R.G.J., Turner D.R., Millward G.E. and Worsfold P.J., 1994. Shipboard flow injection determination of seawater pH with spectrophotometric detection. Submitted to *Analytica Chimica Acta*.

Bellerby R.G.J., Turner D.R. and Robertson J.E., 1994. pH as a monitor of the CO_2 system in surface seawater: results from the Bellingshausen Sea, Southern Ocean. Submitted to *Deep-Sea Research*.

Presentations:

Bellerby R.G.J., Millward G.E., Turner D.R. and Worsfold P.J. (1992). Application of FIA to the precise determination of seawater pH. Poster presentation at the *Fourth Winter Conference on Flow Injection Analysis,* Scottsdale, Phoenix, Jan. 11-16.

Bellerby R.G.J., Millward G.E., Turner D.R. and Worsfold P.J. (1993). The continuous spectrophotometric determination of seawater pH - and its rôle in the carbon cycle of the Southern Ocean. Poster presentation at the *Nansen Centennial Symposium* on 'The Role of Polar Oceans in Shaping the Global Environment', Bergen, Norway, June 21-25.

Bellerby R.G.J., Robertson J.E., Turner D.R. and Millward G.E. (1993). A fully automated spectrophotometric technique for the semi-continuous, on-line, shipboard determination of seawater pH. Talk given at the *4th International CO_2 Conference*, Carqueiranne, France, September 13-17.

Bellerby R.G.J., Turner D.R., Millward G.E. and Worsfold P.J. (1994). Seawater pH in the Bellingshausen Sea - the validation of a fully automated, continuous spectrophotometric method. Poster presentation at the 1994 AGU/ASLO Ocean Sciences Meeting, San Diego, February 21-25.

Bellerby R.G.J., Robertson J.E., Turner D.R. and Millward G.E., (1993). Spectrophotometric pH determination and the internal consistency of CO_2 measurements in the Southern Ocean. Talk given at the *Sterna Southern Ocean meeting*, University of Plymouth, April 14-15.

External visits:

Marine Physical Laboratory, Scripps Institute of Oceanography, La Jolla, San Diego, 7th to 8th January 1992. Discussions on seawater pH scales and pH measurement with Dr. Andrew Dickson.

Institute of Marine Sciences, University of South Florida, St. Petersburg, 19th to 20th January 1992. Discussions on spectrophotometric pH measurements with Dr. Robert Byrne.

Courses:

Biological Oceanography, Bermuda Biological Station For Research, Bermuda, 21st July to 21st August, 1993.

Awards:

Royal Society *John Murray Travelling Studentship* to participate in the Sterna expedition to the Southern Ocean aboard *R.R.S. Discovery* as part of the U.K. contribution to the Joint Geochemical Ocean Flux Study.

Plymouth Marine Laboratory/University of Plymouth *Plymouth Marine Fund Award* to present work at the *Nansen Centennial Symposium*, Bergen, Norway.

To Bekkqi,

with all my love.

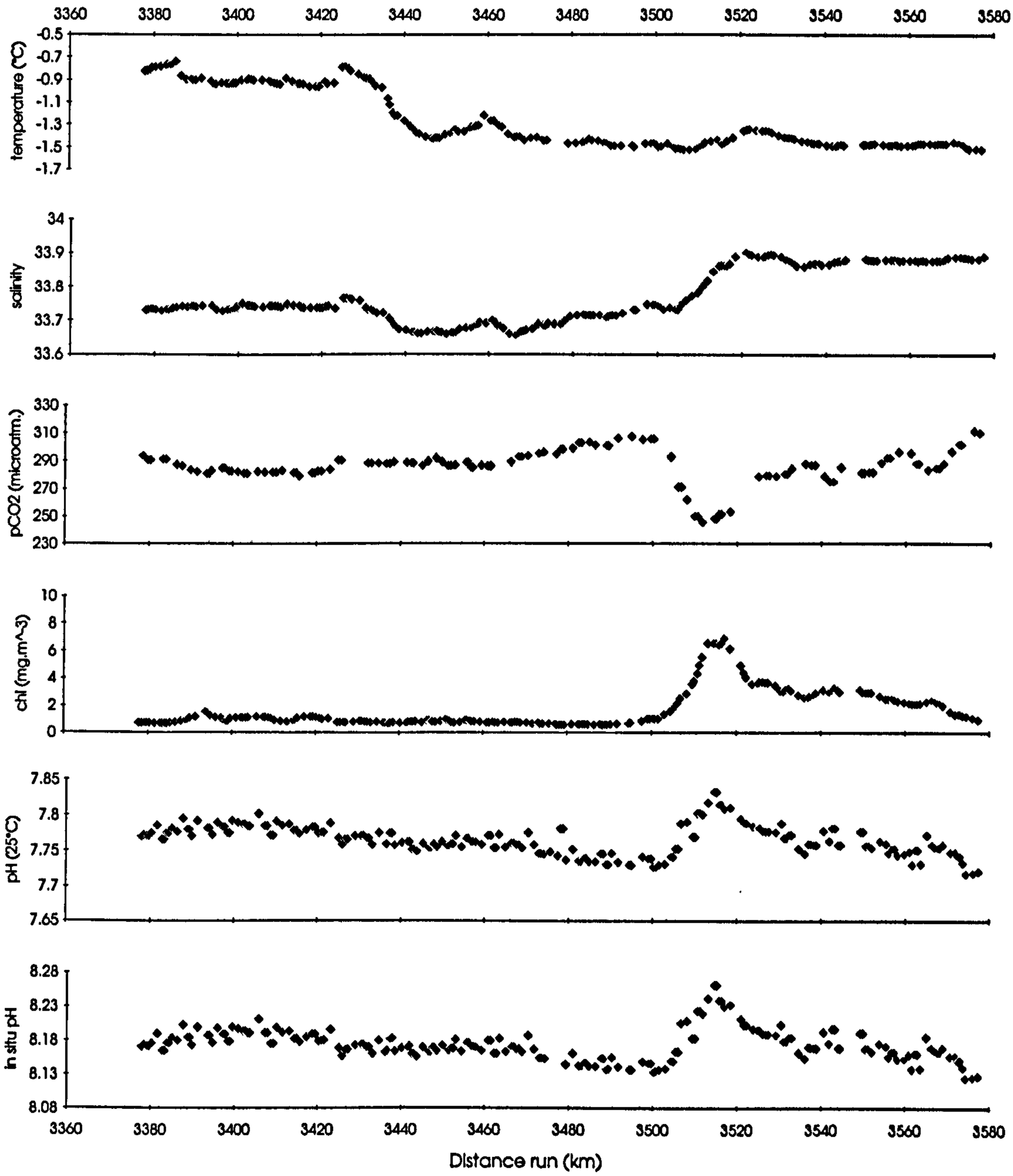

Figure 5.14. Surface profiles of temperature, salinity, pCO2, chlorophyll, pH(25°C) and in situ pH for leg W, survey 1, Bellingshausen Sea

CHAPTER 1.

INTRODUCTION

An improvement in the accuracy of global climate models requires an increase in our understanding of oceanic biogeochemical cycling. Central to this understanding is the accurate characterisation of the oceanic carbon dioxide system, measurements of which are limited to time series stations and to oceanic cruises, both of which are limited in number and do not give a fair global representation on a spatial and temporal scale. Selectivity of sampling site may provide bias towards a certain area during cruises, whether it be due to a particular oceanographical feature, or simply due to accessibility and cost. The ability to model the carbon dioxide system would be greatly enhanced through high density carbon dioxide measurements on a global and inter-annual scale, however, due to the high costs involved such measurements are not possible using conventional cruise methods, and it would therefore be favourable to develop instrumentation enabling the carbon dioxide system to be determined *in situ*. Fully automated instrumentation could then be employed on buoys and autonomous submarines, and additionally take advantage of ships of opportunity.

The carbon dioxide system can be thoroughly characterised from the measurement of any two of the parameters pH, alkalinity, total carbon dioxide (TCO_2) and the partial pressure of carbon dioxide (pCO_2) (Skirrow, 1975). The parameter pairing most amenable to *in situ* operations is that of pH and pCO_2 (Johnson *et al.*, 1992; Bellerby *et al.*, 1993)

The measurement of pH in seawater has traditionally been avoided because of problems inherent with the operation of potentiometric methods. The use of a glass electrode has a general accuracy of < 0.01 pH unit (Culberson, 1981), although selected continuous potentiometric methods have illustrated very high precision (Fuhrmann and Zirino, 1988; Mackey *et al.*, 1989; Butler and Mackey,1992). Major errors arise from residual liquid junction potentials, electrode drift between calibration and sample measurement, standing potentials (Culberson, 1981; Covington *et al.*, 1988) and on-line electrical interference, especially during continual shipboard analyses (Bellerby *et al.*, 1993). The sensitivity of the carbon dioxide system to the seawater pH is such that it is necessary to measure the parameter to ± 0.005 pH units. Recently, discrete spectrophotometric methods using the acid-base characteristics of selected sulfonephthalein indicators has been shown to equal or better this level of precision (Robert-Baldo *et al.*, 1985; Byrne and Breland, 1989; Clayton and Byrne, 1993), and it was therefore the objective of this work to

develop a highly precise continuous spectrophotometric method for seawater pH.

This thesis reports on the carbon dioxide system in seawater, and the intimate relationship between the CO_2 parameters, air-sea gas exchange and the productivity of the marine biosphere is summarised. A brief account of the global carbon cycle is presented and the effects of anthropogenic perturbations are documented. The role of the ocean in buffering atmospheric CO_2 is discussed.

The assignment of pH values to standard buffers is explained and the merits of each scale are discussed along with their inter-relation. The theory of potentiometric and spectrophotometric pH measurement is presented and a chronological literature review of fieldwork is given for both techniques.

The development and automation within this study of both continuous potentiometric and spectrophotometric techniques for seawater pH measurement is described and the operation of the instrumentation in the Bellingshausen Sea, Southern Ocean is documented along with the relationships between the CO_2 system and the hydrography and biology of the surface waters.

CHAPTER 2.

THE OCEANIC CARBON CYCLE

2.1. Introduction

The dissolution of atmospheric CO_2 in the surface ocean, hydration and subsequent dissociation of the CO_2 results in equilibrium partitioning between the dissolved CO_2 species. Knowledge of the equilibrium conditions, relating this partitioning to temperature and salinity, enables the calculation of a carbon dioxide parameter (pH, pCO_2, TCO_2 and alkalinity) from any pair of measured parameters. Biological activity in the euphotic zone of the oceans fixes dissolved inorganic carbon dioxide to organic carbon and particulate inorganic forms. Sequestration of this biologically modified material in the marine sediments is a major sink for CO_2. The exchange of CO_2 between the ocean and the atmosphere is a function of the carbon dioxide concentration gradient, and the rate of gas transfer, across the ocean surface.

The cycling of carbon between the global reservoirs is influenced on a geological timescale by the equilibrium between the lithogenic exchange of carbon dioxide with the atmosphere and ocean. Net exchange is a corollary of the relative influences of the silica, organic carbon and carbonate cycles. The size of the atmospheric carbon dioxide reservoir is variable, and significantly controlled by ocean-atmosphere interactions and the interplay between chemical buffering and biological modifications in the ocean. The consequences of anthropogenic perturbations of the atmospheric CO_2 concentration with respect to future climate change are unknown. It is paramount that the significance of the oceanic carbon sink be evaluated in order for it to be incorporated accurately into climate models.

This chapter aims to introduce the inorganic oceanic carbon cycle, the relationship between the carbonate parameters and the intimate association of the CO_2 system with the biology of the surface ocean. Carbon dioxide exchange across the surface ocean is discussed along with its parameterisation. The significance of anthropogenic perturbations of the global carbon cycle on the atmospheric CO_2 is summarised.

2.2. Marine Carbonate Chemistry

When carbon dioxide transfers across the air-sea interface there exists a chemical buffering due to the non-conservative properties of the gas in seawater. The carbon dioxide gas undergoes hydration, and subsequent dissociation, until equilibrium for all carbon species, gaseous and aqueous, is attained.

Considering carbon dioxide transfer from the atmosphere into the ocean; carbon dioxide gas $CO_2(g)$ first dissolves in seawater to form dissolved $CO_2(aq)$

$$CO_2(g) \leftrightarrow CO_2(aq) \qquad 2.1.$$

and some of the dissolved CO_2 is hydrated to carbonic acid

$$CO_2(aq) + H_2O(l) \leftrightarrow H_2CO_3 \qquad 2.2.$$

There is dissociation of carbonic acid to bicarbonate and carbonate ions through the reactions

$$H_2CO_3^* \leftrightarrow H^+ + HCO_3^- \qquad 2.3.$$

$$HCO_3^- \leftrightarrow H^+ + CO_3^{2-} \qquad 2.4.$$

where $H_2CO_3^*$ represents both H_2CO_3 and $CO_2(aq)$, *i.e.* total undissociated dissolved carbon dioxide, and the first order process for Equation 2.3. is the hydration of dissolved CO_2 to bicarbonate (Skirrow, 1975). Equilibria for reactions 2.3. and 2.4. are written, respectively,

$$K_1 = \frac{h.[HCO_3^-]}{[H_2CO_3^*]} \qquad 2.5.$$

$$K_2 = \frac{h.[CO_3^{2-}]}{[HCO_3^-]} \qquad 2.6.$$

Where K_1 and K_2 are the first and second dissociation constants of carbonic acid respectively (Hansson, 1973a; Mehrbach *et al.*, 1973; Dickson and Millero, 1987; Goyet

and Poisson, 1990; Roy *et al.*, 1993b). Bracketed constituents refer to their stoichiometric concentrations, *i.e.* they include ion-pairings and hydrated forms as well as the free ion concentrations and total CO_2(aq) (Hansson, 1973a). The term $h = 10^{-pH}$ and is related to $[H^+]$ in a manner dependent on the chosen pH scale, which in turn dictates the values of the dissociation constants used to characterise the carbon dioxide system.

It would at this point be sufficient to measure pH and pCO_2 to fully characterise the inorganic carbon constituents, namely $[H_2CO_3^*]$, $[HCO_3^-]$ and $[CO_3^{2-}]$. However, under certain circumstances it may be favourable to determine directly the alkalinity and total carbon dioxide. These variables are conservative with respect to temperature and pressure if expressed as mol.kg^{-1} seawater (Unesco, 1987) and can be used to identify and quantify the processes controlling inorganic speciation (Najjar, 1992; Robertson and Watson, 1993). Total carbon dioxide (TCO_2, sometimes termed DIC or ΣC) is a summation of the inorganic carbon species

$$[TCO_2] = [H_2CO_3^*] + [HCO_3^-] + [CO_3^{2-}] \qquad 2.7.$$

Alkalinity (Alk) is equivalent to the excess positive charge in seawater and can generally be assumed to approximate (Dickson, 1981)

$$\begin{aligned} Alk = {} & [HCO_3^-] + 2[CO_3^{2-}] + [B(OH)_4^-] + [OH^-] + 2[HPO_4^{2-}] \\ & + 3[PO_4^{3-}] + [SiO(OH)_3^-] + [HS^-] + 2[S^{2-}] + [NH_3] \\ & - [H^+] - [HSO_4^-] - [HF] - [H_3PO_4] \end{aligned} \qquad 2.8.$$

Most ions are assumed to make up an insignificant part of the total alkalinity. In addition to the carbonate ions only borate has a significant rôle in balancing the charge equivalence when taking into account the analytical precision of current techniques of alkalinity determination (Dickson, 1981). Fortunately, the borate concentration (as well as sulphate and fluoride) may be calculated from their stoichiometric (conservative) relationship with salinity. The alkalinity can therefore be simplified to the proton condition, where the zero level of protons considered is relative to boric acid, water and carbonic acid (Dickson, 1981; Butler, 1992). Alkalinity can now be written as

$$Alk = [HCO_3^-] + 2[CO_3^{2-}] + [B(OH)_4^-] + [OH^-] - [H^+] \qquad 2.9.$$

It is necessary to determine the thermodynamics of boric acid and water in seawater to ascertain their effective contribution to alkalinity. The dissociation of boric acid gives the relationship (Hansson, 1973a; 1973b; Dickson, 1990a; Roy *et al.*, 1993a)

$$K_B = \frac{[B(OH)_4^-].h}{B(OH_3)} \qquad 2.10.$$

Similarly for the dissociation of water (Culberson and Pytkowicz, 1973; Dickson and Riley, 1979)

$$K_W = [OH^-].h \qquad 2.11.$$

To calculate that part of the total alkalinity attributed to the carbonate system, namely the carbonate alkalinity (CA),

$$CA = [HCO_3^-] + 2[CO_3^{2-}] \qquad 2.12.$$

the borate and hydroxide concentrations obtained from Equations 2.10. and 2.11. are subtracted from the total alkalinity.

Through the determination of any two of the four major carbon dioxide variables (TCO_2, pCO_2, alkalinity and pH) it is possible to determine all the other variables of the carbon dioxide system through the equations set out below (Skirrow, 1975; Millero, 1979).

$$[CO_3^{2-}] = CA/(2 + h/K_2) \qquad 2.13.$$

$$[HCO_3^-] = CA/(1 + 2.K_2/h) \qquad 2.14.$$

$$CA = TCO_2(1 + 2K_2/h)/(1+ h/K_1 + K_2/h) \qquad 2.15.$$

$$pCO_2 = [H_2CO_3^*]/ \alpha \qquad 2.16.$$

$$TCO_2 = CA(1 + h/K_1 + K_2/h)/(1 + 2K_2/h) \qquad 2.17.$$

$$h^3 + h^2[K_1(A-1) + K_B)]/A + h[K_1K_B(A - B - 1) + K_1K_2(A - 2)]/A + K_1K_2K_B(A - B - 2)/A = 0 \qquad 2.18.$$

where $A = Alk/TCO_2$, $B = \Sigma B/TCO_2$ and ΣB is the total borate concentration.

Certain parameter couplings are preferable due to their superior analytical precision. Such pairings have been critically appraised by Dickson and Riley (1978). They suggest that, overall, the pairing of CA and TCO_2 is the most suited with, if possible, pCO_2 being measured and not calculated. Analytical techniques have improved since the Dickson and Riley paper and a more up-to-date evaluation is needed of the errors incurred during carbon dioxide parameter calculations using present limits of precision. This has been performed for the analytical techniques used in this study, the details of which are documented in Section 4.5.3.

2.3. Productivity and Sedimentation

2.3.1. The Biological Pump.

Given that light, temperature and nutrients are not limiting, autotrophic and mixotrophic activity in the surface ocean removes carbon dioxide from the water through photosynthesis. This process may be represented by

$$nCO_2 + nH_2O \rightarrow (CH_2O)_n + nO_2 \qquad 2.19.$$

where $(CH_2O)_n$ is an organic product. Removal of CO_2 lowers TCO_2 and pCO_2, raises pH and may increase alkalinity very slightly. The small increase in alkalinity is associated with nutrient uptake (Broecker and Peng, 1989; Robertson and Watson, 1993) and approximates to an increase in alkalinity of 16 $\mu equiv.kg^{-1}$ for each 100 $\mu mol.kg^{-1}$ TCO_2 decrease if nitrate is the only utilised nutrient and assuming a classical Redfield ratio (Broecker and Peng, 1989). A lowering of pCO_2 in surface waters biases the CO_2 transfer across the air-sea interface towards a drawdown of the gas into the mixed layer.

The processes affecting the carbon taken up during photosynthesis are complex. Organic carbon may be remineralised in the mixed layer as a result of cellular excretion or through heterotrophic grazing and subsequent excretion or zooplankton death. Alternatively, the foodchain provides a way of moving carbon through the thermocline into the deep ocean - faecal pellets or dead organisms may be large enough to have a sufficient Stoke's velocity to override any localised advective processes and buoyancy forces. The

pelagic zone of the ocean is generally considered to be in biogeochemical steady-state (Platt *et al.*, 1989) and thus transfer of organic material across the reservoir boundary is a measure of the new production, which has been defined as the stoichiometric index of production in the euphotic zone supported by nutrient transfer from below the thermocline (Eppley and Peterson, 1979) and aeolian input. The supply of transient nutrients is generally limited to areas of vertical advection which are most obviously upwelling areas. However, local events such as eddy pumping (Falkowski *et al.*, 1991) and storms (Platt and Harrison, 1985) may support significant production in the open ocean. Diapycnal nutrient transfer has been suggested to contribute significantly to the nutrient supply in oligotrophic areas (Jenkins and Goldman, 1985), however, using inert tracers these exchange rates have recently been shown to be small (Ledwell *et al.*, 1993).

The majority of the organic material is remineralised in the water column. Microbial consumption converts some of this material to dissolved organic carbon (DOC) which makes up almost 2% of the total carbon pool (Siegenthaler and Sarmiento, 1993) although much of the remainder is oxidised to inorganic forms in a reversal of Equation 2.19. As productivity in the euphotic zone supports life in the deep ocean (discounting chemotrophs) some heterotrophic consumption will occur and only particles which are large or dense enough to sink quickly through the water column reach the sediments (Lampitt, 1985). Re-suspension may result from the effects of bottom currents and bioturbation (Lampitt, 1985). Further oxidation occurs before the particles are eventually sequestered into the sediments prior to the onset of diagenetic processes.

This biologically mediated transfer of carbon dioxide in organic form from the mixed layer to the deep ocean and possible integration with the sediments has been termed the biological pump (Longhurst and Harrison, 1989).

2.3.2. The Carbonate Pump.

In addition to the biological pump, another biologically mediated control of the ocean carbon dioxide system is brought about by the formation of calcareous tests by certain planktonic species - coccolithophorids, foraminifera and pteropods. The tests, as an aggregate, make up the skeletal structure of the organism. Uptake of carbonate and

bicarbonate is through skeletal formation: -

$$Ca^{2+} + 2HCO_3^- \leftrightarrow CaCO_3 + H_2O + CO_2 \qquad 2.20.$$

$$Ca^{2+} + CO_3^{2-} \leftrightarrow CaCO_3 \qquad 2.21.$$

During skeletal formation, one mole of carbonate is taken up per mole of calcium and there is a concordant decrease in the surrounding seawater alkalinity of two equivalents. The sequential equilibrium reached amongst the CO_2 species results in the paradox that although the total inorganic carbon in the surrounding seawater has been reduced, there is an increase in pCO_2. In the short term some of this CO_2(aq) is cycled internally by the organism during photosynthesis, however, respiration results in a net increase in pCO_2 which, with respect to air-sea transfer, counteracts the carbonate removal and, for autotrophs, masks the biological pump attributed to the organism (Robertson *et al.*, 1994). This process has important implications in the use of remote sensing applications when determining air-sea CO_2 exchange from images of sea surface pigment concentrations, temperatures and windspeeds (Balch *et al.*, 1992) using empirical algorithms defined from non-calcareous species.

Upon the death of the organism, the skeleton sinks to a depth dependent on the degree of undersaturation to calcite (from coccolithophorids and foraminifera) or aragonite (from pteropods) - unless specified to the contrary both now referred to as calcite - of the surrounding waters and the Stoke's velocity of the particle. The majority of the surface ocean is saturated with respect to calcite. The depth at which the ocean becomes undersaturated is termed the calcite saturation horizon. Only particles which reach sediments above this horizon will remain in precipitate form. Areas where significant calcite deposition occurs are commonly continental shelves and sea mounts, although where the compensation depth, the depth at which carbonate dissolution occurs in the sediments, deepens considerable deposition is seen on the deep ocean floor. Chen *et al.* (1988) reported sedimentary calcite composition as high as 80% in the equatorial Pacific. If the skeleton has been incorporated into a large marine snow aggregate, and has settled rapidly, it may be incorporated into the sediments before dissolution can occur. Dissolution causes a reversal of Equations 2.20. and 2.21. thus, TCO_2 and alkalinity increase. Importantly, pCO_2 decreases and therefore when the water outcrops at the surface it's potential as a carbon dioxide source is weakened.

2.4. Air-sea gas exchange

Net exchange of carbon dioxide between the atmosphere and the ocean relies on an imbalance between the carbon dioxide concentration in the air above the sea surface and the mixed layer in the ocean. For equilibrium to be satisfied, molecular and advective processes in both media must transport carbon dioxide to, or from, the air-sea interface until the concentration gradient between the two reservoirs is removed. Turbulence is mainly responsible for transfer of the gas to the interface. However, apart from highly reactive, highly soluble gases (*e.g.* H_2O, SO_2, NH_3) (Hasse and Liss, 1980) molecular diffusion through the viscous surface of the ocean governs the rate of transfer across the interface (Jähne *et al.*, 1987). A first order control on the rate of diffusion is the relationship between kinematic viscosity (the ratio between the viscosity and density) of the water and the molecular diffusivity (a measure of the rate of random motion) of the gas in the water (*e.g.* Deacon, 1977; Jähne *et al.*, 1987).

The net flux (F) required to correct any disequilibrium is a function of the concentration gradient and the gas transfer velocity for carbon dioxide (k_{CO2}) across the interface:

$$F = k_{CO2}.\alpha_{ml}.[(pCO_{2atm}) - (pCO_{2ml})] \qquad 2.22.$$

where α is the solubility of carbon dioxide in seawater, and subscripts refer to the atmosphere (atm) and the mixed layer (ml) (Robertson and Watson, 1993).

The difference in carbon dioxide concentrations across the interface can be determined analytically. The solubility of carbon dioxide in seawater has been determined by Weiss (1974) as a function of temperature and salinity such that

$$\ln\alpha = -60.2409 + 93.4517(100/T) + 23.3585.\ln(T/100) + S[0.023517 - 0.023656(T/100) + 0.0047036(T/100)^2] \qquad 2.23.$$

where $T(K) = t\,(°C) + 273.15$, and S is the salinity and α is in $mol.kg^{-1}.atm^{-1}$.

Experimental studies have been undertaken to estimate the gas transfer velocity either under laboratory conditions, on lakes or at sea;

(a) Radiocarbon techniques rely on either natural ^{14}C or bomb-derived ^{14}C. The sole

natural source of ^{14}C is from cosmic ray bombardment of the upper atmosphere, whilst anthropogenic ^{14}C has been introduced to the troposphere during atom bomb testing since 1957. Natural radiocarbon is suitable for long-term global determination of air-sea exchange. Exchange is evaluated, assuming that the ocean ^{14}C inventory is in steady state, from the decay constant of ^{14}C in the oceans, and the isotopic composition, in the atmosphere and ocean (Broecker *et al.*, 1986). Bomb-produced radiocarbon gives a global average for gas exchange over a period of a few years. It can be determined if the oceanic bomb ^{14}C for a particular time and previous ^{14}C to ^{12}C ratios in both the atmospheric and oceanic carbon dioxide are known (Broecker *et al.*, 1986). Neither method is suited to characterise the gas transfer velocity windspeed dependence except on a globally averaged basis.

(b) The radon deficiency method (Broecker and Peng, 1974; Peng *et al.*, 1974; 1979; Smethie *et al.*, 1985; Broecker *et al.* 1986) relies on the natural degradation of ^{226}Ra to ^{222}Ra. The source of ^{222}Ra is the ocean through the decay of dissolved ^{226}Ra (Broecker and Peng, 1974) which is derived from conservatively distributed uranium. From the half life of radon, and measuring the depth profiles of ^{222}Ra and ^{226}Ra from the sea surface through the thermocline, the rate of gas transfer from the ocean to the atmosphere can be calculated from the radon deficit in the mixed layer. Radon depletion measurements are valid for periods of days to a month under constant meteorological conditions. However, as exchange calculations are dependent on a constant mixed layer depth, a highly variable parameter, radon methods are not suitable for characterising the windspeed dependence of the gas transfer velocity.

(c) An eddy correlation technique has been employed to characterise small scale changes in the air-sea flux (Jones and Smith, 1977; Wesely *et al.*, 1982; Ohtaki *et al.*, 1989). The local wind field is combined with rapid CO_2 measurements to obtain net fluxes away from the sea surface. This technique commonly produces estimates that are very different to other methods of gas exchange rates.

(d) Measurements of the loss rate of the inert tracer sulphur hexafluoride SF_6 added to aquatic systems under differing wind regimes have been made (Wanninkhof *et al.*, 1985; Upstill-Goddard *et al.*, 1990; Watson *et al.*, 1991a; Wanninkhof *et al.*, 1993). As dual tracer techniques using the gases SF_6 and ^3He work over short timescales (hours-days) they

have proved useful in characterising the windspeed dependence of gas transfer velocities, particularly at high windspeeds (Watson *et al.*, 1991a).

Once transfer velocities have been determined for a particular gas then conversion to CO_2 is achieved through the relationship (Watson *et al.*, 1991a; Erickson, 1993).

$$k_{CO2} = k_{GAS}\left(\frac{Sc_{GAS}}{Sc_{CO2}}\right)^{n} \qquad 2.24.$$

where the Schmidt number (Sc) is equal to the kinematic viscosity (ν) of the water divided by the molecular diffusivity (D) of the gas

$$Sc = \frac{\nu}{D} \qquad 2.25.$$

The superscript *n* is an empirical relationship termed the Schmidt number dependence (Jähne *et al.*, 1987).

The gas transfer velocity has many controls including wind speed, water temperature, thermal stability, surface microlayer composition and chemical and biological enhancement. Wind-tunnel studies have shown that the relationship between transfer velocity and windspeed is not linear (Hasse and Liss, 1980; Liss and Merlivat, 1986; Wanninkhof, 1992). Liss and Merlivat (1986) have categorised this wind speed dependence for any gas at 20°C, with respect to CO_2, over three ranges of windspeed using data from wind-tunnel and lake experiments combined with theory

$$k_{GAS} = 0.17.U_{10}.\left(\frac{600}{Sc_{GAS}}\right)^{0.6} \qquad 0 \le U_{10} \le 3.6\ m.s^{-1} \qquad 2.26a.$$

$$k_{GAS} = [2.85.U_{10} - 9.65].\left(\frac{600}{Sc_{GAS}}\right)^{0.5} \qquad 3.6\ m.s^{-1} \le U_{10} \le 13 m.s^{-1} \qquad 2.26b.$$

$$k_{GAS} = [5.9.U_{10} - 49.3].\left(\frac{600}{Sc_{GAS}}\right)^{0.5} \qquad U_{10} \ge 13\ m.s^{-1} \qquad 2.26c.$$

where k is calculated in $cm.h^{-1}$, Sc is the Schmidt number of the gas, U_{10} is the average windspeed in $m.s^{1}$ at 10m above the water surface.

Within the first category, where U_{10} is less than 3.6 $m.s^{-1}$, the boundary between air and liquid is a free surface. An increase in transfer velocity when the wind is between 3.6

and 13 $m.s^{-1}$ results mainly from the presence of capillary waves increasing the potential surface area for exchange and a thinning of the viscous sublayer as the surface is stretched (Hasse and Liss, 1980). Transfer when the windspeed exceeds 13 $m.s^{-1}$ is promoted through the onset of breaking waves. The viscous sublayer is partly dissipated, reducing resistance to transfer. Bubble injection increases the surface area for transfer. Subsequently, transfer across a broken interface is approximately fifty times more efficient than for a free surface (Monahan and Spillane, 1984).

Wanninkhof (1992) estimated the windspeed gas exchange relationship using discrete windspeed measurements as

$$k_{GAS} = 0.31(u^2)_{10}\left[\frac{660}{Sc_{GAS}}\right]^{0.5} \qquad 2.27.$$

derived from ^{14}C invasion rates and long-term windspeed relationships but has been adjusted using a normalised Rayleigh windspeed distribution to fit to an average windspeed of 7.4 $m.s^{-1}$. Although derived from globally averaged invasion rates and windspeeds this equation should be suitable for steady (short-term) winds (Wanninkhof, 1992).

The temperature dependence of the rate of gas transfer is reflected in the Schmidt number (Jähne *et al.*, 1987), which cancels out a significant contribution of the effect of temperature on solubility (Wanninkhof, 1992). The combined effect of temperature and solubility on the exchange coefficient (K),

$$K = k.\alpha \qquad 2.28.,$$

has been illustrated by Echeto and Merlivat (1988). For low windspeeds, $U_{10} \leq 3.6$ $m.s^{-1}$, K increases with an increase in water temperature. Under more turbulent conditions, $U_{10} \geq 3.6$ $m.s^{-1}$, K decreases with an increase in temperature. This temperature dependence, although small, is important when calculating global budgets as considerable imbalances may result from the large difference in temperatures between source and sink regions (Wanninkhoff, 1992).

The temperature of the mixed layer may be warmer than the surface skin of the ocean, and it is the latter which is a control on gas exchange. Robertson and Watson (1992)

have shown that the oceanic CO_2 uptake calculated by Tans *et al.* (1990) increases by 0.7 Gt C yr^{-1} when the thermal skin effect is taken into account.

The thermal stability of the air above the water has been shown to affect K (Erickson, 1993). Using a model, enhancement of gas transfer was observed when cold air passed over a warmer ocean. The non-inclusion of thermal stability in calculating transfer velocities *in situ* may account for some of the disagreements between different authors (Erickson, 1993).

The degree of chemical enhancement of the CO_2 flux depends on the relationship between the kinetics of gas exchange and of CO_2 hydration and dehydration. Enhancement is greatest at low windspeeds (Wanninkhof, 1992), when the transfer velocity is small and as such the CO_2 resides in the boundary layer long enough for some conversion to other ionic forms (Whitfield and Turner, 1986). Emerson (1975) determined from a lake study that the invasion of carbon dioxide was 5 to 10 times that which would have occurred with no chemical enhancement. Wanninkhof (1992) calculated that chemical enhancement raised the sea-air transfer in equatorial waters, areas of predominantly low windspeeds, by 20% compared to the Rayleigh probability distribution function of globally averaged ^{14}C transfer velocity, and by 6% over the Liss and Merlivat relationship.

Retardation of surface exchange has been noted by Goldman *et al.*(1988) due to the presence of surfactants on the sea surface resulting from biological and anthropogenic activity (Hasse and Liss, 1980; Goldman *et al.*, 1988). Surfactants act to dampen the size of capillary waves (Hasse and Liss, 1980) and may, by reducing the surface tension of the water, buffer the turbulence arising from small eddies in the water column. This would increase the width of the viscous sublayer and thus reduce the gas transfer rate (Goldman *et al.*, 1988).

A consequence of biological activity which has a positive effect on gas transfer may be chemical enhancement by enzymes such as carbonic anhydrase in the surface microlayer (Berger and Libby, 1969). The extent of this enhancement has been challenged (Goldman and Dennet, 1983). Autotrophic activity in the neuston may significantly effect gas transfer of trace gases (Conrad and Seiler, 1988) although this has not been shown for CO_2.

2.5. Global Carbon Cycling

On a geological timescale, atmospheric CO_2 is mainly influenced by the balance between the uptake of CO_2 during the weathering of siliceous rock, and its subsequent release through metamorphic decarbonation of oceanic carbonaceous precipitates. Additional constraints are imposed through the incorporation of organic material into the lithosphere and the cycling of non-metamorphically modified carbonate minerals.

Carbonates are produced by the weathering of siliceous and carbonaceous rocks. During this weathering there is a respective, concomitant release and uptake of atmospheric CO_2. The carbonates are transported to the sea, predominantly in the form of bicarbonate, where they are precipitated and subsequently may be sequestered in ocean sediments. Carbonate precipitation in the oceans results in a net production of CO_2

$$M^{2+} + 2HCO_3^- \underset{\text{weathering}\leftarrow}{\overset{\text{precipitation}\rightarrow}{\leftrightarrow}} MCO_3 + CO_2 + H_2O \qquad 2.29.$$

where M is either calcium or magnesium. Metamorphism and volcanism results in decarbonation through the exchange of calcium or magnesium from the carbonate precipitate to silicon dioxide

$$CO_2 + MSiO_3 \underset{\text{magmatism}}{\overset{\text{weathering}\rightarrow}{\leftrightarrow}} MCO_3 + SiO_2 \qquad 2.30.$$
$$\text{metamorphism}\leftarrow$$

This CO_2 is released on exposure of the siliceous rock to the ocean or atmosphere. Metamorphism does not always take place and CO_2 is taken up from the atmosphere during the weathering of carbonate rocks (Siegenthaler and Sarmiento, 1993).

Within the organic carbon cycle, CO_2 is incorporated into living material. The organic material settles to the seafloor and is lithified. CO_2 is returned to the atmosphere upon weathering and oxygenation of exposed rock (Siegenthaler and Sarmiento, 1993). The organic carbon cycle may be represented as

$$CO_2 + H_2O \underset{\text{metamorphism and air oxidation}}{\overset{\text{organic burial}\rightarrow}{\leftrightarrow}} CH_2O + O_2 \qquad 2.31.$$
$$\leftarrow \text{weathering}$$

Berner (1991) stresses that the relationship in Equation 2.31. does not represent photosynthesis and respiration in the purely biological sense but addresses the balance between net photosynthesis and georespiration.

The amount of carbon in each of the reservoirs - atmosphere, terrestrial biosphere and ocean for the pre-industrial era is shown in Figure 2.1a. The sediments contain about 20,000,000 Gt C (UNEP, 1988) and it is apparent that a perturbation of the deep ocean and sedimentary inventories would have a significant effect on the much smaller atmospheric carbon reservoir.

Carbon fluxes between the above reservoirs generally exist in a *quasi*-steady state, particularly if viewed on a millenium timescale. Nevertheless, there have been some significant shifts in the atmospheric concentration of CO_2 associated with transformations between glacial and interglacial environments verified by CO_2 analysis of air bubbles trapped in ice (*e.g.* Barnola *et al.*, 1987; Neftel *et al.*, 1988). Reasons for these changes remain speculative. Boyle (1988) and Broecker and Peng (1989) suggest that the cause may be changes in the alkalinity of Antarctic waters, brought about by the turning on and off of the thermohaline circulation of the Atlantic. This process would be responsible for changing the influx of low-alkalinity waters into the Southern Ocean (Broecker and Peng, 1989). Alternatively, an increase in the efficiency of the biological pump (see Section 2.1.3.) in Antarctic surface waters through changes in the Redfield ratio of marine organisms (Broecker, 1982), or an increase in aeolian trace nutrient input (Martin, 1990; Martin *et al.*, 1990), would have decreased the TCO_2 concentration in surface waters and lowered the atmospheric CO_2 concentration via an increased air-sea flux.

2.6. Post-industrialisation cycling

Anthropogenic activity has perturbed the global carbon cycle by modifying the short-term equilibrium between sediment and atmosphere. Combustion of fossil fuels has changed the organic carbon cycle and land-use changes such as deforestation have altered the carbon balance between the terrestrial biosphere and the atmosphere. Consequences of these perturbations are mainly speculative. It is predicted that, as a result of the radiative forcing due to the increase in carbon dioxide and other trace gases in the atmosphere, global

temperatures will rise. The weightings to the many suggested feedback mechanisms to this warming are unknown. The following sections will discuss the atmospheric increase, scenarios for the ensuing rise in temperature and sea level, and several proposed oceanic uptake and feedback mechanisms for the control of atmospheric CO_2 levels.

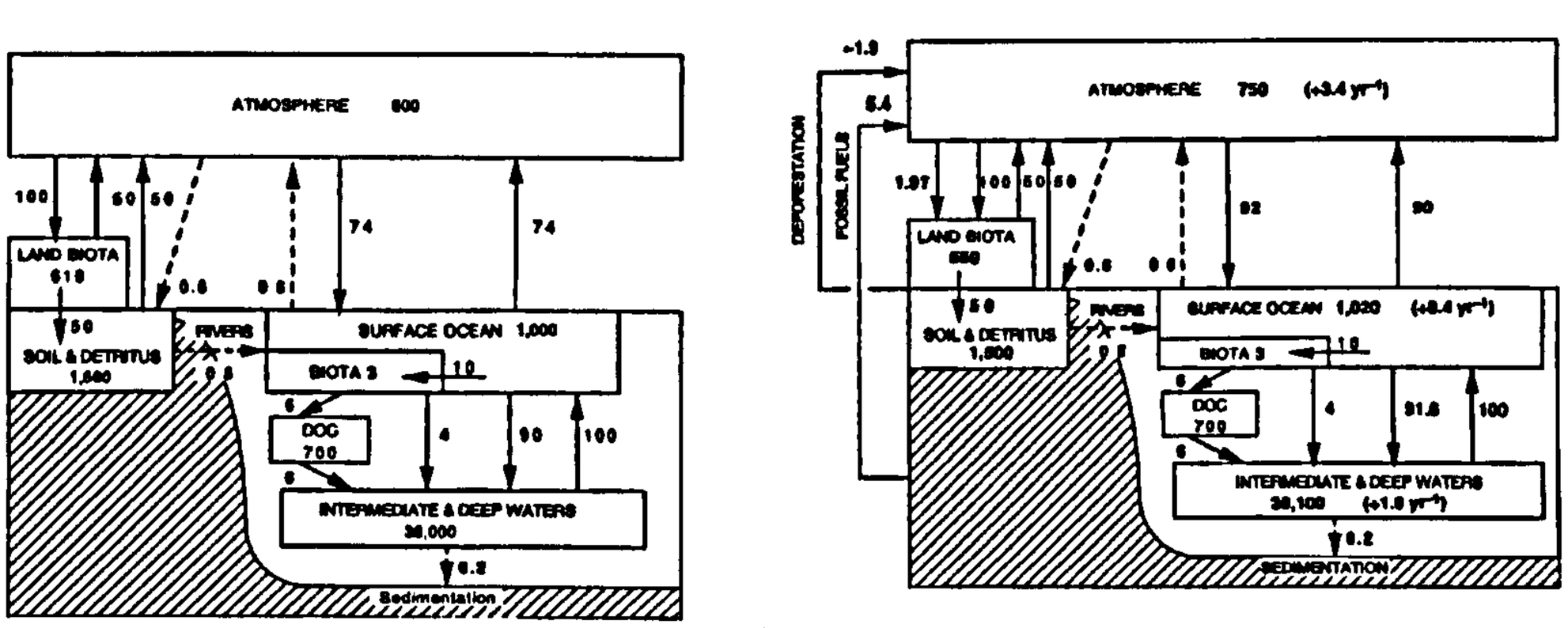

Figure 2.1. Global carbon reservoirs and fluxes (Gt C, gigatonnes carbon, 1 Gt = 10^{15}g) for (a) the pre-industrial era and (b) the period 1980-89 (from Siegenthaler and Sarmiento, 1993).

2.6.1. Atmospheric CO_2 Increase

The pre-industrial atmospheric concentration of carbon dioxide is thought to have been about 280ppmv (IPCC, 1990). As a consequence to the combustion of fossil fuels, cement production and land-use changes (Keeling, 1973; Rotty, 1983), atmospheric carbon dioxide concentration has increased (Figure 2.1b.) By 1990 the concentration had reached 353ppmv and is presently rising at about 1.8ppmv.yr^{-1} (IPCC, 1990). Predictions for future atmospheric rises suggest that levels may more than double by the end of the 21st century (IPCC, 1990; Wigley and Raper, 1992). Carbon dioxide gas absorbs strongly in the wavelength of longwave terrestrial radiation. As a direct result of increased levels of radiative gases (mainly carbon dioxide, chlorofluorocarbons, methane, carbon monoxide and nitrous oxide) there is now an enhanced greenhouse effect (IPCC, 1990; Lashof and Ahuja, 1990). CO_2 contributes most to this forcing and there is considerable

correspondence between the rise in CO_2 and the global temperature rise (Kuo *et al.*, 1990). Models by Schlesinger and Jiang (1991) predict that warming relative to the 1990 global temperature will be between 0.62-5.15°C (best scenario) and 1.61-5.15°C (worst scenario) by 2100. Revised projection for a doubling of CO_2 from the 1990 level suggest a warming of 3.4°C (Wigley and Raper, 1992).

2.6.2. Uptake and Feedback Mechanisms Affecting the Oceanic Carbon Cycle

At present, only about half of the CO_2 released through anthropogenic activity has remained in the atmosphere (Liss and Crane, 1983). When all known sources and sinks are accounted for there remains a missing sink of 1.6 ± 1.4 Gt C (IPCC, 1990) and our ignorance of the net fluxes between both the terrestrial biosphere and the oceans, and the atmosphere, generate uncertainties in understanding the fate of this missing CO_2. The consensus amongst the oceanographic community is that the oceans are the largest short term carbon sink (*e.g.* Siegenthaler, 1983; IPCC, 1990) having taken up about 40 % of the anthropogenic carbon output. However, a general circulation model, constrained by empirical oceanic pCO_2 gradients and monthly climatological wind speeds, was used to suggest that the total oceanic uptake is at most 1 Gt C.yr^{-1} (Tans *et al.*, 1990). Therefore, to balance the known atmospheric inputs there must be a terrestrial sink in the temporal northern latitudes of about 2.6 Gt C.yr^{-1} (Tans *et al.*, 1990). Sarmiento *et al.* (1992) forced their model with the Siple ice core data and Mauna Loa atmospheric pCO_2 values. They gave support to the IPCC (1990) scenario that there is an oceanic uptake of about 2 Gt C. yr^{-1} which is confirmed by a recent estimate of 2.0 ± 0.6 Gt C yr^{-1} (Siegenthaler and Sarmiento, 1993).

An obvious sink for some of the excess atmospheric carbon dioxide is the solubility pump in the ocean. An increase in the partial pressure gradient across the air-sea interface will enhance the downward flux into the mixed layer. Subsequent mixing, and particularly incorporation into the deep water formed at high latitudes, will sequester carbon dioxide in the deep ocean for up to a 1000 years before it outcrops at the surface releasing the gas back into the atmosphere. Back-calculating deep ocean TCO_2 values to represent pre-industrial surface concentrations suggest that surface TCO_2 concentrations have increased

by approximately 40μmol.kg^{-1} (Kroopnick, 1985). This is consistent with the increase shown between Figures 2.1a and b. where 100 Gt C. has reached the deep ocean (Siegenthaler and Sarmiento, 1993).

The missing carbon dioxide may be hidden amongst the ranges of estimates for sinks and sources. Chen (1993) has estimated the excess carbon in the oceans and suggests that the high estimates for the oceanic sinks balance the low estimates of the sources of carbon dioxide from fossil fuel release and land use changes. The accuracy of the inverse methods used by Chen and others in determining excess CO_2 is, however, very low (Sarmiento, 1991).

A biologically initiated control of anthropogenic CO_2 may be through increased dissolution of suspended and sedimentary calcite (Byrne *et al.*, 1984). The increase in dissolution is due to the lower pH of the CO_2 - rich water. Dissolution of carbonate consumes CO_2 through a reversal of Equations 2.20. and 2.21., and on outcropping at the surface the seawater will be a 'negative source' of CO_2 relative to it's original composition on transfer to depth.

2.6.3. Speculative uptake mechanisms

Although a speculative sink, and a cause for heated debate (*e.g.* Smith and Mackenzie, 1991; Broecker, 1991; Sarmiento, 1991), the biological pump may have a rôle to play in moderating the atmospheric increase (Reibesell *et al.*, 1993). It has been argued that because inorganic carbon is not limiting in oceanic waters then an increase in the TCO_2 content of the water would not enhance productivity (Broecker, 1991). Thus many global carbon models do not include biology, considering CO_2 a fixed quantity and thus a passive tracer (*e.g.* Maier-Reimer and Hasselmann, 1987; Sarmiento *et al.*, 1992). The CO_2(aq) concentration in seawater is very low, and it is this carbon source that is mainly used in photosynthesis (as opposed to HCO_3^- and CO_3^{2-}), therefore, during an intense diatom bloom, photosynthesis could strip the water of most of the CO_2(aq) as the kinetics for gas exchange and carbonate dehydration are comparatively slow (Raven, 1993; Reibesell *et al.*, 1993). Using Michaelis-Menten kinetics and the Redfield ratio it has been shown that CO_2 can be the limiting nutrient and, therefore, an increase in the carbon dioxide content of

surface waters may promote the rate of productivity (Reibesell *et al.*, 1993).

There is the possibility of changes in species composition induced by a warming of the surface waters. Taylor *et al.* (1991) suggested that an increase in coccolithophorids '..might be anticipated in a warmer world' and would decrease the uptake of CO_2. Alternatively, an increased occurrence of diatoms, with their high C:N ratio, could increase the carbon transport, in relation to the available nutrients, due to differential nutrient respiration rates with depth (A.F. Michaels, personal communication, 1993).

2.7. Conclusions

On dissolution in the ocean, atmospheric CO_2 is partitioned between the various inorganic carbon species and it is this buffering that dictates the large size of the inorganic carbon pool. The relationship between the carbon species allows the determination of a parameter from pH, pCO_2, TCO_2 and alkalinity from the measurement of one parameter pairing. There is an intimate association between the marine carbonate system and biological productivity through the processes of photosynthesis and respiration, and through the production of carbonate shells. CO_2 exchange between the atmosphere and the ocean has been heavily researched. However, there are large discrepancies apparent between investigators over the windspeed dependence of gas exchange, the knowledge of which is important in assessing the net flux of CO_2 from empirical CO_2 parameter measurements.

Modifications of the natural CO_2 cycle, through fossil fuel combustion and land use changes, has led to an increase in the atmospheric CO_2 concentration and a consequence for this increase is thought to be a global temperature rise. Changes in atmospheric CO_2 concentrations are ultimately buffered by the sediments, however, short-term feedback mechanisms are quantitatively unknown. The solubility pump is thought to have moved 40 % of the atmospheric CO_2 into the oceans and there is no evidence for an increase in the biological and carbonate pumps. Uncertainties in the importance of the ocean as a sink for anthropogenic atmospheric CO_2 will be reduced through greater spatial mapping of the CO_2 parameters.

CHAPTER 3.

pH MEASUREMENT - THEORY AND PRACTICE

3.1. Introduction

The concept of pH is unusual in that it is defined as a property related not to concentration, as is for example the measurement of other single species such as oxygen, but is related to the activity of hydrogen ions in a solution. As single ion activity coefficients cannot be measured it has been necessary to adopt conventions either for their estimation or to define a standard state in which their value is unity. Evolution of pH theory has resulted in the development of many different pH scales, none of which have been universally adopted. pH measurements are routinely taken in general water quality tests, however, the measurement of seawater pH has been limited to a handful of investigators using a wide range of pH scales and methodologies and traditionally, potentiometric methods using glass electrodes have been used both in discrete and continuous modes. More recently discrete spectrophotometric techniques have also been employed and shown to be very precise.

This chapter details the pH scales, the limits of their usage and their inter-relation. The theory of potentiometric and spectrophotometric pH measurement is explained and a review of past and present techniques is given.

3.2. pH Scales

The chemical potential of a species in an ideal solution may be related to its concentration by the equation (Whitfield, 1975; Stumm and Morgan, 1981)

$$\mu_i = \mu^\circ_i + \text{R.T. } \ln m_i/m^\circ_i \qquad 3.1.$$

where μ_i is the chemical potential and m_i is the molal concentration of species i. R is the gas constant (8.31433 $J.K^{-1}.mol^{-1}$) and T is the absolute temperature (K). x°_i is a defined standard state of x, an arbitrary property which is pressure and temperature dependent (Bates, 1973). Because of the non-ideal behaviour of a system, especially in electrolyte solutions (Whitfield, 1975), the activity of an ion is related to the concentration by

$$a_i = m_i.\gamma_i \qquad 3.2.$$

where m_i is the concentration and γ is the activity coefficient of species *i*. The cell potential (E) of a reversible electrode may be written

$$E_i = E°_i + \frac{R.T}{F} \ln a_i/a°_i \qquad 3.3.$$

where F is the Faraday constant (96,487 C.mol^{-1}).

Single ion activity coefficients cannot be measured and are only defined on the basis of conventions for dividing the mean ion activity coefficient of an electrolyte into single ion activity coefficients (Dickson and Whitfield, 1981; Clegg and Whitfield, 1991). A comparison of models used to estimate single ion activity coefficients is given by Nesbitt (1980). There are variations in the values produced by these models and, therefore, it is necessary to define a standard state where the activity coefficient is unity and as such the standard potential will equal unity (Whitfield, 1975). Two conventions have been developed: the *infinite dilution scale* where the activity coefficient approaches unity as solute concentration approaches zero, and the *constant ionic medium scale* where the activity coefficient becomes unity as the concentration of the component approaches zero in a pure ionic medium (Culberson, 1981; Stumm and Morgan, 1981).

3.2.1. Infinite Dilution Scales

The realisation that the electromotive force of a galvanic cell was illustrative of changes in the activity of the hydrogen ion (a_H) rather than its concentration (Equation 3.3) led Sørenson and Linderstrøm-Lang (1924) to suggest that

$$pa_H = -\log a_H \qquad 3.4.$$

and it was therefore necessary to develop standard solutions of known hydrogen ion activities. Values of pa_H can be *operationally* assigned to a solution by measuring cell potentials following varying additions of the chloride ion using the cell A (Covington *et al.*, 1983; Dickson, 1984)

$$Ag(s) \mid AgCl \mid Solution, m_{Cl} \mid H_2(g, 1\ atm.) \mid Pt(s) \qquad (A)$$

The potential of cell A is represented by

$$E = E^\circ - \frac{R.T}{F}.\ln a_H a_{Cl} \qquad 3.5.$$

where E° is the standard potential of the silver-silver chloride half cell. Equation 3.5. may be arranged such that

$$p(a_H\gamma_{Cl}) = \frac{F(E - E^\circ)}{R.T.\ln 10} + \log m_{Cl} \qquad 3.6.$$

where $p(a_H\gamma_{Cl})$ is the thermodynamically defined acidity function. Through the measurement of the cell potential at varying values of m_{Cl}, and extrapolation of the curve $p(a_H\gamma_{Cl})$ *versus* m_{Cl} to $m_{Cl} = 0$, a value for $p(a_H\gamma_{Cl})^\circ$ can be determined. Thus at the zero chloride level, Equation 3.6. may be written (Bates, 1973)

$$pa_H = p(a_H\gamma_{Cl})^\circ + \log\gamma_{Cl} \qquad 3.7.$$

From the Bates-Guggenheim convention, which uses an extended form of Debye-Hückel theory and is the key to assigning single ion activities, the activity coefficient of the chloride ion may be represented as a function of the ionic strength of the solution where

$$\log\gamma_{Cl} = \frac{A.I^{1/2}}{(1 + 1.5I^{1/2})} \qquad 3.8.$$

and A is the Debye-Hückel slope (Bates, 1973). Combining Equations 3.7 and 3.8, a pa_H value may be assigned to the standard buffer solution.

3.2.1.1. The National Bureau of Standards pH scale

There are many infinite dilution scales (Bates, 1973; Kristensen *et al.*, 1991). however, only the National Bureau of Standards (NBS) (now the National Institute of Standards and Technology (NIST)) scale has been comprehensively employed in seawater measurement (Zirino, 1975; Zirino *et al.*, 1983; Johnson *et al.*, 1977; Culberson, 1981). Within the NBS scale, values have been assigned to seven primary standards and these are

listed at 25°C in Table 3.1. They encompass the range pa_H(NBS) 3.7 to 10.0 and have been shown to be internally consistent to ± 0.006 units at 25°C (Bates, 1973). Preparatory methods for NBS buffers are catalogued in Whitfield (1971).

3.2.2. Constant Ionic Medium Scales

If seawater is considered to be of constant ionic strength and there is constant stoichiometry amongst the major constituents with respect to salinity, and the activity coefficients of minor reactants are regulated by the bulk electrolyte, then the concentration of a minor ion may be determined directly (Hansson, 1973c; Dickson, 1981). These conditions apply in the design of constant ionic medium pH scales which rely on the hypothesis that when the hydrogen ion concentration approaches zero in the ionic medium then the activity coefficient tends to unity. This has been suggested to apply providing the concentration of the species is less than 10% of that of the bulk electrolyte (Sillén, 1967), in this case NaCl. Whitfield (1979) states that this limit should be 1% of the total ionic strength of the medium. There are two main pH scales which follow the ionic medium convention: the total hydrogen ion scale and the free hydrogen ion scale. The derivation of each scale is discussed below.

3.2.2.1. Total Hydrogen Ion Scale

In answer to criticisms of the NBS scale mainly over problems arising from unknown liquid junction potentials (discussed in Section 3.3.) Smith and Hood (1964) proposed the use of pH scales based on seawater-amine buffers. Hansson (1973c) defined the total hydrogen ion concentration scale assigning values to standard buffers composed of equimolal (0.005 mol.kg^{-1} solution) tris(hydroxymethyl)-aminomethane, referred to as tris, and its hydrochloride, tris.HCl, in synthetic seawater without fluoride, over the salinities 10 to 40 and temperatures 5 to 30°C. Buffer pH was established using the cell

Glass electrode	Buffer solution + m_{Cl} in synthetic seawater	Synthetic seawater saturated with AgCl	Ag; AgCl	(B)

The composition of the synthetic seawater dictates that the total hydrogen ion concentration, m_H(SWS), defined by this method is the sum of free, uncomplexed hydrogen ions and those associated with sulphate

$$m_H(SWS) = m_H + m_{HSO_4} \qquad 3.9a.$$

Small errors are inherent in the use of Equation 3.9a. when measuring the pH of natural seawater due to the exclusion of fluoride on the total concentration of hydrogen ions. These errors are believed to be negligible within the applied accuracy of the scale (Dickson, 1993). Nevertheless, the total hydrogen scale has been expressed as the sum of free, uncomplexed hydrogen ions and those associated with sulphate and fluoride (Equation 3.9b) and has been termed the seawater scale (Dickson and Millero, 1987; Dickson, 1990b)

$$m_H(SWS) = m_H + m_{HSO_4} + m_{HF} \qquad 3.9b.$$

Using the total hydrogen scale (*i.e.* without fluoride) and data from Hansson (1973), Almgren *et al.* (1975) obtained the algorithm for the pH value of the standard equimolal tris buffer in relation to temperature and salinity, where

$$pm_H(SWS) = (2559.7 + 4.5S)/T - 0.01391S - 0.5523 \qquad 3.10$$

The standard deviation from the original experimental data and those from Equation 3.10. is 0.0035 pH units.

The assignment of pH values to tris buffers related to their salinity, temperature and concentration of tris was further extended and refined by Millero (1986) who defined pm_H(SWS) values for equimolal tris buffers (m_{TRIS} = 0.005 to 0.06) to encompass salinities found both in oceanic and estuarine environments. The relationship (Ramette *et al.*, 1977; Millero, 1986)

$$pH = pK^* + am_{TRIS} \qquad 3.11.$$

Table 3.1. Composition and assigned pH value of NBS primary standard buffers at 5, 15, and 25°C (adapted from Bates ,1973).

Buffer solution	temperature 5°C	15°C	25°C
Saturated (at 25°C) potassium hydrogen tartrate	-	-	3.557
0.05*m* potassium dihydrogen citrate	3.840	3.802	3.776
0.05*m* potassium hydrogen phthalate	3.999	3.999	4.002
0.025 *m* potassium dihydrogen phosphate + 0.025*m* disodium hydrogen phosphate	6.951	6.900	6.865
0.008695*m* potassium dihydrogen phosphate + 0.3043*m* + 0.025*m* disodium hydrogen phosphate	7.500	7.448	7.413
0.01*m* borax	9.395	9.276	9.180
0.025*m* sodium bicarbonate + 0.025*m* disodium carbonate	10.245	10.118	10.012

holds for both the total and free hydrogen scale where a varies with salinity such that

$$a = -9.73 \times 10^{-2}S + 6.988 \times 10^{-5}S^2 \qquad 3.12.$$

The stoichiometric dissociation constant pK^* was evaluated at m_{TRIS} extrapolated to zero and fitted to the equation

$$pK^* = pK + A + B/T \qquad 3.13.$$

Using data from Bates and Hetzer (1961) on the dissociation constant of Tris, Millero (1986) fitted the temperature dependence of pK as shown in Equation 3.14.

$$pK = -22.5575 + 3477.5496/T + 3.32867\ \ln T \qquad 3.14.$$

Further, the variables A and B were determined with respect to salinity (S) for the total hydrogen ion scale to be

$$A = -2.3755 \times 10^{-2}S + 6.165 \times 10^{-5}S^2 \qquad 3.15a.$$

$$B = 6.313S \qquad 3.15b.$$

Values of pm_H(SWS), at $m_{TRIS} = 0$, can be calculated by substituting Equations 3.14 and

3.15 into 3.13. Small corrections have to be applied to these values to account for the concentration of tris used as shown in Equation 3.11.

Dickson (1993) has proposed the temperature - pH relationship for equimolal 0.04*m* tris buffer to be

$$\text{pH(SWS)} = 11997/T + 3.7669S/T + 0.00178S^2/T - 381.3088 - 0.011634S + 67.63163\ \ln T - 0.121538T \qquad 3.16$$

3.2.2.2. Free Hydrogen Ion Scale

Several authors (Hansson *et al.*, 1975; Bates and Macaskill, 1975; Ramette *et al.*, 1977; Dickson, 1990a) determined the electromotive force of tris buffers in fluoride and sulphate free synthetic seawater using the cell (C)

Pt; H_2(g, 1 atm.)	Equimolal buffer solution in artificial seawater	Ag; AgCl (C)

This scale is conceptually the clearer of the three (Dickson, 1984; 1990a). However, there are uncertainties in using the scale due to the unknown errors in the extent of dissociation of hydrogen sulphate. Values for $\beta_{HSO_4^-}$ depend on the form of activity coefficient model used (Millero, 1986; Dickson, 1990; 1993).

pH values on the free hydrogen scale can be calculated from the concentration of tris buffer and buffer temperature using Equations 3.11. to 3.14. inclusive and then calculating the constants A and B from Millero (1986)

$$A = 2.065 \times 10^{-3}S - 1.770 \times 10^{-4}S^2 \qquad 3.17a.$$

$$B = 0.64S \qquad 3.17b.$$

The constants include implicitly the difference in concentration scale between the total hydrogen scale, moles per kilogram seawater (Hansson, 1973c), and the free hydrogen scale, moles per kilogram water (Bates and Macaskill, 1975).

3.2.3. Conversion between different pH scales

There is disagreement as to which pH scale is the most suitable for pH measurements in seawater and, therefore, no common scale has been accorded. It is necessary to understand the relationships between scales if pH measurements on different scales are to be compared. The total hydrogen ion scale has recently been suggested to be the most suitable for seawater pH measurements (Dickson, 1993). Therefore the other scales will be compared to this scale.

pH on the total hydrogen ion scale may be converted from pH on the free hydrogen ion scale through the relationship (Dickson, 1993)

$$\mathrm{pH(SWS)} = \mathrm{p}m_{\mathrm{H}} - \log(1 - 0.00106S) - \log(1 + m_{\mathrm{SO_4}}\beta_{\mathrm{HSO_4}}) \qquad 3.18.$$

The difference in the concentration scales between the two pH scales is compensated by the second term on the right in Equation 3.18., where S is the salinity of the seawater sample.

The NBS scale is related to the total hydrogen ion scale such that

$$\mathrm{pH(SWS)} = \frac{\mathrm{p}a'_{\mathrm{H}}}{f_{\mathrm{H}}} \qquad 3.19.$$

where a'_{H} is the apparent activity of the hydrogen ion and f_{H} is the apparent activity coefficient of total hydrogen ions (Culberson and Pytkowicz, 1973, Perez and Fraga, 1987; Covington and Whitfield, 1988). Values of f_{H} are specific to an individual pH system and depend on the type of electrodes and the type of liquid junction used (Hansson, 1973c; Johnson *et al.*, 1977; Covington *et al.*, 1988). Therefore conversion to pH values on the total hydrogen scale requires f_{H} values to be determined for each pH system. This is achieved in two ways: firstly, by comparing the $\mathrm{p}a'_{\mathrm{H}}$ change compared to the theoretical change due to the amount of acid added during an alkalinity titration (Culberson *et al.*, 1970; Culberson and Pytkowicz, 1973; Johnson *et al.*, 1977) and secondly by measuring the pH of ionic medium buffers using glass electrodes calibrated with NBS buffers (Hansson, 1973c; Butler *et al*, 1985).

3.3. Potentiometry

The now standardised buffer solution on any scale can now be used to measure the pH of an unknown test solution using a cell of the type (Dickson, 1984)

reference electrode	concentrated KCl solution	Standard or Test solution	Electrode reversible to the hydrogen ion	(D)

The potential across the cell in both the standard and test solutions is measured and from Nernstian theory, the operationally defined pH of the unknown solution pH(X) may be determined using Equation 3.20.

$$pH(X) = pH(S) + \frac{(E_S - E_X)}{(RT\ln 10/F)} - \frac{(E_{jB} - E_{jX})}{(RT\ln 10/F)} \qquad 3.20.$$

where pH(S) is the assigned pH value of the standard buffer. The residual liquid junction potential ($\Delta E_j = E_{jB} - E_{jX}$) depends on the mobilities of the ionic species on the two sides of the boundaries (Bates, 1973) and an estimation of ΔE_j is possible in simple solutions where the composition of the solutions forming the bridge are known. Problems with accurate determinations of pa_H arise due to large liquid junction potentials when solutions of low ionic strength, *i.e.* rainwaters (Jones *et al.*, 1987), and high ionic strength, *i.e.* seawater (Culberson, 1981) and brines (Ben-Yaakov and Lorch, 1983), are investigated. The use of the extended Debye-Hückel theory (Equation 3.7) in the assignment of pa_H values to standard buffer solutions only stands for test solutions with $0.01 < I < 0.1$ mol.kg^{-1}. Therefore, when using NBS buffers in solutions of considerably higher ionic strength, *i.e.* seawater $I \approx 0.7$ mol.kg^{-1}, inaccuracies are incurred during pH measurements due to non-thermodynamic assumptions in the calculation of the chloride ion activity coefficient and the unknown size of the residual liquid junction potential. The measured parameter is therefore the apparent hydrogen ion activity

$$pa'_H = pa_H \times \text{constant} \qquad 3.21.$$

The constant is representative of the size of the residual liquid junction potential (Johnson *et*

al., 1977). This does not mean that acid-base systems cannot be studied using infinite dilution scales. Proton transfer reactions can be measured within the reproducibility of $p\alpha'_H$ measurements (Johnson *et al.*, 1977) if the apparent constants and solution pH are determined using the same electrode combination (Mehrbach, 1973; Johnson *et al.*, 1977; Perez and Fraga, 1987). Similarly, thermodynamic continuity is maintained if the same stoichiometric pH scale is used to calculate the pH and dissociation constant for a reaction (Hansson, 1973c; Dickson, 1984).

Historically, the reporting of seawater pH has generally been avoided due to an appreciation of the apparent difficulties involved, which are discussed above. Measurement had been reserved for accomplished operators. Recent developments in the methodology have led to an increase in the documentation of seawater pH measurements. Selected investigations are discussed in the following two sections for both discrete and continuous seawater pH determinations.

3.3.1. Discrete Potentiometric Analysis

Commonly, seawater pH measurements are made on discrete samples which have been collected aboard ship and stored in bottles prior to analysis. Park (1966) inserted glass and reference electrodes directly into a bottle full with seawater, the rubber support to the electrodes and thermometer displacing seawater thus preventing seawater equilibrium with the air. Measurements were made on the NBS scale. A reproducibility of ± 0.02 pH unit was reported from replicate measurements on single samples (Park, 1966).

Micro-electrodes have shown a precision on replicate pairs of ± 0.0026 pH unit during routine use at sea (Zirino, 1975). He added that 87% of the pairs were within 0.004 units of the individual mean. pH was measured on the NBS scale on stirred samples. Stirring increased the pH by 0.010 pH unit. However, a steady potential was attained more quickly with stirring. Charging times for the electrode to equilibrate with the new environment was initially 15 minutes after calibration. Response times for the ensuing seawater samples was then about 6 minutes (Zirino, 1975).

Comparison of the performance of different glass electrode - reference electrode

pairings, when measuring seawater on the NBS scale, was reported by Johnson *et al.* (1977). Electrodes were supported in the media in a rubber bung as in Park (1966). The cell was, however, constructed to allow filling and emptying with seawater or buffer to be performed without moving the electrodes. Precision relative to the pH 7.413 NBS buffer was ± 0.01 pH unit. Johnson *et al.* (1977) asserted, from a comparison of reference electrodes having different liquid junction types, that a change to a pH scale aiming to reduce ΔE_j (*i.e.* ionic medium scales) would result only in a partial improvement in precision. The total difference in ΔE_j of 0.006 pH unit reported by Johnson *et al.* (1977) was later described as considerable by Millero (1986).

Shipboard measurements of seawater pH on the total hydrogen scale were first reported by Almgren *et al.* (1975). Measurements were made using tris buffer according to Hansson (1973c). Water samples were brought to room temperature by immersing 1 litre bottles in a water bath. For potential measurements temperature was controlled by placing beakers of buffer and seawater in a thermo-equilibrating block. No precision or sampling times were given for the technique. However, an inter-calibration exercise on the ship with a method using an infinite dilution scale highlighted a large difference between results on the different scales (Almgren *et al.*1975).

Culberson (1981) designed a cell into which seawater or buffer was injected from a plastic syringe. A sharp junction was formed between the KCl and sample or buffer on the initial injection. The junction did not have to be renewed between successive seawater injections. A series of twenty seawater injections did not vary in potential by more than 0.1mV. This is equivalent to better than 0.002 pH unit, although the precision is later reported to be 0.002-0.005 pH unit (Culberson, 1981). Potentials were steady about 30 seconds after the injection and pH was noted about 3 minutes later. However, the frequency of measurements is limited by the time taken for the syringes plus solution to equilibrate in a water bath prior to injection and the delivery of the sample (Culberson, 1981). The extensive utility of this cell has been illustrated by its successful application to estuarine waters (Butler *et al.*, 1985) and fresh waters (Covington *et al.*, 1983).

A recent inter-laboratory comparison of discrete seawater pH measurements revealed large discrepancies between different operators (Unesco, 1990). Measurements were made on the NBS scale, on the total proton scale (from alkalinity titrations) and others

on the total hydrogen ion scale. The titration and total hydrogen scale agreed to within 0.02-0.03 pH unit. Results using the NBS scale exhibited a scatter of 0.3 pH unit, however, the reproducibility of individual methods was better than the discrepancies exposed between operators (Unesco, 1990). It should be noted that measurements of samples with time and between bottles used in the study showed no significant changes (Poisson *et al.*, 1990).

3.3.2. Continuous Potentiometric Analysis

Whilst studying the speciation of copper in the surface waters of the Eastern Tropical Eastern Ocean, Zirino *et al.* (1983) used a flow pH system consisting of a combination microelectrode, with AgCl reference, mounted in a teflon manifold. The electrodes were calibrated on the NBS scale every two days. This method was run together with the discrete method developed by Zirino (1975) and pH measurements using both methods agreed to ± 0.04 pH unit. The same system was later used by Zirino *et al.* (1986) although the system was calibrated only once during a two week cruise - the second calibration was ignored as it produced 'an erroneous discontinuity in the pH' (Zirino *et al.*, 1986).

Fuhrmann and Zirino (1988) calibrated their glass electrodes in tris secondary buffers as assigned by Smith and Hood (1964) every 2-3 days. A glass electrode was supported in a plexiglas holder with the tip immersed in a flowing stream of either buffer for calibration or seawater pumped from a hull penetration. The flow system was shown to have a operating precision of ± 0.003 pH unit within a limited calibration period (in this case equivalent to a 5km transect). Comparison of flow pH values and the discrete values obtained by the method of Zirino (1975) illustrate an agreement of better than ± 0.02 pH units for samples for CTD (conductivity, temperature, depth) casts to 100m (Fuhrmann and Zirino, 1988). The maximum disagreement at any one depth is about 0.04 pH unit.

Two types of continuous pH methods were employed by Mackey *et al.* (1989). A double junction electrode calibrated at the surface, sealed and lowered on a CTD frame, and a system similar to the one described in Zirino *et al.*(1983) and Fuhrmann and Zirino (1988). The former double junction method was not calibrated for pressure and data is only reported as being consistent, detailing fine structure, over the top 500m on nine replicate

casts to 5000m. The short term reproducibility of the second, surface, pH system was better than ± 0.0003 pH unit. Electrode potential variation during calibration of the system over a 2 week period was equivalent to about ± 0.002 pH unit. Taking into account errors associated with the assignment of pH to the standard buffers and limitations in temperature control Mackey *et al.* (1989) claimed an accuracy of ± 0.008 pH unit.

3.4. Spectrophotometric pH measurement

3.4.1. Theory

The spectrophotometric determination of seawater pH utilises the acid-base properties of selected sulfonephthalein indicators through the measurement of their absorption characteristics under differing states of protonation (*e.g.* Robert-Baldo *et al.*, 1985; Byrne, 1987; Byrne and Breland, 1989; Clayton and Byrne, 1993). All sulfonephthalein indicators are weak diprotic acids (King and Kester, 1989) and have two protonation steps which exhibit associated colour changes (Breland and Byrne, 1993; Clayton and Byrne, 1993). Mass balance equations for an indicator (ligand, L) going from a fully protonated to an unprotonated state are shown in Equations 3.22. and 3.23. with their respective equilibria represented by Equations 3.24. and 3.25.

$$H_2L \leftrightarrow H^+ + HL^- \qquad 3.22.$$

$$HL^- \leftrightarrow H^+ + L^{2-} \qquad 3.23.$$

$$K_1 = \frac{h.[HL^-]}{[H_2L]} \qquad 3.24.$$

$$K_2 = \frac{h.[L^{2-}]}{[HL^-]} \qquad 3.25.$$

As in Chapter 2, all bracketed species refer to their stoichiometric concentrations, and $h = 10^{-pH} \approx [H^+]$. K_1 and K_2 are the first and second dissociation constants of the indicator. The total concentration of the indicator is then

$$[L] = [L^{2-}] + [HL^{-}] + [H_2L] \qquad 3.26.$$

Under normal oceanic conditions $[H_2L]$ is very small and thus can be ignored (Byrne, 1987; Clayton and Byrne, 1993). Equation 3.28. may then be written

$$[L] = [HL](1 + K_2.h^{-1}) \qquad 3.29.$$

The absorbance of a chemical species at a given wavelength is a function of the molar absorptivity (absorbance per centimetre per mole) of the species, assuming Beer's law, and the distance over which the attenuation occurs. This may be represented as (Byrne and Kester, 1978; Byrne *et al.*, 1981)

$$_{\lambda}A_i = \ell \,.\, _{\lambda}\varepsilon_i.[i] \qquad 3.30.$$

where λ is the wavelength, i is the indicator species in question, ε is the molar absorptivity of the species and ℓ is the optical pathlength. Therefore, the total absorbance of the indicator, $_{\lambda}A$, is a summation of the absorbances attributed to the individual indicator species

$$_{\lambda}A = (_{\lambda}\varepsilon_{HL}.[HL^{-}] + _{\lambda}\varepsilon_{L}.[L^{2-}]).\ \ell\ . \qquad 3.31.$$

The absorbance may then be written as

$$_{\lambda}A = [HL^{-}](_{\lambda}\varepsilon_{HL}. + _{\lambda}\varepsilon_{L}.K_2.h^{-1}).\ \ell\ . \qquad 3.32.$$

Dividing Equation 3.32. by the total indicator concentration [L] from Equation 3.29. gives

$$_{\lambda}a = \frac{_{\lambda}A}{\ell\ .\ [L]} = \frac{_{\lambda}\varepsilon_{HL} + _{\lambda}\varepsilon_{L}.K_2.h^{-1}}{1 + K_2.h^{-1}} \qquad 3.33.$$

Rearranging Equation 3.33.

$$_{\lambda}a + _{\lambda}aK_2.h^{-1} = _{\lambda}\varepsilon_{HL} + _{\lambda}\varepsilon_{L}.K_2.h^{-1} \qquad 3.34.$$

$$ {}_{\lambda}a - {}_{\lambda}\varepsilon_{HL} = K_2.h^{-1}({}_{\lambda}\varepsilon_{L^-} - {}_{\lambda}a) \qquad 3.35 $$

provides the pH of the solution according to the dissociation constant and absorption properties at a single wavelength

$$ pH = pK_2 + \log_{10}\left[\frac{{}_{\lambda}a - {}_{\lambda}\varepsilon_{HL}}{{}_{\lambda}\varepsilon_{L^-} - {}_{\lambda}a}\right] \qquad 3.36. $$

where $pH = -\log h$, $pK_2 = -\log K_2$.

If absorption measurements are made at two wavelengths, then the ratio of two absorptions (R) may be represented by

$$ R = \frac{{}_2A}{{}_1A} = \frac{{}_2\varepsilon_{HL} + {}_2\varepsilon_L K_2.h^{-1}}{{}_1\varepsilon_{HL} + {}_1\varepsilon_L K_2.h^{-1}} \qquad 3.37. $$

assuming ℓ, [L] and $(1 + K_2.h^{-1})$ are constant. Equation 3.37. may be re-written

$$ R.{}_1\varepsilon_{HL} + R.{}_1\varepsilon_L.K_2.h^{-1} = {}_2\varepsilon_{HL} + {}_2\varepsilon_L K_2.h^{-1} \qquad 3.38. $$

$$ R.{}_1\varepsilon_{HL} - {}_2\varepsilon_{HL} = K_2.h^{-1}({}_2\varepsilon_L - R.{}_1\varepsilon_L) \qquad 3.39. $$

Dividing by ${}_1\varepsilon_{HL}$ gives,

$$ R - {}_2\varepsilon_{HL}/{}_1\varepsilon_{HL} = K_2.h^{-1}({}_2\varepsilon_L/{}_1\varepsilon_{HL} - R.{}_1\varepsilon_L/{}_1\varepsilon_{HL}) \qquad 3.40. $$

$$ \frac{R - {}_2\varepsilon_{HL}/{}_1\varepsilon_{HL}}{({}_2\varepsilon_L/{}_1\varepsilon_{HL} - R.{}_1\varepsilon_L/{}_1\varepsilon_{HL})} = K_2.h^{-1} \qquad 3.41. $$

Rearranging to make pH the conditional variable as a function of the dissociation constant, the absorption and molar absorptivity ratios at the chosen wavelengths of measurement

$$ pH = pK_2 + \log_{10}\left[\frac{R - {}_2\varepsilon_{HL}/{}_1\varepsilon_{HL}}{({}_2\varepsilon_L/{}_1\varepsilon_{HL} - R.{}_1\varepsilon_L/{}_1\varepsilon_{HL})}\right] \qquad 3.42. $$

By measuring the absorbance of a colorometric indicator, at either one or two (or

more) wavelengths, it is possible to determine the pH of a translucent solution knowing the dissociation constants and the molar absorptivities, and with regard to single wavelength determinations the concentration, of the indicator in question. The pH scale of measurement is dependent on the scale used to determine the pK. Due to changes with respect to temperature and ionic composition of the pK value it is necessary both to characterise these dependences and also have good control of solution temperature during pH analysis. These characteristics have been determined for selected sulfonephthaleins and spectrophotometric pH measurements have been obtained successfully in seawater. The following section chronicles recent methodologies used for these measurements.

3.4.2. Discrete Spectrophotometric Analysis

Robert-Baldo *et al.* (1985) were the first to reintroduce the spectrophotometric technique for measurement of seawater pH. They developed a single wavelength method using phenol red to aid the determination of marine aragonite dissolution kinetics (Acker *et al.*, 1987). Robert-Baldo *et al.* (1985) used potentiometric pm_H values of seawater solutions to characterise the temperature and salinity dependence of the dissociation constant (pK_2) for $33 \leq S \leq 37$ and $273\ K \leq T \leq 303\ K$ with an average residual of pK ± 0.004. They found that the molar absorptivites of phenol red displayed very little dependency on medium composition.

Although well defined, the composition of a standard buffer for potentiometric pH determinations is open to operator error, contamination from CO_2 exchange and biological activity (Bates, 1973). Byrne (1987) used the indicators thymol blue, bromothymol blue and phenol red to measure the pH of 0.04*m* equimolal tris, 0.025*m* equimolal phosphate and 1:3:5 phosphate buffers respectively. The multiwavelength method employed was able to determine changes in buffer pH of 0.001 unit (Byrne, 1987).

The first at-sea comparison of spectrophotometric and potentiometric methods was performed by Byrne *et al.* (1988). On samples from the Indian Ocean, using phenol red and a single wavelength technique (free hydrogen ion scale, 20°C), pH determinations differed from potentiometric values (NBS scale, 25°C) by 0.012 ± 0.010 pH unit. The imprecisions in both methods were thus less than 0.01 pH unit.

A multiwavelength technique used by Byrne and Breland (1989) showed that measurements on replicate samples agreed to 0.001 pH unit or better. Their highly precise determinations were conducted using cresol red indicator. They proposed that with improvements in salinity measurements and a spectrophotometer with absorption resolution to 0.0001A, pH could be measured with a precision near to 0.0001 pH unit.

King and Kester (1989) have determined the dissociation constants of thymol blue, bromophenol blue, bromocresol green, bromocresol purple and phenol red in seawater. They advocate the use of a multi-indicator method to measure the pH of a seawater solution over the pH range 1.5-8.5. Simultaneous potentiometric and spectrophotometric measurements agreed over this range to ± 0.005 pH units.

More recently, Clayton and Byrne (1993) have reported at-sea pH measurements with a precision of 0.0004 pH unit. They used a multiwavelength technique employing *m*-cresol purple as the indicator. Following from the suggestion that the total hydrogen ion scale was the most suitable for seawater analysis (Dickson, 1993), pH was measured on this scale as opposed to the free hydrogen scale adopted by previous investigators.

The utility of spectrophotometry has been extended to solutions other than seawater. Yamazaki *et al.* (1992), using standards of acetic acid and aqueous ammonia, have characterised the pK of bromocresol green over the range I = 0-1 at 25°C, and thymol blue over the range I = 0.02-3 and t = 25-65°C. They claim an overall error of ± 0.008 and 0.002 pH unit respectively for each indicator.

3.4.3. Continuous Spectrophotometric Analysis

Discrete spectrophotometric analyses are slow and labour intensive and thus the methods outlined in Section 3.4.2. are impractical for the evaluation of kinetic or other dynamic studies. The advancement of flow analysis techniques in recent years has allowed for the introduction of automated methods for the continual spectrophotometric analysis of solution pH within the field of analytical chemistry. Rapid analysis is now available although errors associated with refraction in low ionic strength solutions is a problem for accurate determinations. This section aims to document the methods presently used.

Single wavelength flow injection analysis of solution pH was performed by Pia *et al.*

(1990). This was a multi-indicator method relying on the linearity of absorbance with pH over the pH range 1 to 8. A frequency of 100 samples per hour was attained with a precision and accuracy of ± 0.2 pH unit. Serra *et al.* (1990) used phenol red indicator isolated in resin as a base for fibre-optic pH measurements on seawater samples but did not determine the precision of the method.

Spectrophotometric measurements are widely used in analytical chemistry for measuring pH gradients during continual, pH-sensitive determinations (Nørgaard, 1991; Vives *et al.*, 1992). These measurements are thus limited to species which do not react with the indicator (Vives *et al.*, 1992). A multi-indicator stock solution is usually added to the sample or carrier solution. pH is determined simultaneously with the analyte using diode array spectrophotometry (Nørgaard, 1991; Vives *et al.*, 1992). Levels of precision and accuracy are not well documented. It appears that the limit of precision of pH measurements is less than ± 0.01 pH unit. Accuracies in pH are limited to the accuracy of pK determinations. Vithanage and Dasgupta (1986) obtained the pK values of bromocresol green and non-sulfonephthalein indicators (quinaldine red, methyl red and (thiazolyl) azoresorcinol) to better than ± 0.1 unit and methyl orange to ± 0.03 unit. Vives *et al.* (1992) measured pK of bromothymol blue, phenol red and neutral red with precisions of ± 0.01, 0.04 and 0.04 units respectively. This variability was attributed mainly to problems in correcting for refractive index changes.

3.4. Conclusions

There is no general agreement between operators on the correct pH scale to use when measuring seawater pH, although there has been a recent promotion of the total hydrogen ion scale. During potentiometric analyses there are uncertainties associated with the unknown extent of the residual liquid junction potential when using the infinite dilution scales, and for highly accurate thermodynamic studies equilibrium constants should be calculated for each instrument system used. Implementing the ionic medium scales reduces the uncertainty in the residual liquid junction potential but there are still problems associated with electrode drift, electrical interference and stirring potentials.

Potentiometric pH measurements have been shown to be highly precise if careful operational procedures are followed, and are certainly suitable for daily water quality testing, however, their use for accurate pH work is suspect due to problems including electrode drift, electrical interference and unknown residual liquid junction potentials.

Measuring the acid-base characteristics of selected colorometric indicators for the determination of solution pH is readily becoming accepted as a alternative to potentiometry; details of the performances of both potentiometric and spectrophotometric techniques are summarised in Table 3.2. Spectrophotometric pH determinations do not require calibration, which is inherent in the characterisation of the absorbance properties of the indicator used, and in discrete mode simple absorbance ratios can be used to furnish very precise measurements. However, to date no spectrophotometric flow system has been developed with a precision suitable to aid characterisation of the marine carbonate system.

Table 3.2. Performance and methodologies of selected investigations in the measurement of seawater pH.

Method	Scale	Precision	Reference
Discrete Potentiometric Analysis			
Micro-electrode insertion	NBS	0.02	Park (1966)
Micro-combined-electrode, sample injection	NBS	0.0026	Zirino (1975)
Various electrode pairings, sample injection	NBS	0.01	Johnson *et al.* (1977)
Electrode insertion	pH(SWS)	not given	Almgren *et al.* (1975)
Sample insertion, micro-assembly	NBS	0.002-0.005	Culberson (1981)
Continuous Potentiometric Analysis			
Combination electrode	NBS	not given	Zirino *et al.* (1983)
Combination electrode	NBS*	0.003	Fuhrmann and Zirino (1988)
Combination electrode	NBS*	0.0003	Mackey *et al.* (1989)
Discrete Spectrophotometric Analysis			
Single wavelength, phenol red	pm_H	< 0.01	Byrne *et al.* (1988)
Multi-wavelength, cresol red	pm_H	0.001	Byrne and Breland (1989)
Multi-wavelength, multi-indicator	pm_H	0.005	King and Kester (1989)
Multiwavelength, *m*-cresol purple	pH(SWS)	0.0004	Clayton and Byrne (1993)
Continuous Spectrophotometric Analysis			
Single wavelength, multi-indicator	NBS	0.2	Pia *et al.* (1990)
Fibre-optic	pm_H	not given	Serra *et al.* (1990)

* - tris buffers calibrated against NBS standard buffers.

CHAPTER 4.

ANALYTICAL DEVELOPMENT

4.1. Introduction

An improvement in the accuracy of global carbon budget models will be facilitated through more rigorous empirical constraints implied from greater global mapping of the CO_2 system in seawater. This will require the introduction of rapid, real-time, highly precise, automated instrumentation for measuring the CO_2 parameters concurrently, thus making the most efficient use of the available shiptime.

The recent interest in the applicability of spectrophotometry to the measurement of seawater pH has illustrated the highly precise nature of discrete analysis. High density measurements of seawater pH cannot be obtained by discrete measurements and although there is no doubt that continuous potentiometric methods can provide highly precise results, the accuracy of such methods has not been fully tested. There is a great need for a highly precise continuous method for seawater pH measurement. This chapter reports on the development and automation of potentiometric and spectrophotometric techniques for continuous seawater pH measurement.

The instruments for pH measurement were subsequently used in the Southern Ocean aboard R.R.S. *Discovery* as part of the Biogeochemical Ocean Flux Study (BOFS), the UK contribution to the Joint Geochemical Ocean Flux Study (JGOFS). The characteristics of surface seawater pH and an appraisal of the controls of the carbon dioxide system is given in Chapter 5. To characterise the surface water carbon dioxide system, all four system parameters (pH, pCO_2, TCO_2 and alkalinity) were to be measured concurrently. The methodologies for both the spectrophotometric and potentiometric determination of seawater pH are re-defined, instigated both by their integration and additionally to conform to a shipboard environment. The operation of both pH techniques is assessed. An evaluation of the performance of the pH, pCO_2 and TCO_2 methods is enabled through the determination of their internal consistency during the cruise.

4.2. Potentiometry

4.2.1. Buffer solutions

(a) NBS buffer solutions

NBS buffer solutions were prepared according to Whitfield (1971). Solutions were stored in a refrigerator (4°C) when not in use and replaced every 2-3 weeks to avoid biological degradation.

Equimolar phosphate buffer

The salts di-sodium hydrogen phosphate and potassium di-hydrogen phosphate were oven-dried for 2h at 120°C and then cooled in a dessicator. Weighed amounts, 3.388g potassium di-hydrogen phosphate and 3.533g sodium di-hydrogen phosphate, were dissolved in water to 1 litre at 25°C. The resultant solution had a nominal pH of 6.865 at 25°C (Whitfield, 1971; Bates, 1973).

Phthalate buffer

Although implied as an unnecessary step (Whitfield, 1971) potassium hydrogen phthalate salt was dried at 120°C for 2h and cooled in a dessicator. This salt can be dried safely at temperatures less than 135°C (Bates, 1973). To make up pH 4.008 buffer, at 25°C, 10.12g of the salt was dissolved in water to 1 litre at 25°C.

(b) Tris buffer solution

Tris buffer solutions, based on an original artificial seawater recipe of Khoo *et al.* (1977) with appropriate concentration changes in NaCl accounting for additions of equimolal tris and tris.HCl salts (Millero, 1986), were made up according to Millero, (1986). The salts in Table 4.1. were oven dried at 120°C for 2h, except for tris and tris.HCl which were dried for 1h at 100°C (Hansson, 1973c), and then cooled in a desiccator. Stock solutions of $MgCl_2$ and $CaCl_2$ were made up and their exact concentrations determined by silver nitrate titration (Millero, 1986) although Almgren *et al.* (1975) stated that direct addition of hydrated forms was acceptable. To remove dissolved carbon dioxide, oxygen-

free nitrogen (BOC) was bubbled for 24 hours through water which had previously been boiled for 2 hours in a beaker covered with a watch glass. Appropriate weights of stock solution and salts, from Table 4.1., were added to the degassed water to 1kg.

Table 4.1. Composition of 0.06m tris buffer for S = 35 seawater (from Millero, 1986)

Solute	molinity	$g.kg^{-1}$
NaCl	0.34933	20.416
Na_2SO_4	0.02788	3.960
KCl	0.01008	0.752
$CaCl_2$	0.01026	1.139
$MgCl_2$	0.05258	5.006
Tris	0.05717	6.926
Tris.HCl	0.05717	9.010

4.2.2. Instrumentation and procedures

4.2.2.1. Electrode care and testing

Glass electrodes are inherently temperamental and their behaviour depends on electrode age, history of use and conditions of storage. In order to attain optimum performance glass electrodes must be conditioned prior to use as failure to do so may result in excessive and irreproducible electrode potential drift (Bates, 1973). Conditioning is normally achieved by soaking the electrodes in a solution of ionic strength approximating that of the test solution. Bates (1973) stated that for test solutions below pH 9 electrodes may be soaked in water or phosphate buffer. When testing the reproducibility of the flow system NBS buffer was used and thus the glass and reference electrodes were conditioned in solutions of either phosphate buffer or 0.1M HCl. Analyses of seawater samples necessitated the use of high ionic strength buffers and as such the electrodes were soaked in tris buffer acidified to approximately pH 3 with 1M HCl. Hansson (1973c) stored his electrodes in synthetic seawater at pH 3. Reference electrodes for discrete measurements

were regular refilled with saturated KCl filling solution (Ciba-Corning Cat. 001 56 001M). The reference electrode used for flow analysis is shown in Figure 4.1. The outer skin was wrapped in black tape to prevent light penetrating to the electrode as the Ag; AgCl internal reference is light sensitive under high KCl concentrations (Bates, 1973). When not in use, the electrode was filled with 3.5M KCl and the system closed by attaching the input to the output with 0.8mm diameter PTFE tubing (Anachem).

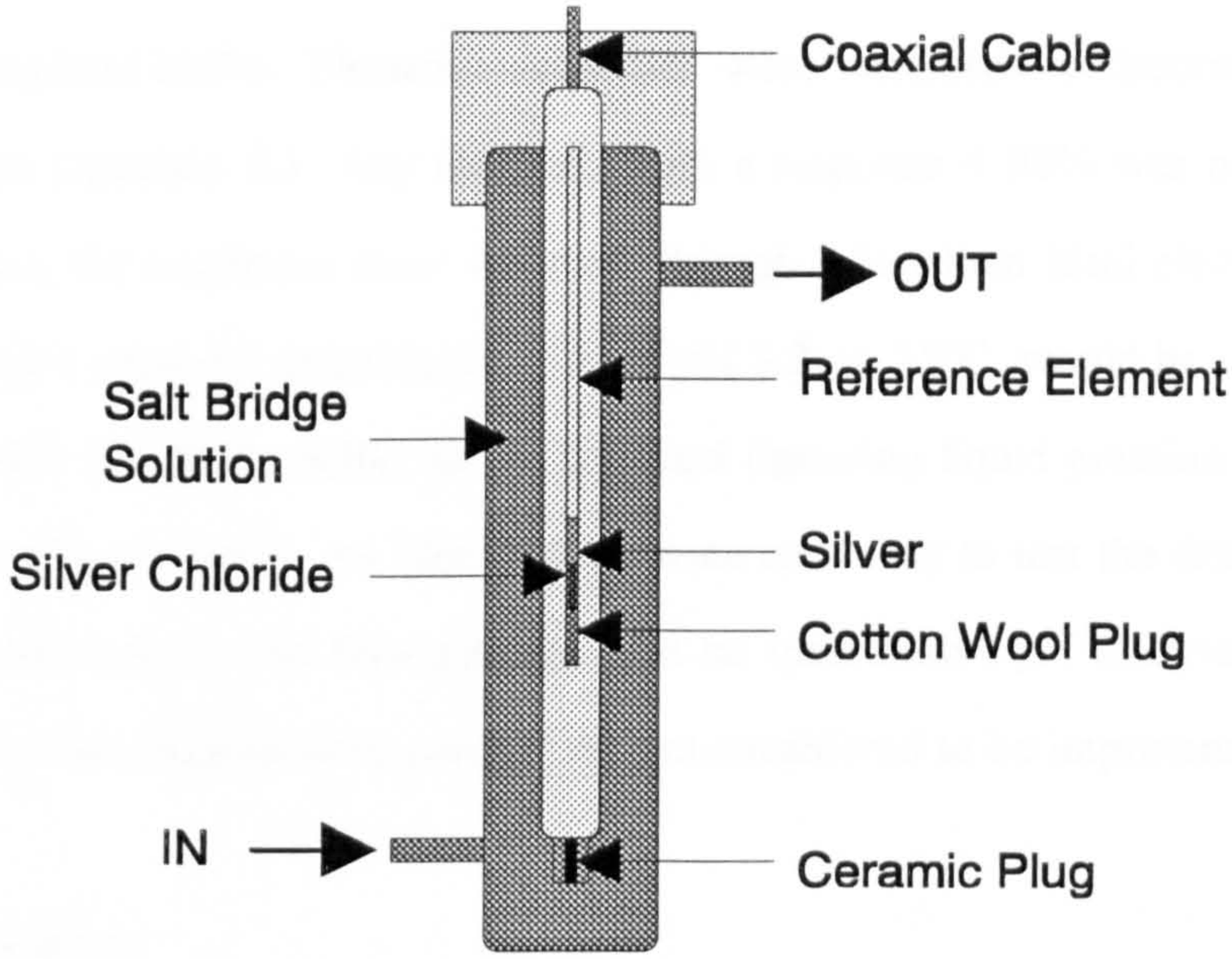

Figure 4.1. Reference electrode used for potentiometric flow measurements.

4.2.2.2. Electrode responses

Glass electrodes respond to changes in the hydrogen ion activity (Bates, 1973). This response can be represented by Equation 4.1.

$$E_2 - E_1 = \frac{RT\ln 10}{F} .(pH_1 - pH_2) \qquad 4.1.$$

The potential difference ($E_2 - E_1$), assuming constant liquid junction potential, for an ideal response will equal RTln10/F for each pH unit difference between $pH_1 - pH_2$. Values of RTln10/F are tabulated in Bates (1973). This ideal or Nernstian response is used as a

reference to compare the actual response of the glass electrodes.

Glass and reference electrodes, once correctly conditioned, were twice rinsed with water and padded dry with acid-free tissue. In pairs, the glass and reference electrodes were supported in an electrode clamp and lowered into a beaker containing NBS phthalate buffer being constantly mixed with a magnetic stirrer. The absolute potential was monitored using a digital pH meter (Beckman Model 4500) and when stable was noted along with the solution temperature measured with a thermometer. This procedure was repeated for the equimolar phosphate buffer. Electrode responses were compared to theoretical responses calculated from Equation 4.1. Any electrode with a response < 98% was not used (Table 4.2.). Therefore, the maximum error incurred through a less than ideal electrode response when measuring a seawater solution ($S = 35$) of pH 8.2, at 25°C, would be - 0.027 pH unit when using NBS phosphate buffer as the standard (ignoring liquid junction effects), and - 0.003 pH unit with tris buffer. As NBS buffers were used only to test the drift and response times of the electrodes in the flow system, with no quantitative pH analyses, the possible offset caused by less than ideal responses was not considered to be important.

4.2.2.3. Automation

Computer programs in the FORTRAN language were written for system control and data acquisition and analysis. A schematic diagram of the system is illustrated in Figure 4.2. All programs were run on an IBM PS/2 Model 55 SX. System control and data acquisition were through a microlink (BIODATA 2). Modules used were PH4 for reading electrode potentials, RTDH for thermistor data, Q12DA for pump speed control, BCD8 and 08 8DC modules controlled the power supply to pumps (Gilson Minipuls 2) and Altex valve through MBA317 and MBA375 units. Both MBA units were designed and built at the Plymouth Marine Laboratory.

Table 4.2. Responses of glass electrodes tested in this study.

Electrode code	E (mV) pH7(a)	E (mV) pH4(b)	T (°C)	Response (%)
S(c,j)	-32.3	132.3	20.5	98.0
T(c,j)	1.2	159.8	22.5	93.9
R(c,j)	-30.6	134.2	22.1	97.7
Q(c,j)	-28.5	131.4	22.0	94.9
31(d,k)	2.3	165.9	21.7	97.0
16(d,k)	-6.0	155.8	21.7	96.8
17(e,k)	-4.9	157.3	14.5	99.0
14(f,k)	17.6	182.4	21.0	98.1
16(f,k)	unstable			
19(f,k)	16.0	179.1	21.0	97.1
31(f,k)	21.2	181.7	21.0	95.6
54(g,k)	-0.1	167.1	21.0	100.3
53(g,k)	1.1	168.3	21.0	100.3
55(g,k)	1.7	168.7	21.5	99.9
53(h,k)	-69.3	101.9	31.0	100.1
50(h,k)	-71.0	95.9	29.0	98.0
R1(i,l)	-11.4	154.2	24.7	98.1
R2(i,l)	-11.7	157.2	25.0	99.9
52(i,l)	-5.1	162.0	25.0	98.9
53(i,l)	-5.3	169.0	25.0	98.2
55(i,l)	-3.5	163.7	25.0	98.9
R1(i,k)	-1.7	165.8	25.0	99.1
R2(i,k)	2.7	170.0	25.0	99.0
52(i,k)	10.2	177.6	25.0	99.0
53(i,k)	9.0	176.5	25.0	99.1
55(i,k)	11.7	179.7	25.0	99.4

(a) Nominal pH 6.685 at 25°C.
(b) Nominal pH 4.008 at 25°C.

Test date :
(c) 12-12-90;
(d) 06-02-91;
(e) 07-02-91;
(f) 23-04-91;
(g) 30-10-91;
(h) 17-02-92;
(i) 09-11-92.

(j) Reference electrode 63
(k) Russel reference electrode 26
(l) Russel reference electrode 25

S,T,R and Q were Kent All-Purpose pH Electrodes. All other glass electrodes were Russell Electrodes (SWL/B14, A=70mm).

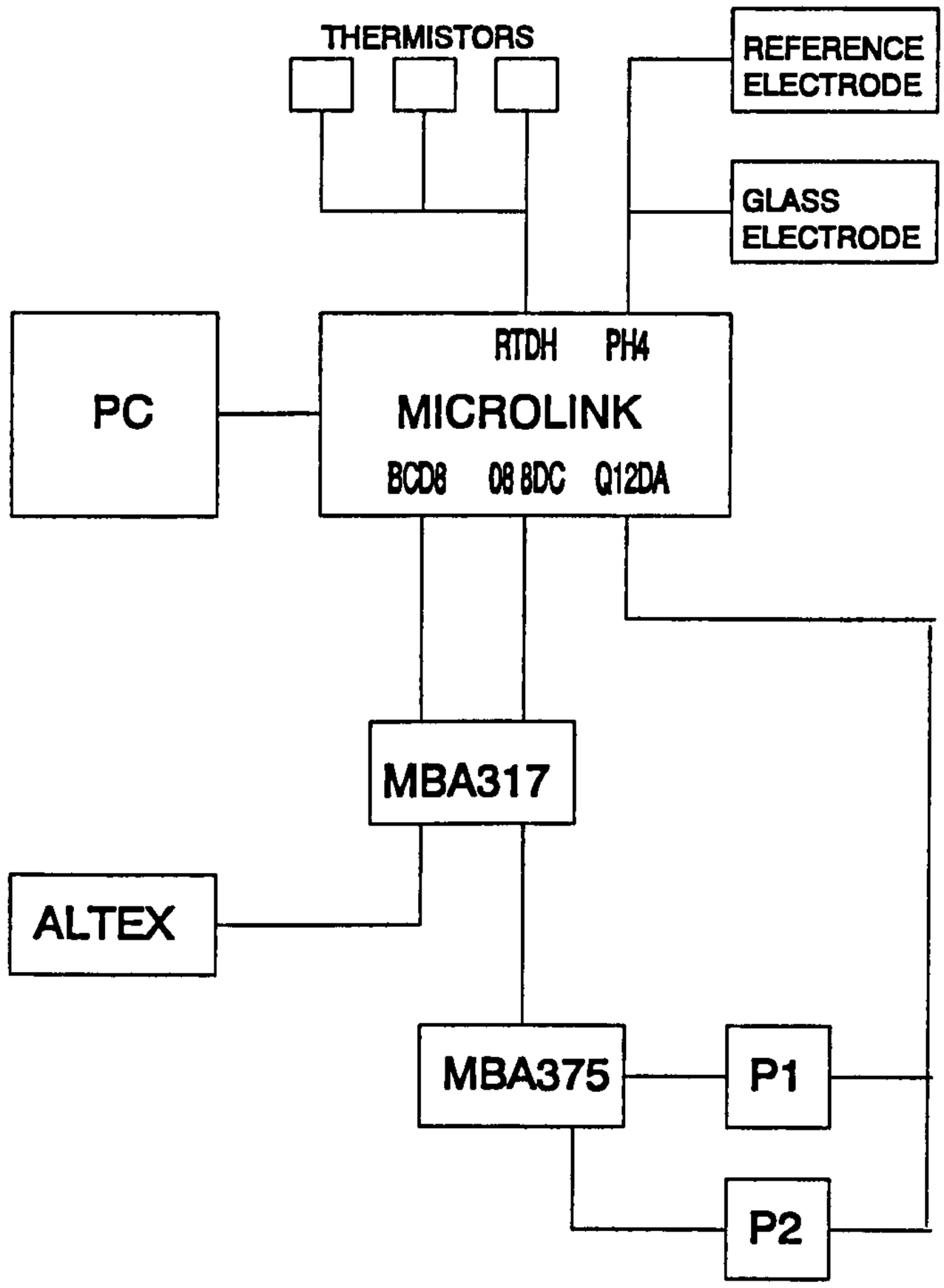

Figure 4.2. Schematic diagram of control network developed for the continuous potentiometric measurements. Units MBA375 and MBA317 controlled power supply to peristaltic pumps (P1 and P2) and the switching valve (Altex). Microlink modules are described in the text. All commands were sent from an IBM PS/2 Model 55 SX computer (PC).

4.2.2.4. Optimisation of potentiometric flow system

All on-line potentiometric pH measurements were made using cell D (Section 3.3). The schematic flow diagram of the manifold is shown in Figure 4.3.

Discrete analysis of solution pH may be affected by ion desorption from the glass electrode (Covington *et al.*, 1988). This may be due to dissolution of the glass membrane or as a release of ions previously adsorbed from other samples or buffer (Covington *et al.*,

1988). The use of a flow system considerably reduces the effect of these phenomena by diluting any impurities by their carriage away from the electrode bulb. Flow analysis systems continually renew the liquid junction and with constant solution and reference solution flow rates, the geometry of the liquid junction is consistent, *i.e.* all chemical and potential gradients are parallel (Brezinski, 1983). The set-up described here provides a greater frequency of measurement than methods which rely on discrete, syringe delivery of a sample (Culberson, 1981; Diamond and Walshe, 1991).

The flow system inherited at the beginning of this project was very temperamental with regular bubble formation and significant electrical contamination, particularly at sea (S.Knox and D.R. Turner, pers. comm.).

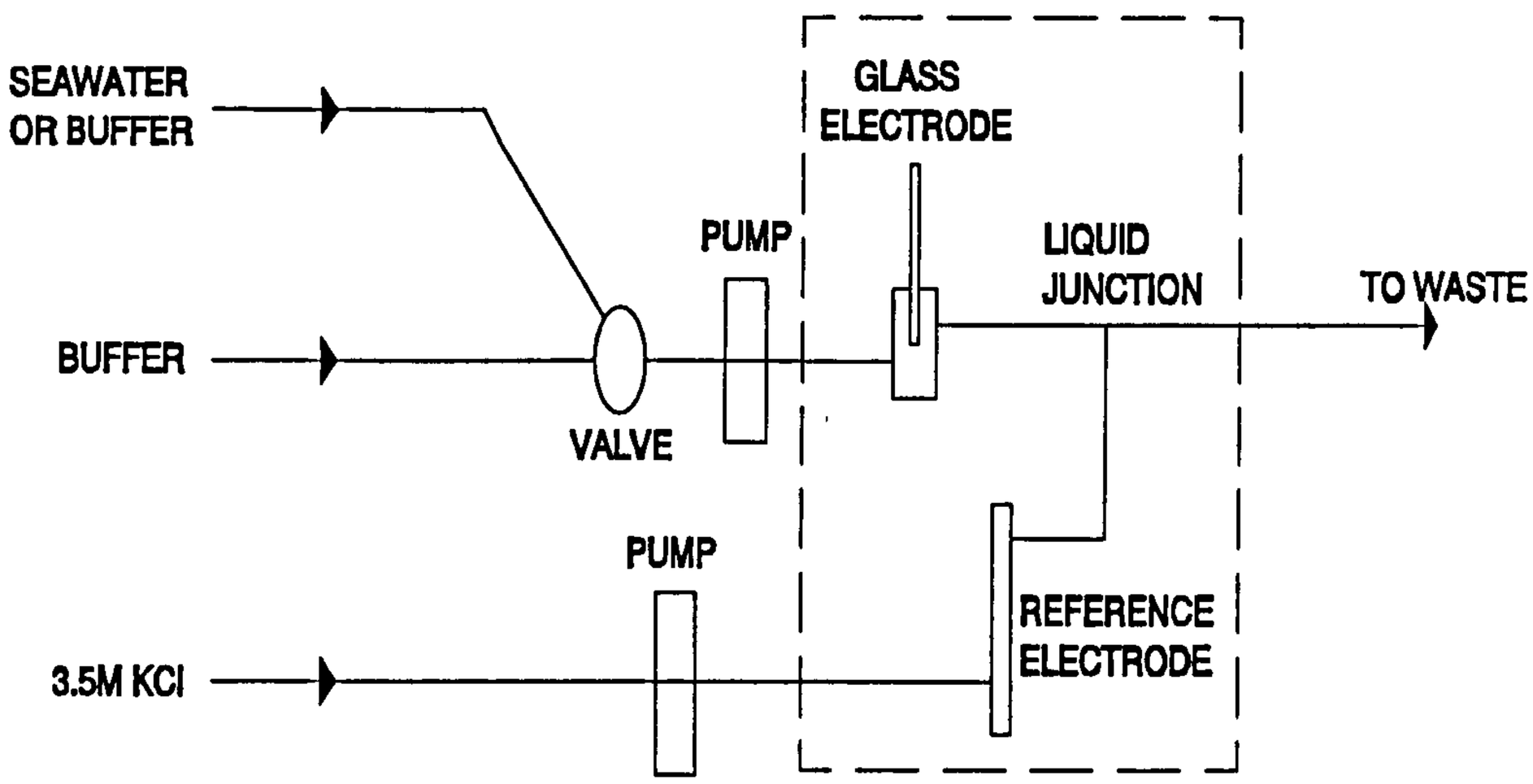

Figure 4.3. Schematic diagram of the potentiometric flow manifold. The dashed line surrounds the potentiometric cell D

Bubble formation is common in flow systems when the working temperature is above that of the initial test solution. The old system was run to test the electrode drift and to ascertain the significance of bubble formation on the electrode potential. The electrodes were taken from their conditioning solution (equimolar phosphate buffer) at room temperature (approximately 18°C), rinsed with water, dried with acid free tissue and positioned in the flow cell. NBS buffer was pumped through the system at 0.44 $mL.min^{-1}$. Spikes in potential were observed if a bubble touched the glass membrane of the electrode (Figure 4.4.). It was occasionally necessary to halt analysis and release the bubble by manipulating the position of the electrode within the flow cell. The design of the flow cell was such that bubbles forming in the intake tubing regularly became trapped in the flow cell. Small bubbles were seen to congregate in the flow cell, amalgamating to form one large bubble which, when escaping from the cell, was often noted to partly block the liquid junction. This also caused the potential to become unstable, possibly due to the breakdown of the cylindrical properties of the transition zone in the junction.

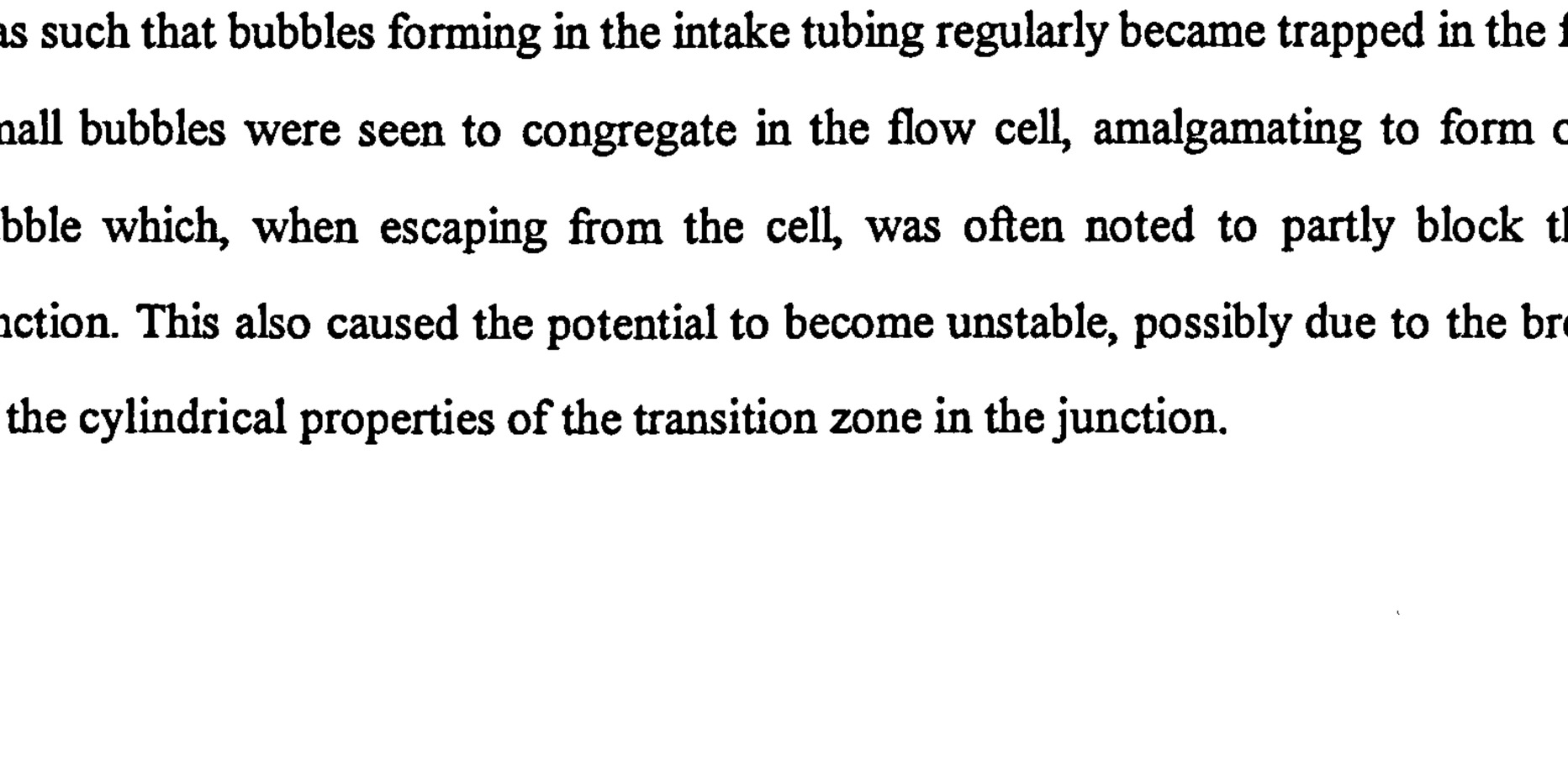

Figure 4.4. Typical change in potential on the passage of a bubble through the flow cell.

The significance of potential spiking with reference to continuous pH analysis is shown in Figure 4.4. The potential difference (≈ 0.2mV) between the readings at 3 and 7 minutes corresponds to 0.003 pH units at 25°C. If this were the case when analysing the pH of a test solution, then, after the bubble has passed, results would be in error until the next standard is run. It was thus necessary to design a system which would reduce bubble formation and accommodate a flow cell allowing greater ease of passage of bubbles past the electrode.

Both the new and the original flow cells are shown in Figure 4.5. All tubing was 0.8mm i.d. PTFE tubing connected to the cells through Rheodyne fittings. The cell cavity was isolated from the air with an O-ring when an electrode was in place. The original flow cell (Figure 4.5a.) was designed to accommodate Kent pH electrodes which are flat-bottomed and as such there is little dead volume in the cell cavity. The angle of introduction and exit of solution to and from the flow cell, combined with the small cell cavity, leads to conditions favourable for bubbles becoming lodged. The new flow cell (Figure 4.5b) was designed to facilitate the passage of bubbles through the cell. The inflow port at the base and the exit at the top of the electrode chamber determined that bubbles quickly passed the H^+-sensitive bulb. Further, it was generally seen that bubbles escaped fully from the cell.

Very rarely was it necessary to remove the electrode from the flow cell to release bubbles. Reducing the bubble size, indirectly resulting from lowering the residence time of smaller bubbles in the cell reducing their accession, helped maintain the integrity of the liquid junction, and thus avoiding errors associated with a junction collapse (Howson *et al.*, 1986).

This study supported the findings of Covington *et al.* (1988) that it is favourable to deliver the more dense reference solution to the lower port of the T-piece promoting a more stable liquid junction. Indicator dye added to the reference solution illustrated the unstable, convective nature of solution across the liquid boundary when reference solution enters the T-piece over the test solution.

The system was made more isothermal through the construction of a new perspex frame to fit a temperature controlled water bath. All buffer reservoirs were supported on a shelf in the bath. The reference electrode was held in the water such that the top, just above the outlet tubing, was at the surface. The glass electrode was held in a support such that the

flow cell was wholly immersed. The tubing array was arranged in order that the minimum length was exposed to the air.

Once the improved system was running, continuous electrode potential measurements in phthalate buffer, as performed on the old system, were repeated for comparison. The temperature control, afforded by supporting the buffer reservoirs, flow cell, reference electrode, liquid junction and tubing in the water bath at constant temperature, resulted in a considerable reduction in potential drift. Comparison of Figures 4.6. and 4.7. illustrates the reduced electrode drift during continuous analysis of phthalate buffer prior to and after the development of the new system. The charging times, the times for the electrodes to settle down and acclimatise to their new environment, were halved from about 80 min to 40 min. The average rate of potential drift, after this initial settling in period, was significantly reduced from -0.56 $mV.h^{-1}$ to -0.25 $mV.h^{-1}$. This later time compares very favourably with the 0.6 $mV.h^{-1}$ considered stable by Whitfield *et al.* (1985). More importantly, maximum deviation from the line of regression of this drift decreased from an equivalent of 0.16 to 0.002 pH unit.

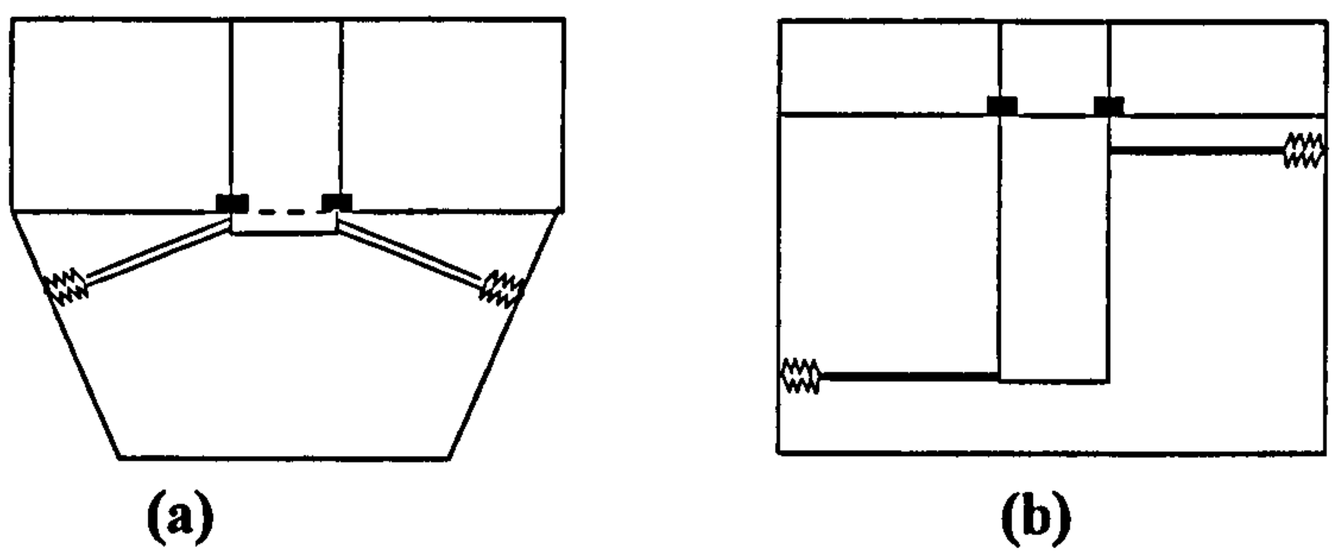

Figure 4.5. Flow cells used in this study. (a) original flowcell. (b) new flowcell. Glass electrodes are inserted into the top of the cell. Input to cell 'b' is through the lower port.

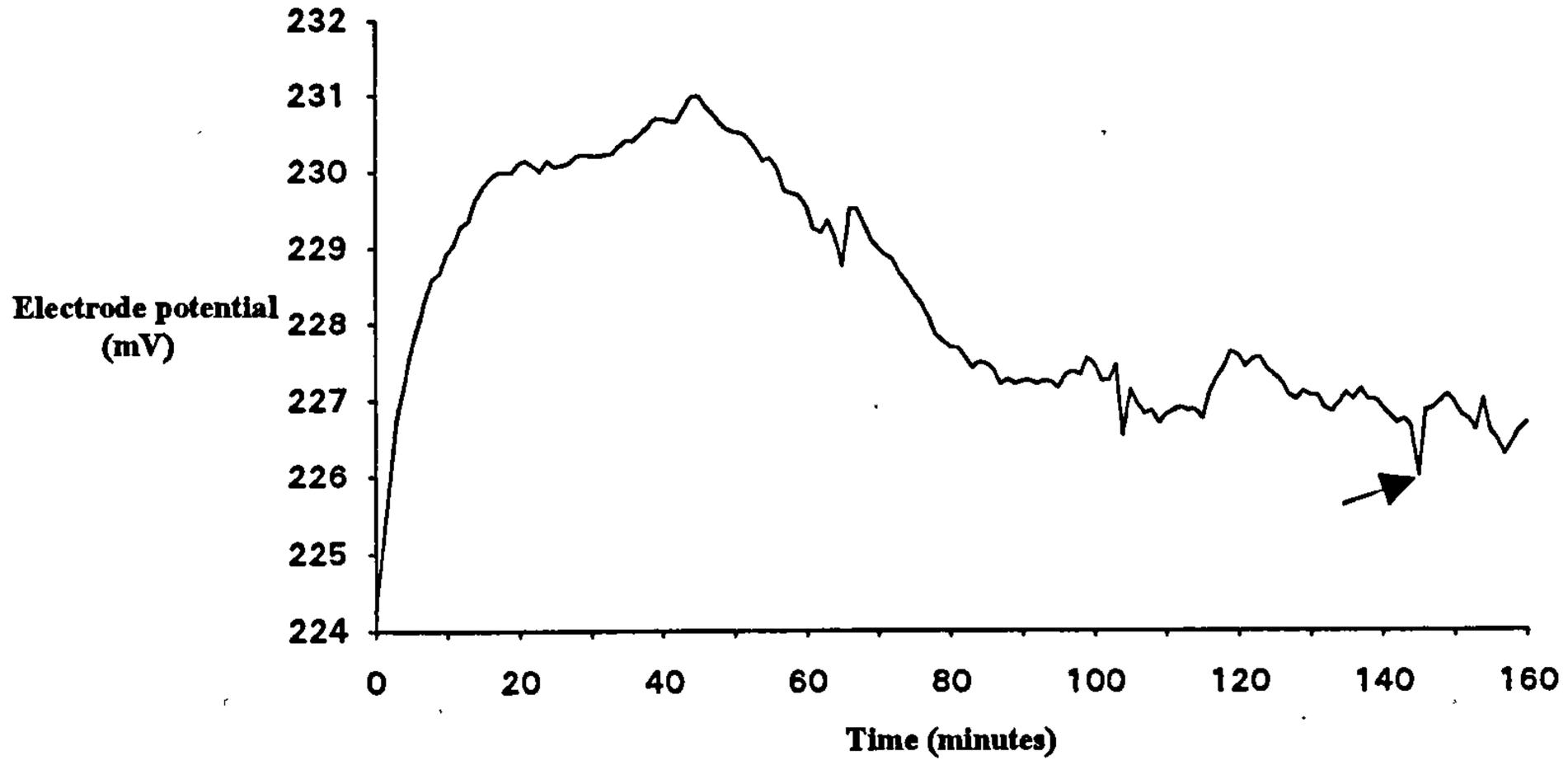

Figure 4.6. Potential drift of electrode in phthalate buffer using original flowcell. The arrow indicates maximum deviation in potential from the regression line of the drift after the charging time. This is equivalent to 0.016 pH units.

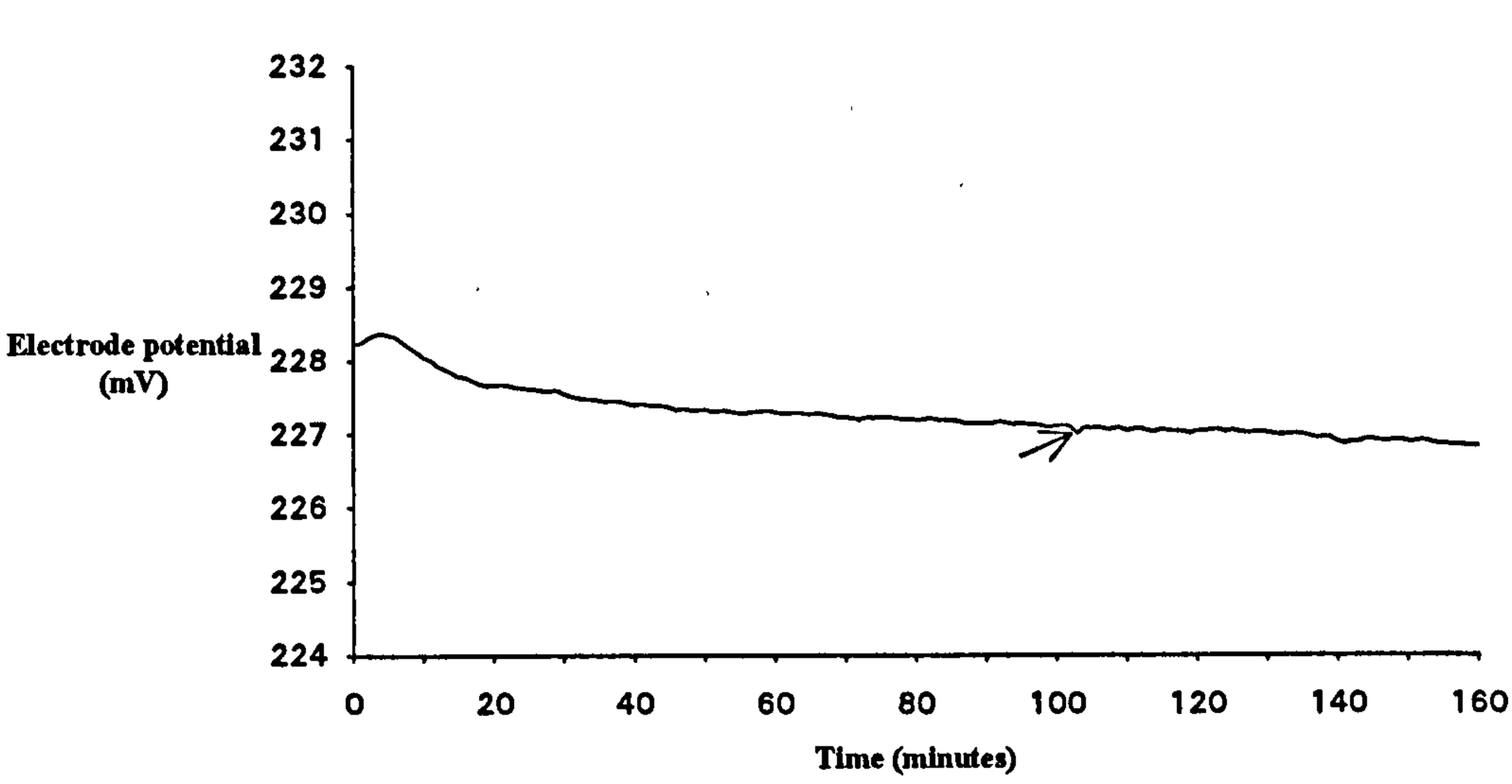

Figure 4.7. Potential drift of electrode in phthalate buffer using new flowcell and incorporating increased temperature control. The maximum deviation from the regression of drift after the charging time is indicated by the arrow and is equivalent to 0.002 pH units.

To achieve rapid analyses with limited buffer consumption it was necessary to optimise the system further by determining the flow regime across the electrode resulting in the optimum response time when changing from one buffer to another. This was achieved by adjusting, through systematic adaptations of the computer program, the flushing times, and rates of solution so as to obtain a short, reproducible response time, and yet provide limited buffer consumption. The flushing time is the length of time the buffer rate was increased above its normal operating value after the switching valve had been operated. This increased value is termed the flushing rate. The response time is defined as the time between switching the buffers and the electrode producing a voltage reading within 0.1 mV of the final reading (Howson *et al.*, 1986). This is the equivalent to 0.0017 pH units from the final pH at 25°C.

Figures 4.8.a-e. show response curves when changing from the phosphate to the phthalate buffer under different flushing regimes. Once flushing had finished the pump speed was returned to 0.44 $mL.min^{-1}$. To compensate for electrode drift, and to ease the comparison of the electrode responses, all curves were normalised by converting the equilibrium potential to 222.9 mV and changing the previous potentials accordingly. Figure 4.8a. illustrates the electrode potentials of repeat runs with a flushing rate of 1.84 $mL.min^{-1}$ for 30s. The short-term response is irreproducible and the equilibrium potential takes more than 15 minutes to be reached. The responses shown in Figures 4.8b. and 4.8c. are also obtained with a flushing rate of 1.84 $mL.min^{-1}$, but with flushing times of 45 and 60s respectively. The former illustrates reasonable reproducibility although Run 2 does not reach equilibrium in 15 minutes. The disparity shown in Run 2 may be an artefact - possibly due to bubble passage. The responses in Figure 4.8c. show excellent reproducibility and a rapid attainment of equilibrium potential with a response time of about 5 minutes. Figures 4.8d. and 4.8e. record the electrode response characteristics with a constant flushing time of 30s and flushing rates of 3.55 $mL.min^{-1}$ and 5.40 $mL.min^{-1}$ respectively. The former response is very reproducible yet slow with a response time of about 10 minutes. The highest flushing rate (Figure 4.8e.) has a very erratic short-term response. However, the response time is also about 10 minutes. The mean responses under each flushing regime have been grouped into two categories: those with a constant flow rate of 1.84 $mL.min^{-1}$ and varying flushing times; and those with a constant flushing time of 30s and varying

flushing rates. The response characteristics are shown in Figures 4.9a. and 4.9b. The response of Figure 4.8a. is common to both categories and has already been shown to be slow and irreproducible. The response time is shorter under the conditions in Figure 4.9a with both combinations attaining maximum response in under 5 minutes. The response times of the combinations in Figure 4.9b. are over 10 minutes.

It is suggested that the flushing parameters 1.84 $mL.min^{-1}$ for 60s provide the optimum conditions in this study. An average response rate of 0.7 $mV.s^{-1}$ under these conditions is favourably comparable with that calculable from the data reported by Howson *et al.* (1986) of 0.69 $mV.s^{-1}$. Especially so as this latter value was obtained using a constant flow rate of 3 $mL.min^{-1}$ and a final buffer consumption of 12 mL as opposed to under 3.5 mL for optimum response times in this work.

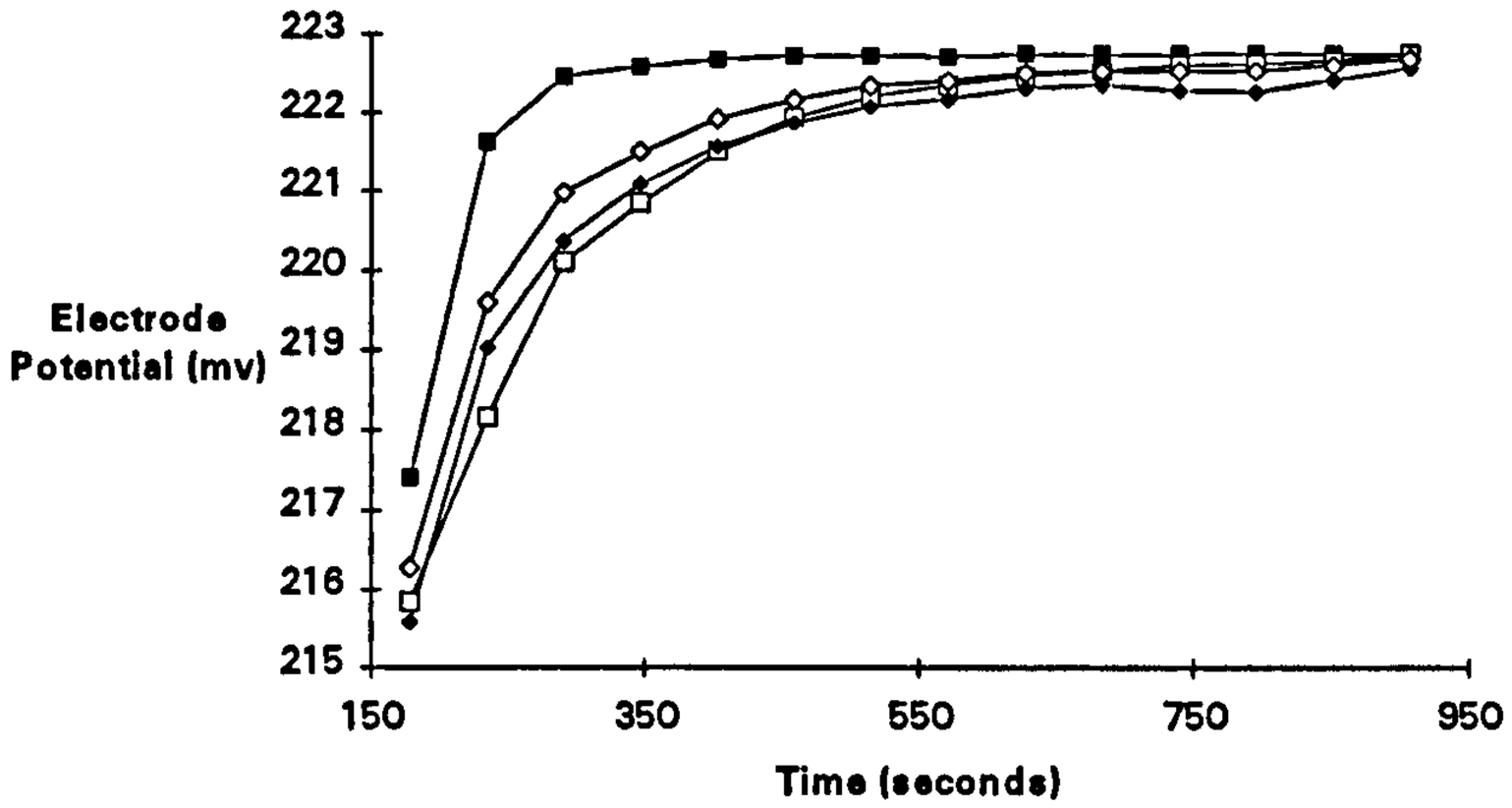

Figure 4.8a. Electrode response times when changing from phosphate buffer to phthalate buffer. Flushing rate 1.84mL.min^{-1}, flushing time 30s. Run 1 —■— ; Run 2 —□— ; Run 3 —◆— ; Mean —◇—

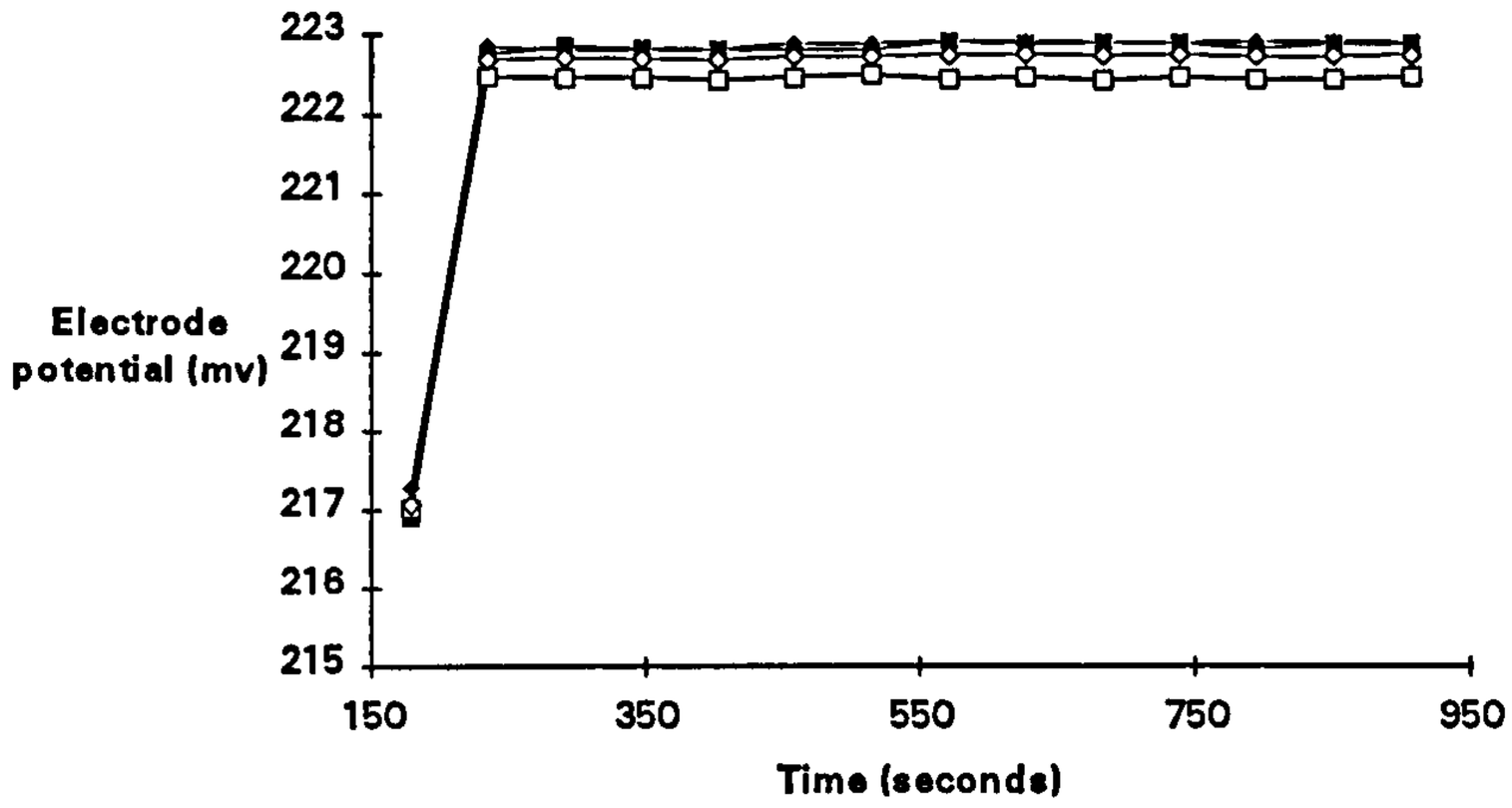

Figure 4.8b. Electrode response times when changing from phosphate buffer to phthalate buffer. Flushing rate 1.84mL.min^{-1}, flushing time 45s. Run 1 —▪— ; Run 2 –□— ; Run 3 —◆— ; Mean —⟡—

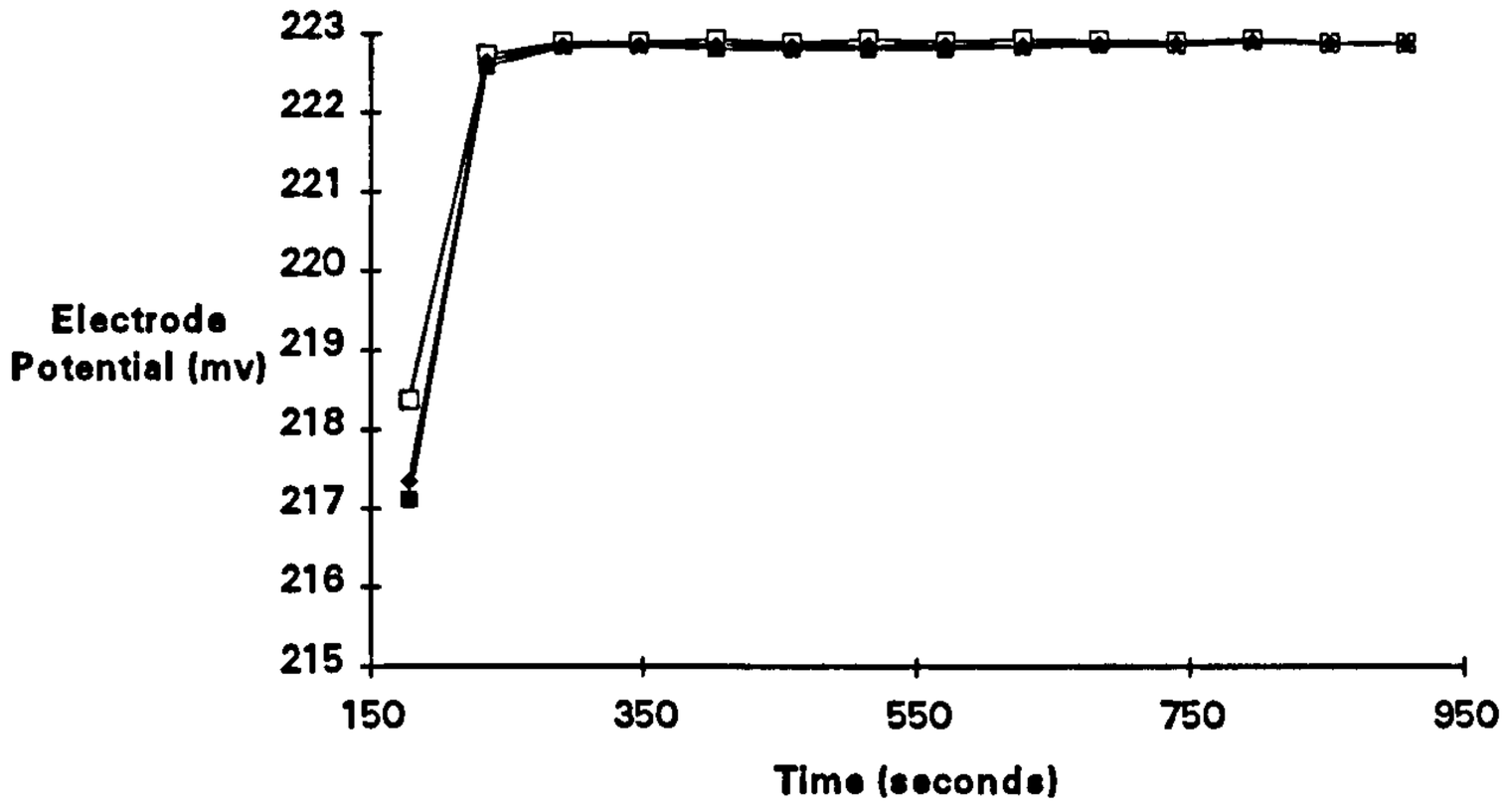

Figure 4.8c. Electrode response times when changing from phosphate buffer to phthalate buffer. Flushing rate 1.84mL.min^{-1}, flushing time 60s. Run 1 —▪— ; Run 2 –□— ; Mean —◆—

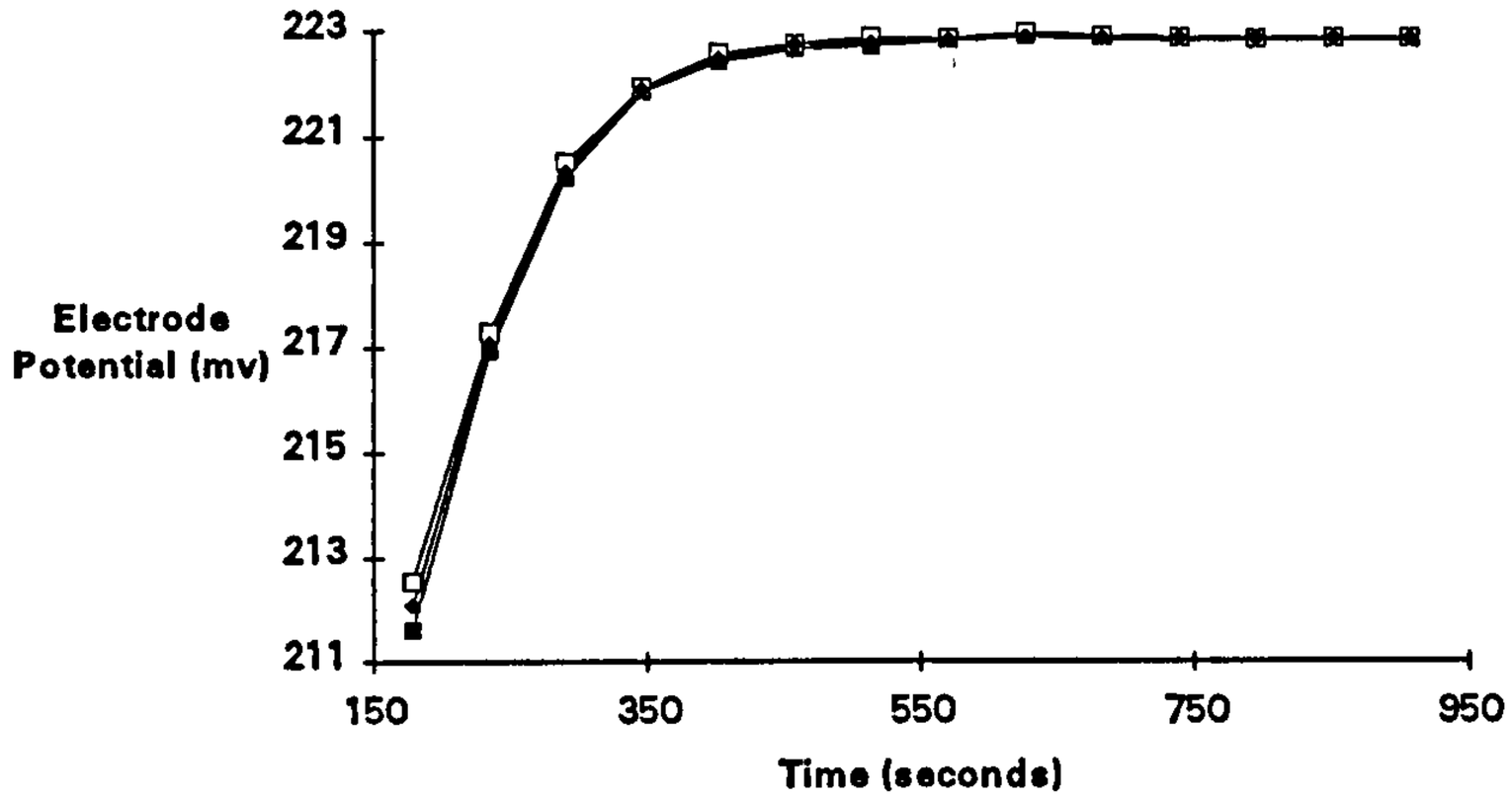

Figure 4.8d. Electrode response times when changing from phosphate buffer to phthalate buffer. Flushing rate 3.55mL.min^{-1}, flushing time 30s.
Run 1 —▪— ; Run 2 —▫— ; Mean —◆—

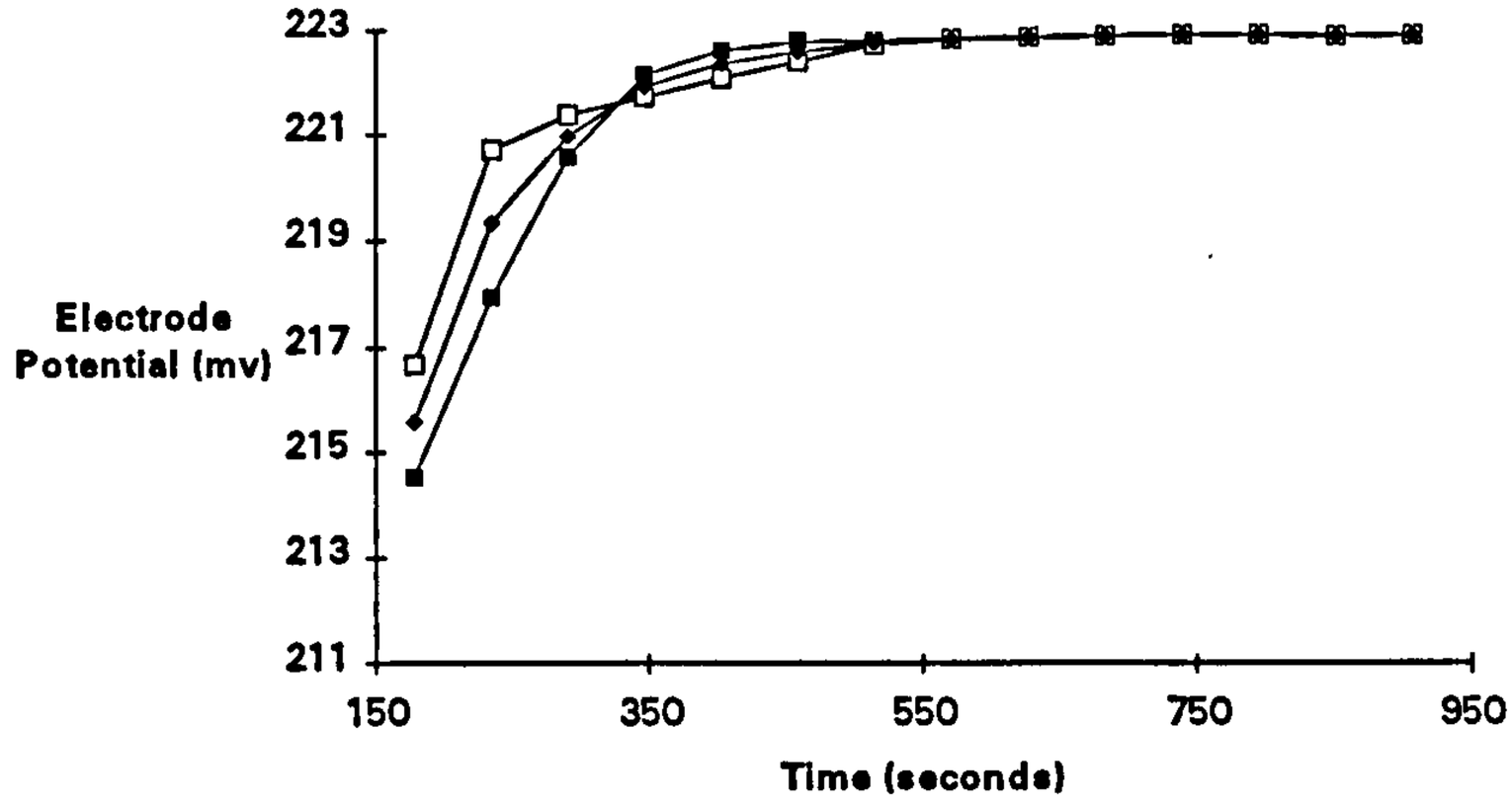

Figure 4.8e. Electrode response times when changing from phosphate buffer to phthalate buffer. Flushing rate 5.40mL.min^{-1}, flushing time 30s.
Run 1 —▪— ; Run 2 —▫— ; Mean —◆—

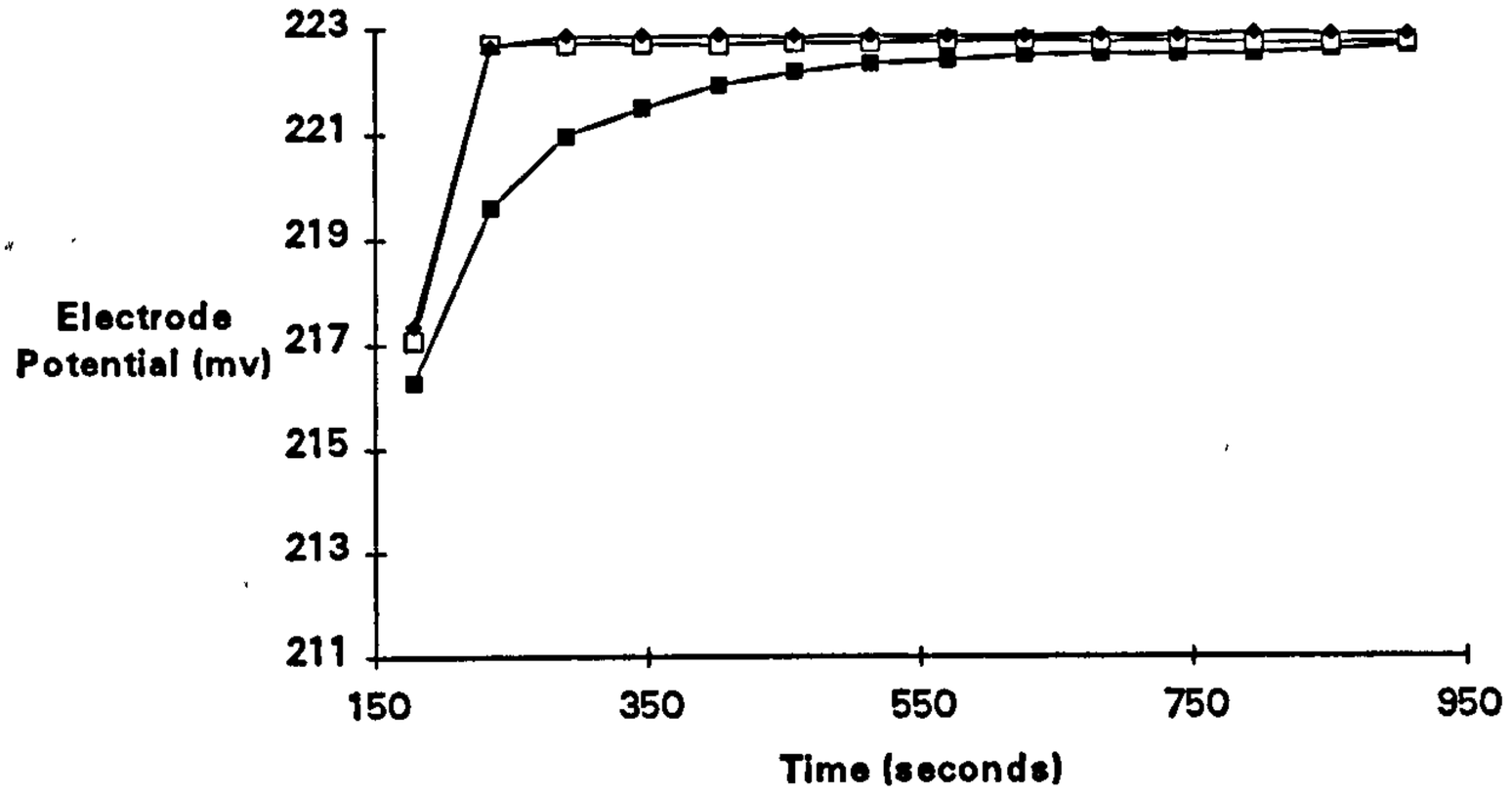

Figure 4.9a. Mean electrode response times when changing from phosphate buffer to phthalate buffer. Flushing rate 1.84mL.min^{-1}, flushing times: —■— 30s, —□— 45s, —◆— 60s.

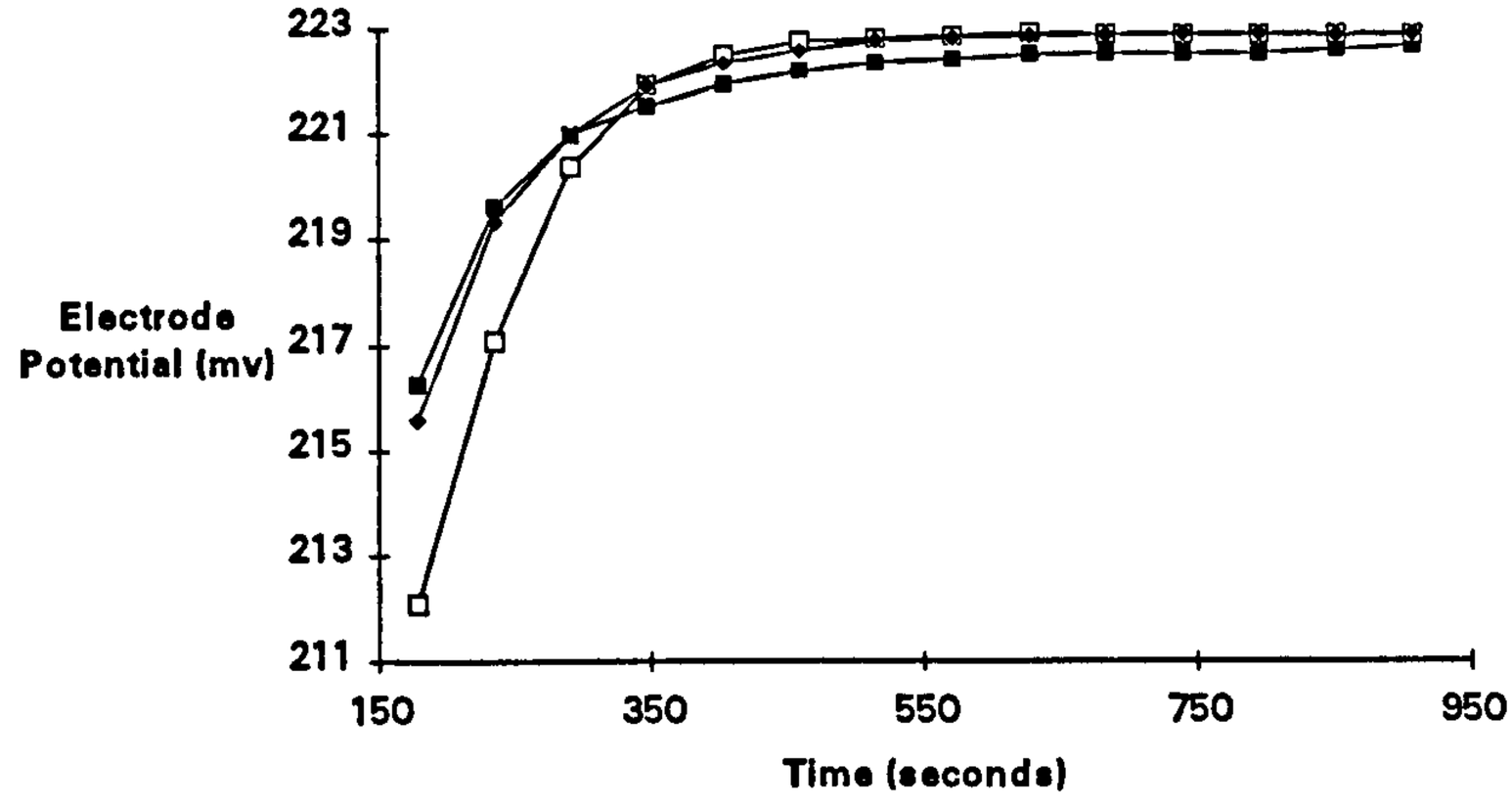

Figure 4.9b. Mean electrode response times when changing from phosphate buffer to phthalate buffer. Flushing time 30s, flushing rates: —■— 1.84mL.min^{-1}, —□— 3.55mL.min^{-1}, —◆— 5.40mL.min^{-1}.

4.3. Spectrophotometry

4.3.1. Instrumentation and procedures

A dedicated spectrophotometer (Cecil CE2020) was used throughout this study to measure solution absorbance. The instrument was chosen from a large range of available models as it fulfilled our selection criteria; *i.e.* it covered the required wavelength range, had excellent baseline stability, rapid wavelength change and interface potential, was compact, lightweight and met the price stipulation. The specifications of the instrument are given in Appendix A.

The instrument could be operated in two modes:

(1) For discrete measurements a 1cm cuvette (Hellma) was held in a single cell holder in the instrument. Wavelength changes and absorbance readings were manually obtained from the control panel. No temperature control was available; (2) For remote operation, commands were sent, and data acquired, via the computer through a bi-directional RS232C link to the spectrophotometer using FORTRAN routines written as part of this study. No manual control was possible as the control panel is locked when the instrument is started up with the RS232 console occupied. Temperature control was enabled through a Peltier thermostated temperature controller (Cecil CE2024) which was linked to a 4-way cell holder. The cooling system was a constant supply of fresh water to the cell holder delivered through black laboratory tubing to reduce biofouling. A 30μL, 1cm flow-through compact cell (Hellma-178.711 QS) with SUPRASIL windows was used for all flow analysis. A sample injection valve (Burkard Scientific) was operated through the microlink (Biodata 2) via the MBA375. Pump (Gilson Minipuls 2) control was enabled as in Section 4.2.2.1.

4.3.2. Discrete measurement

As a precursor to the development of the continuous system, and to become more familiar with spectrophotometric techniques for seawater pH measurement, the pH value of an equimolal phosphate buffer was measured discretely using an approach similar to that of Byrne (1987). Bromothymol blue in the solid form was added to the buffer in a 1cm cuvette

(Hellma), warmed to 25°C in a thermostatted water bath, and the absorbance measured at 415, 615 and 730nm. Indicator concentration in the solution was modified to furnish an absorbance of between 0.9 and 1.0 at 615nm. This was achieved by either adding more indicator or diluting the solution with buffer. Absorption of the blank at the three wavelengths were also taken and the appropriate corrections made to indicator absorptions. Using the formula from Byrne (1987), giving the pK_2 value and molar absorptivity ratios for bromothymol blue at 25°C, buffer pH was calculated from

$$pH = 7.098 + \log\left(\frac{R - 0.0046}{2.3774 - R*0.396}\right) \qquad 4.2.$$

where $R = (A_{615} - A_{730}) / (A_{415} - A_{730})$. Replicate analysis of the buffer gave pH = 6.862 ± 0.002, n = 4. There is good agreement with the theoretical pH(NBS) value of pH 6.865 (Bates, 1973).

4.3.3. Continuous measurement

In order to achieve rapid, autonomous pH determination it was necessary to develop a method of continual spectrophotometric analysis. This involved characterising the flow regime, the injection properties and determining the working precision of the system.

To test the reproducibility of the peristaltic pump, water was pumped through the system (Figure 4.10.) at 2.8mL.min^{-1}. The injection valve was switched and phenol red indicator from the indicator reservoir was injected for 0.4s into the sample at a rate of 0.32mL.min^{-1}, corresponding to an injection of 2μL. The resulting plug was homogenised in a 30cm mixing coil and transported to the detector when the pump was stopped. The plug was held in the flow cell for 10s prior to absorbance readings being taken at 558nm. The pump was then restarted and the plug discharged to waste. The system was flushed until all indicator had stopped being entrained in the sample flow and the whole procedure repeated.

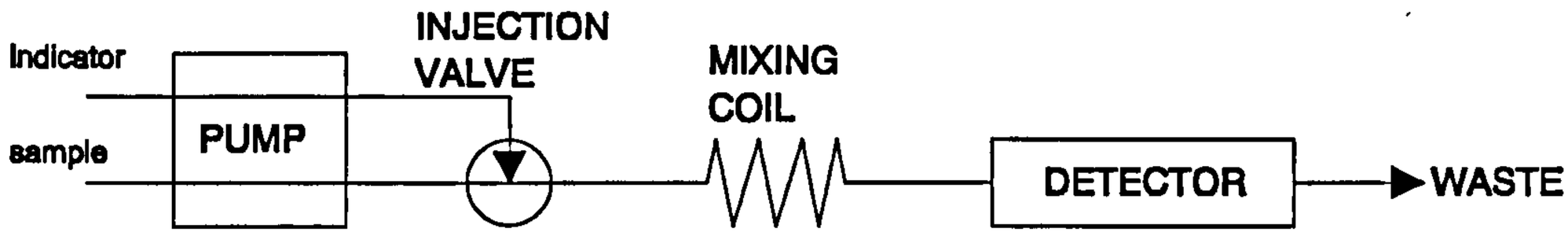

Figure 4.10. Schematic flow diagram of the spectrophotometric pH system used to characterise the reproducibility of the peristaltic pump.

The resultant time lapse between the indicator injection and the absorption maximum varied between injections (Figure 4.11.) and, additionally, variations in peak height were observed. This nullified the determination of pH by measuring the absorption at the two wavelengths from alternate injections as Equation 3.42. assumes constant indicator concentration for both A_1 and A_2 in Equation 3.37. The irregularity in indicator concentration can be attributed to the peristaltic nature of the pump. The sinusoidal flow driven by peristaltic pumps causes variation in the instantaneous flow speed of both the sample and indicator solutions and concurrent variation in their relative concentrations on mixing and the timing of this mixing. This problem of timing with regard to determination of the time of maximum absorption is magnified if the flow rate of the indicator solution is considerable compared to the rate of the sample flow. The extent of this magnification depends on the degree of pulsing from the pump and whether the pulsing in the indicator flow is in phase with the pulsing in the sample flow.

It is important to measure absorption at, or near to, the maximum absorbance in stop-flow systems because of the possibility of lateral movement of the plug once the pump has stopped. Movement may result from either back pressure in the system due to previous forcing by the pump, or the motion of bubbles through the tubing when the pump has been stopped. The rate of change of absorption per degree of lateral movement is greatest on the rise and fall of the absorption peak and reduces to a minimum at the top of the peak. It is therefore preferable to have a broad absorption peak with a flattened top with absorption measurements taken in the middle of the plug where the rate of change of absorbance will be near constant.

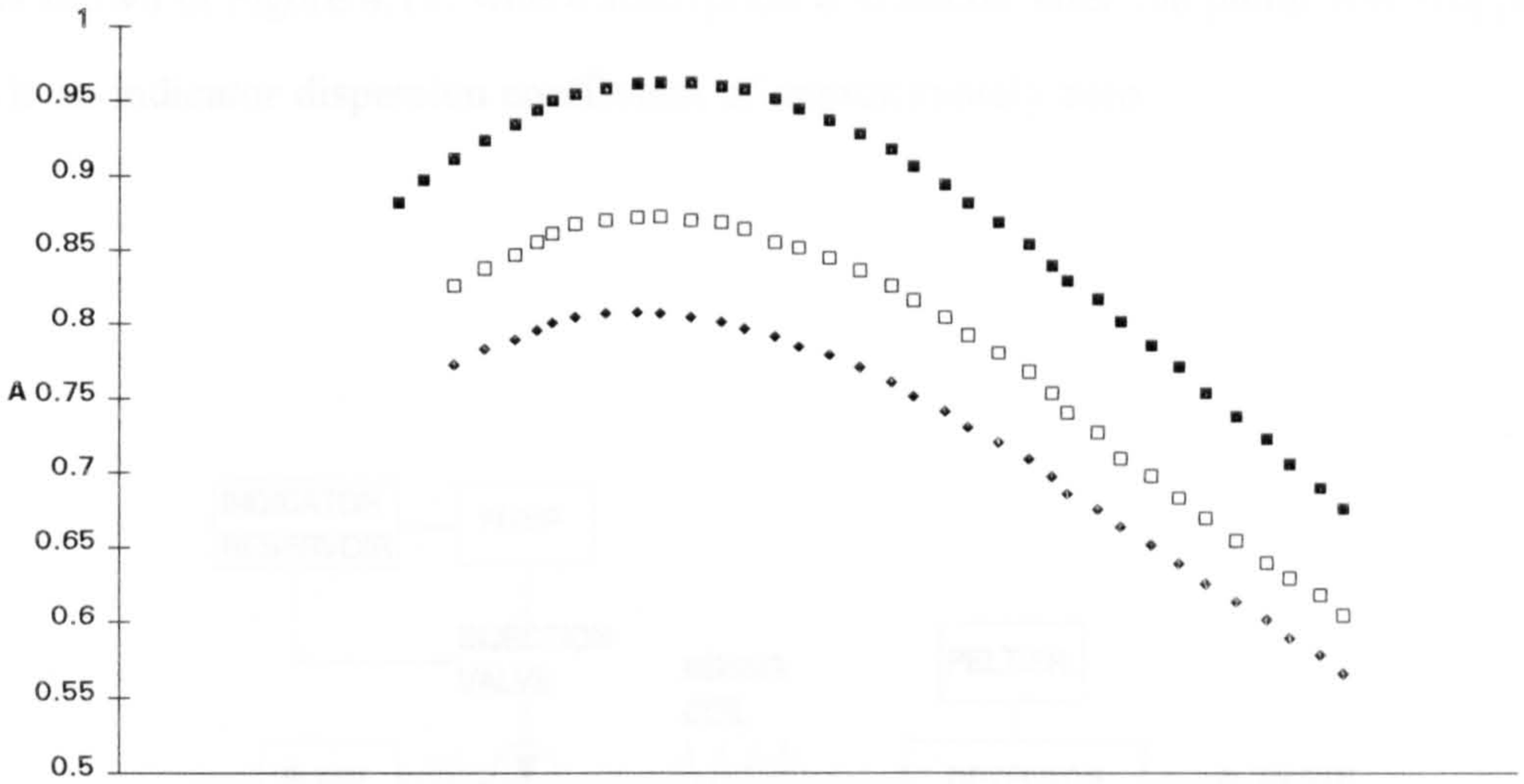

Figure 4.11. Variability in peak characteristics of replicate runs with phenol red injections in water. A is absorbance.

It was assumed that the dilution of a seawater medium by ≈ 1% through the addition of the indicator solution would not change the ionic speciation of the seawater significantly if the indicator stock solution was made up from the sample. The dilution used above when determining the degree of pulsing was ≈ 10% and thus was unacceptable. As the sampling frequency of the other carbon dioxide variables (pCO_2, TCO_2 and alkalinity) is at best $3min^{-1}$ it was adjudged that the sampling frequency for pH measurement could be compensated to allow for greater reproducibility of sample pH through reducing the dilution of the sample by the indicator solution and broadening the peak width by increasing the injection time and the mixing of the indicator plug.

The flow speeds were, therefore, changed to 12.0 $mL.min^{-1}$ for sample and 0.1 $mL.min^{-1}$ for indicator solution incorporating an independent peristaltic pump for the indicator solution (Figure 4.12). The indicator injection time was lengthened to 5s (total injection 8.3 μL), and the mixing coil length increased to 1 metre to maximise the homogeneity of the plug and increase the peak width. Figure 4.13. illustrates the constancy of absorbance over the peak maximum suggesting the problem with pump pulsing had been reduced and, due to a near constant indicator dispersion coefficient over a broad peak maximum, any lateral movement of the indicator plug would cause a small change in absorption. The dispersion coefficient is the rate of change of the indicator concentration.

This is shown in Figure 4.14. where absorption is constant after the pump was stopped, *i.e.* there is an indicator dispersion coefficient of approximately zero.

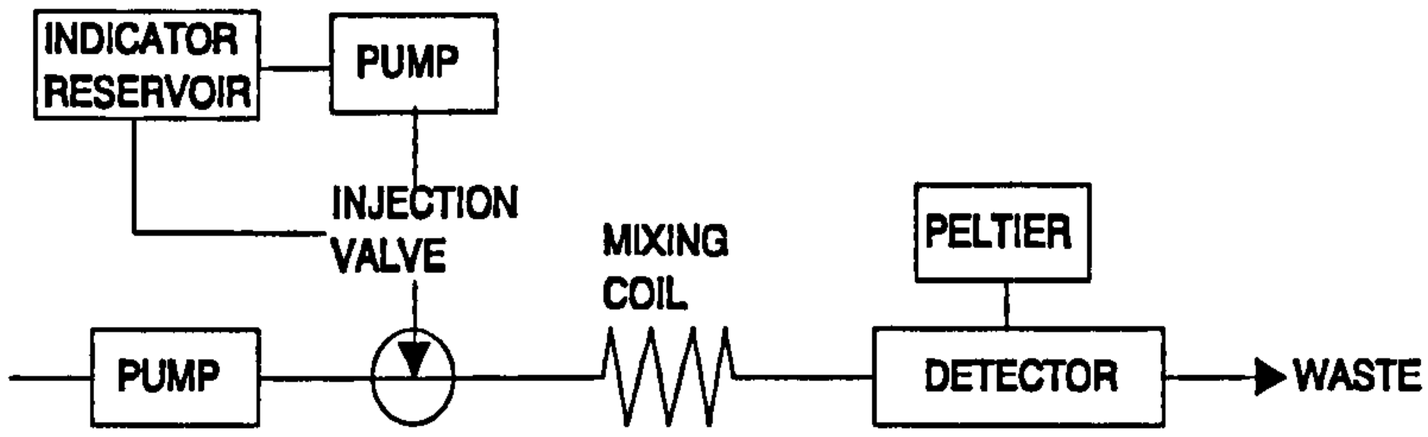

Figure 4.12. Schematic flow diagram of the spectrophotometric pH system (adapted from Bellerby et al. (1993))

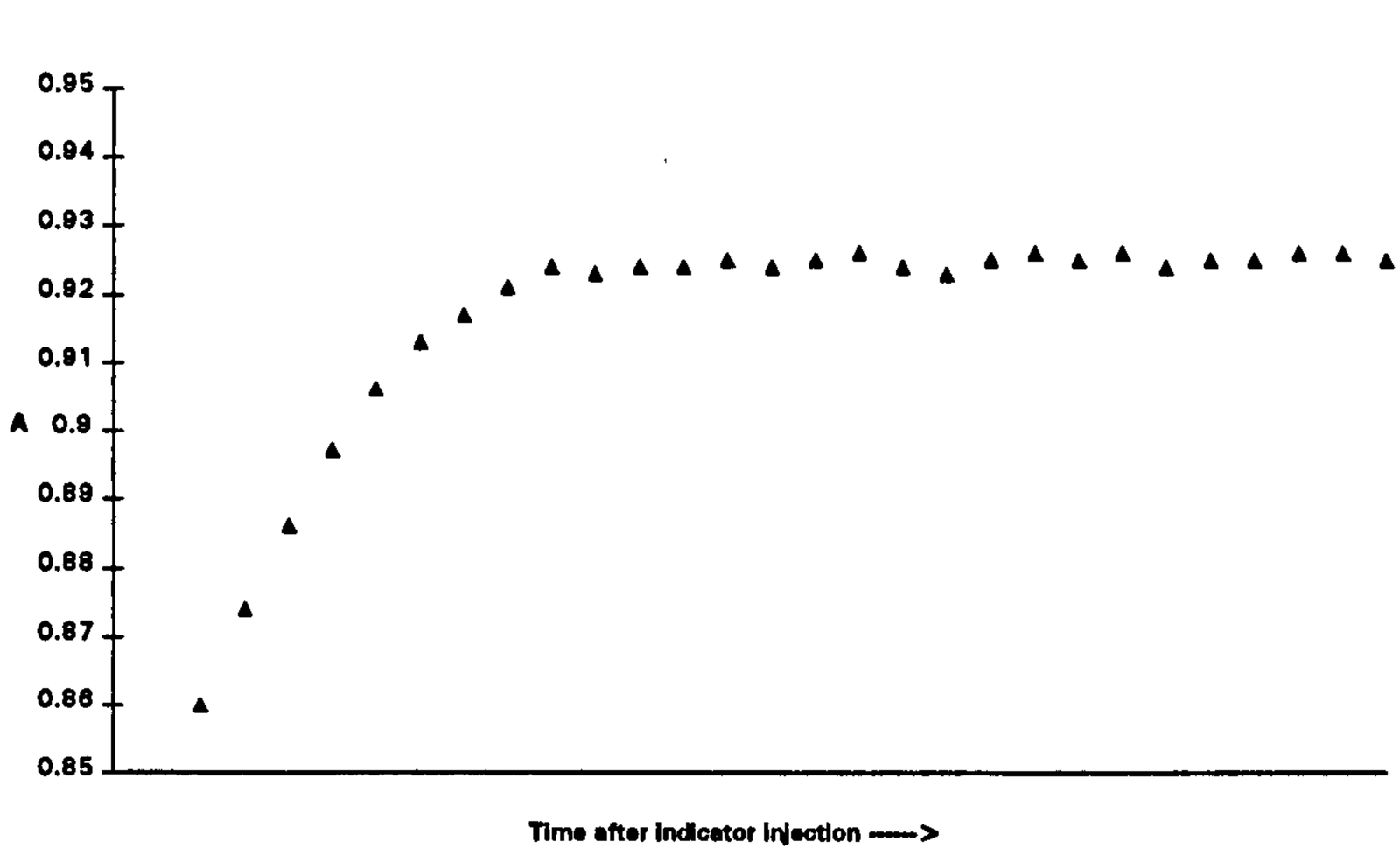

Figure 4.13. Characteristics of absorption rise and peak of the indicator solution plug. The dispersion coefficient of the indicator is approximately unity at the absorption maximum. A is absorbance.

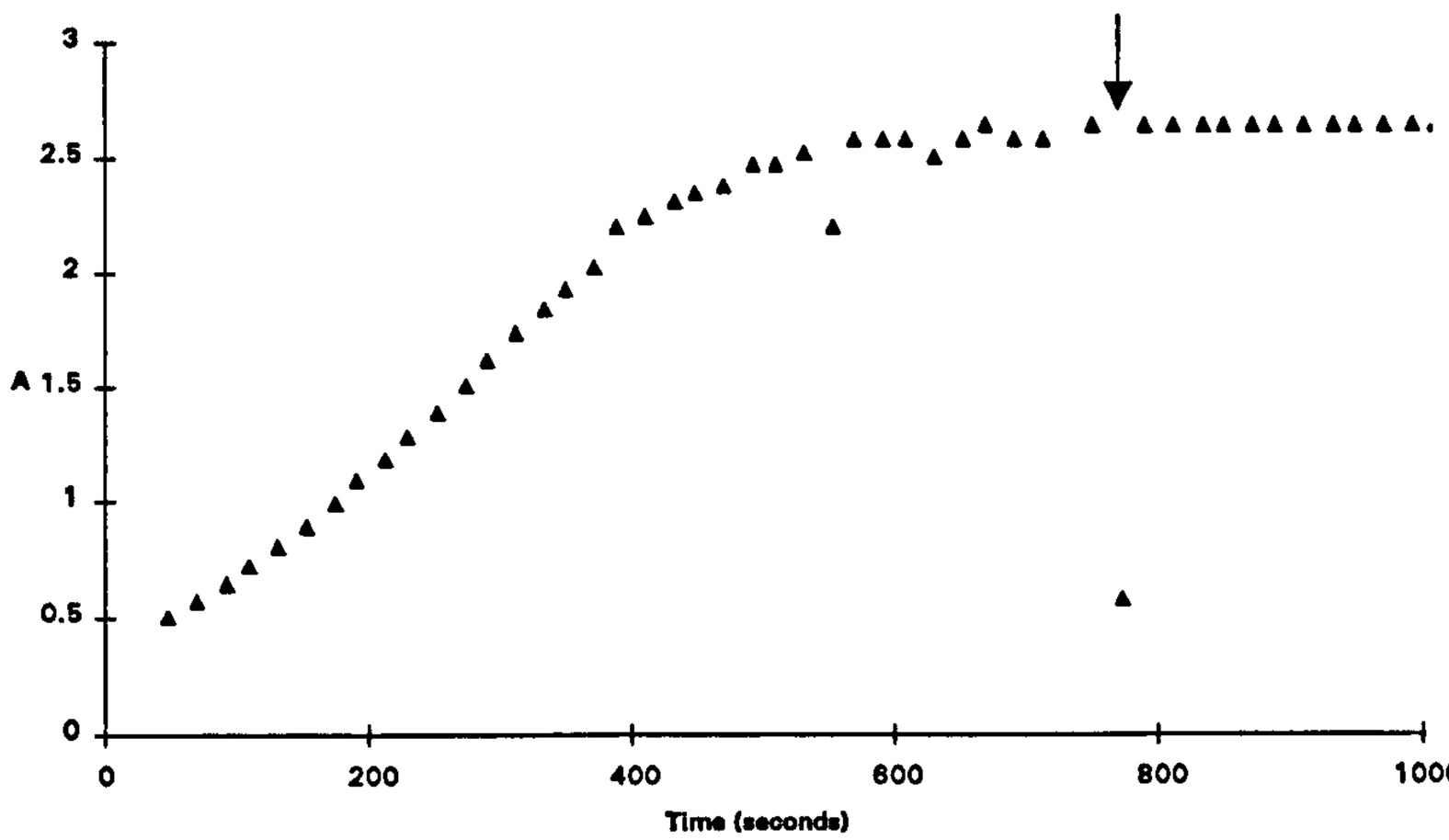

Figure 4.14. Constancy of absorbance of the indicator solution plug with time after the pump has stopped. The arrow indicates when the pump was halted. The wayward points are representative of problems with data acquisition which were later overcome. A is absorbance.

An experiment to determine the precision of the new method employed the injection of phenol red to solutions of tap water under the modified flow conditions specified above. The tap water was made progressively more acidic through the addition of drops of 0.1M HCl between sets of replicate analyses. No temperature control was administered. Calculating the molar absorptivity ratios for phenol red from Robert-Baldo *et al.* (1985), see Equation 6.1., values of pH - pK were calculated and are listed in Table 4.3., (represented not as pH because the pK of phenol red in fresh water has not been determined), and show a S.D. of between ± 0.003 and 0.022 units. Considering the buffer capacity of fresh water is very poor, this level of precision is encouraging and is markedly better than the precision of ± 0.2 pH units found by Pia *et al.* (1990) for measurements of pH in low ionic strength solutions. What is also apparent is the general trend of increased precision as R decreases, *i.e.* the pH of the solution nears the pK_2 of the indicator.

Table 4.3. Absorption characteristics and values of pH - pK for replicate analyses of tapwater using phenol red

	Absorption ratio (R)	A_{558}	pH - pK
Sample 1	11.940	1.224	1.019
	12.315	1.240	1.051
	12.273	1.242	1.047
	12.094	1.217	1.032
	12.408	1.211	1.058
	11.789	1.203	1.007
	12.018	1.216	1.026
Average	12.120	1.222	1.034
SD	0.223	0.015	0.019
Sample 2	11.470	1.192	0.980
	11.556	1.209	0.987
	11.459	1.201	0.979
	11.469	1.205	0.980
	11.232	1.195	0.961
Average	11.534	1.203	0.986
SD	0.261	0.009	0.022
Sample 3	10.866	1.164	0.930
	10.673	1.166	0.915
	10.858	1.178	0.930
	11.041	1.189	0.945
	10.944	1.184	0.937
	11.143	1.184	0.953
	10.985	1.189	0.940
	10.960	1.177	0.938
Average	10.943	1.181	0.937
SD	0.148	0.008	0.012
Sample 4	10.503	1.164	0.901
	10.585	1.166	0.907
	10.697	1.176	0.917
	10.710	1.159	0.918
	10.645	1.190	0.912
Average	10.683	1.172	0.916
SD	0.156	0.011	0.013
Sample 5	4.769	0.906	0.371
	4.864	0.897	0.382
	4.882	0.915	0.384
	4.882	0.921	0.384
	4.876	0.917	0.384
	4.836	0.914	0.379
	4.803	0.912	0.375
	4.850	0.913	0.381
	4.842	0.919	0.380
Average	4.853	0.916	0.381
SD	0.029	0.003	0.003

4.4. Shipboard methodology and experimentation

The experimental basis for pH measurements at sea was essentially the same as that described for the laboratory in Section 4.2. and 4.3., although, for continuous on-line measurements, seawater was pumped through PTFE tubing (0.8 mm i.d.) from the overhead non-toxic laboratory supply originating from an inlet at the bow of the ship at a depth of 4m (Turner, 1993). The on-line seawater for both methods was divided at a glass 'Y' junction immediately prior to pump 'P3' enabling the diameter of the pump tubing and the speed of the pump to determine the flow regime through one instrument independent of the other. A schematic diagram of the integrated hardware used for shipboard analyses is illustrated in Figure 4.15.

For potentiometric measurements, tris buffer (0.06*m*) was made up according to the recipe of Millero (1986), see Table 4.1. To prevent biological contamination of the buffer during transit to the Southern Ocean and throughout the cruise, saturated mercuric chloride solution was added to a final concentration of 0.02% (v/v). Seawater was pumped through the Altex valve to the electrode flowcell at a rate of 4.3 $mL.min^{-1}$ and, similarly during calibration, tris buffer was pumped at 0.5 $mL.min^{-1}$, after an initial flush at 2.0 $mL.min^{-1}$ for 60 seconds. For potential measurements, an average of 50 readings was reported along with standard deviation. The seawater stream was earthed using a platinum tube attaching the PTFE tubing to the liquid junction T-piece. The integration of the two methods with respect to hardware, and also to compensate for differences in the respective lengths of tubing between the on-line supply and each 'detector', meant that it was impractical to flush the electrode with seawater exactly as documented in Section 4.2.2.2. and the maintenance of a regular flow regime through the spectrophotometer was considered essential. Solution temperature was measured by a thermistor inserted into the stream immediately after the electrode flowcell.

During spectrophotometric analyses, seawater was pumped at 12 $mL.min^{-1}$ from the laboratory supply through the spectrophotometer to waste. Phenol red stock solution (solid phenol red dissolved in seawater from the non-toxic supply) was circulated through the injection valve at 0.1 $mL.min^{-1}$ and injected for 5 seconds into the seawater stream approximately every 3 minutes. The approximation is another artifact of the integrative

nature of the pH set-up employed aboard ship; one main FORTRAN program directed instrument control and data acquisition for both techniques, and as the potentiometric readings during tris calibration waited for near constant potential (*i.e.* a drift in E_s of less than 0.6 $mV.min^{-1}$), there was variation in the timing of each command dependent on the electrode response rate. The frequency of measurements increased to $30h^{-1}$ when spectrophotometric measurements were made on their own. Absorption readings were reported as the mean of 20 measurements with standard deviation. pCO_2 was measured on-line using a GC method with showerhead equilibrator (Robertson *et al.*, 1993) approximately every 17 minutes (Robertson, 1993). TCO_2 was measured discretely using a coulometric method adapted from Robinson and Williams (1991). Sampling frequency was, at best, 20 analyses per day (Debney and Robertson, 1993). Total alkalinity was determined using a novel photometric method which suffered problems both with instrumentation and computer software (Knox, 1993). The data is presently being analysed (S. Knox, personal communication, 1994.).

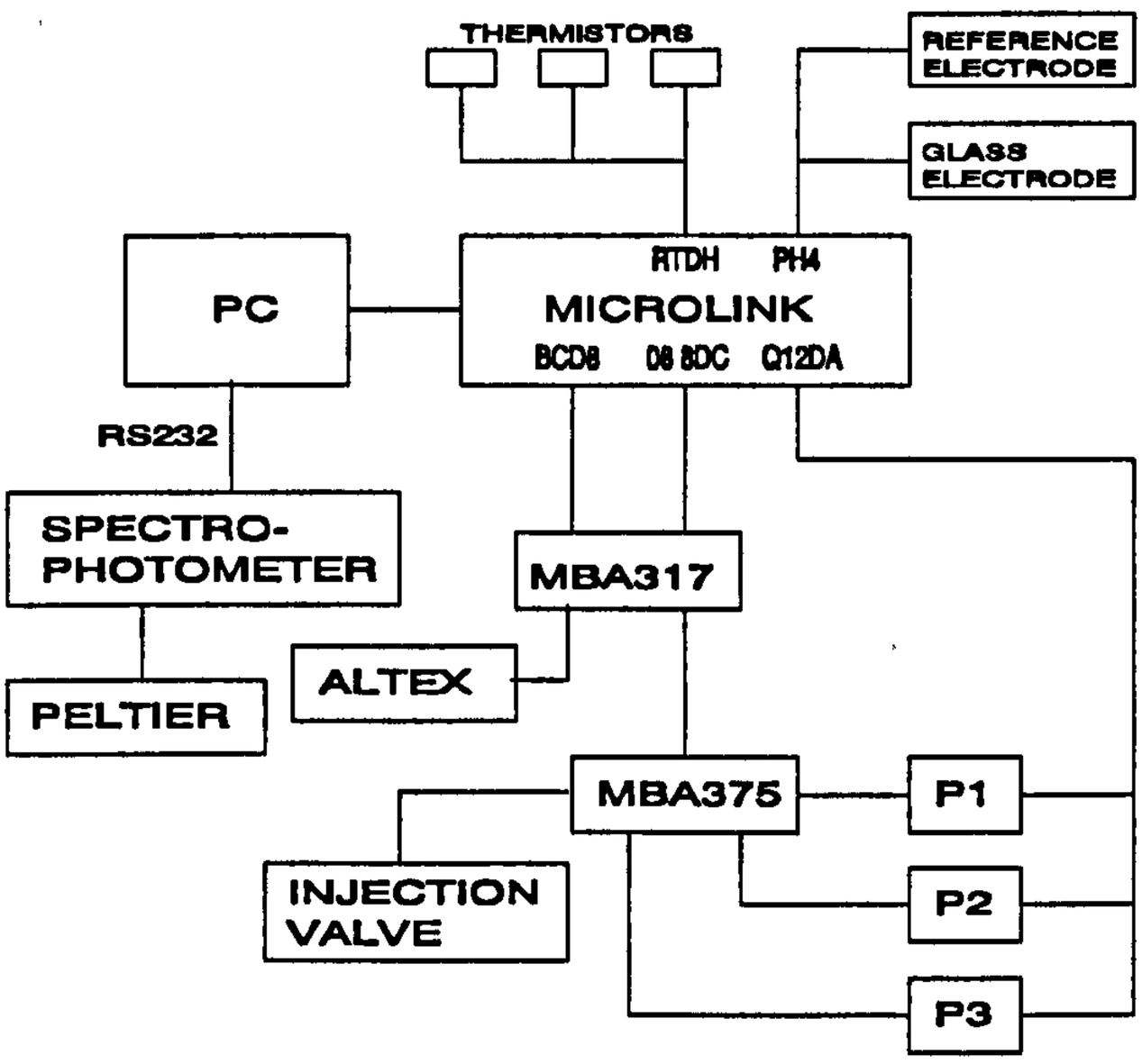

Figure 4.15. Schematic diagram of the hardware employed for the simultaneous determination of seawater pH using spectrophotometry and potentiometry. Units MBA375 and MBA317 controlled power supply to peristaltic pumps (P1, P2 and P3), the switching valve (Altex) and the injection valve. Microlink modules are described in the text (Section 4.2.2.3). Peltier thermostat was controlled by the computer via the spectrophotometer. Spectrophotometer control and data acquisition was via a bi-directional RS232C connection.

4.5. Results

4.5.1. At-sea spectrophotometric pH measurements

For all spectrophotometric seawater pH measurements on the cruise, values were calculated using the equation (Robert-Baldo *et al.*, 1985)

$$pH = pK_2 + \log\left(\frac{R - 0.0038}{(2.6155 - (R*0.1234))}\right) + 0.004\,(35 - S) \qquad 4.3.$$

where, $pK_2 = 7.491$ at 25°C, and $R = R_{25}$, the absorption ratio at 25°C, and S is salinity. The average residual for the pK - temperature relationship is 0.004 units (Robert-Baldo *et al.*, 1985).

As pK_2 was determined on the free hydrogen ion scale (Robert-Baldo *et al.*, 1985) and the carbonic acid constants used in this study (Equations 4.8. and 4.9.) are expressed on the total hydrogen ion scale including fluoride it was necessary to account for the effect of sulphate and fluoride association on the free hydrogen ion concentration in the seawater and thus convert pH values to the total hydrogen ion scale. Additionally, as the carbonic acid constants were determined, and TCO_2 measurements made, on the molinity scale, pH values were converted to this scale from the molality scale. All these corrections are fulfilled in the equation (Dickson, 1990b; 1993)

$$pH(SWS) = pm_H - \log(1 - 0.00106S) - \log(1 + m_{SO_4}\beta_{HSO_4}) - \log(1 + m_{HF}\beta_{HF}). \qquad 4.4.$$

The sulphate formation constant was calculated from the work of Dickson (1990b) and the fluoride formation constant from Dickson and Riley (1979).

An example of the data obtained by the spectrophotometric method is illustrated in Figure 4.16. Unfiltered, *i.e.* all values reported, data is plotted for the 1st survey across the South Polar Front in the Bellingshausen Sea. No x-axis labelling is used as the data is plotted against date and there is no geographical significance to the profile. A full report on pH in this area and for the rest of the cruise track is given in Chapter 5.

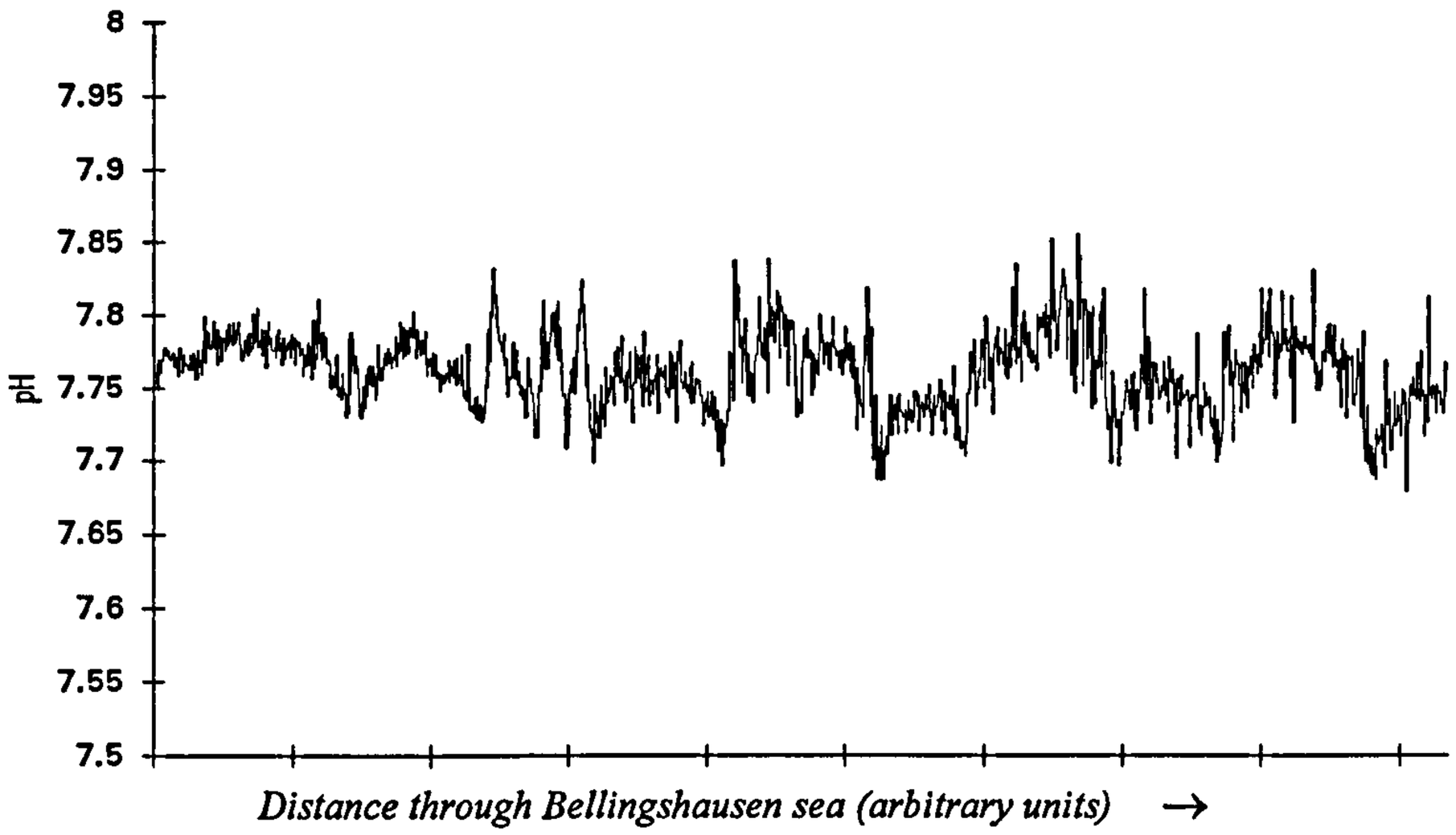

Figure 4.16. Example of unfiltered surface spectrophotometric pH(SWS) 25°C values. The profile is for survey 1 across the South Polar Front, Bellingshausen Sea.

4.5.1.1. Precision testing

Five discrete seawater samples were taken from the on-line supply over a period of 3 hours and their pH measured spectrophotometrically. The absorbance measurements at 433 and 558nm, the absorbance ratio (R) at the temperature of measurement (10°C), the ratio adjusted to 25°C, and the calculated pm_H (25°C) are listed in Table 4.4. The absorption ratio temperature conversion will be explained later in Section 4.5.1.2. Standard deviations of pH for each sample are also in Table 4.4. The weighted standard deviation over all of the five samples can be expressed as

$$SD = [(n_i * SD_i) + (n_j * SD_j) + \ldots)]/(n_i + n_j + \ldots) \qquad 4.5.$$

and corresponds to ± 0.005 unit, n = 106. This level of precision is consistent with the criterion for spectrophotometric pH measurements defined at the beginning of this study.

Table 4.4. Absorption measurements and associated absorption ratios and pH values obtained during precision testing on seawater samples.

A433	A558	Rt	R25	pmH
Sample 1				
0.230	1.040	4.522	4.997	8.058
0.173	0.795	4.594	5.077	8.067
0.174	0.802	4.609	5.093	8.068
0.180	0.825	4.578	5.059	8.065
0.176	0 805	4.581	5.062	8.065
0.179	0.818	4.573	5.053	8.064
0.183	0.830	4.542	5.018	8.060
0.179	0.808	4.508	4.981	8.056
0.179	0.815	4.567	5.046	8.063
0.171	0.786	4.589	5.071	8.066
0.175	0.797	4.554	5.032	8.062
0.180	0.819	4.550	5.028	8.061
0.180	0.814	4.532	5.008	8.059
0.176	0.797	4.526	5.001	8.058
			Mean	**8.062**
			SD	**0.004**
Sample 2				
0.190	0.881	4.633	5.119	8.071
0.192	0.880	4.585	5.067	8.066
0.192	0.881	4.593	5.075	8.066
0.190	0.875	4.601	5.084	8.067
0.191	0.880	4.595	5.078	8.067
0.189	0 872	4.620	5.105	8.070
0.193	0.888	4.597	5.079	8 067
0.186	0.874	4.688	5.181	8.078
0.194	0.890	4.586	5.068	8.066
0.189	0.864	4.564	5.043	8.063
0.185	0.853	4.622	5.107	8.070
0.187	0.865	4.629	5.115	8.071
0.194	0.885	4.566	5.045	8.063
0.186	0.848	4.556	5.034	8.062
0.184	0.846	4.603	5.086	8.068
0.186	0.844	4.542	5.019	8.060
0.191	0.871	4.567	5.047	8.063
0.183	0.830	4.538	5.014	8.060
0.187	0.853	4.574	5.054	8.064
0.183	0.846	4.633	5.119	8.071
0.179	0.825	4.608	5.092	8.068
0.175	0.807	4.619	5.104	8.070
0.181	0.834	4.612	5.097	8.069
0.184	0.837	4.550	5.027	8.061
0.188	0.848	4.521	4.996	8.057
0.177	0.816	4.611	5.095	8.069
0.168	0.773	4.614	5.098	8.069
0.182	0.838	4.615	5.099	8.069
0.178	0.814	4.586	5.068	8.066
0.170	0.777	4.564	5.043	8.063
0.169	0.801	4.732	5.229	8.084
0.167	0.779	4.672	5.163	8.076
0.169	0.783	4.637	5.124	8.072
0.165	0.768	4.649	5.137	8.073
0.169	0.779	4.610	5.094	8.069
			Mean	**8.068**
			SD	**0.005**
Sample 3				
0.197	0.880	4.466	4.935	8.050
0.191	0.854	4.477	4.947	8.052
0.200	0.905	4.526	5.002	8.058
0.201	0.900	4.476	4.946	8.052
0.200	0.892	4.468	4.937	8.051
0.196	0.884	4.519	4.994	8.057
0.195	0.863	4.433	4.899	8.046
0.200	0.891	4.454	4.921	8.049
0.197	0.876	4.437	4.903	8.047
0.193	0.885	4.597	5.080	8.067
0.189	0.876	4.631	5.117	8.071
0.193	0.866	4.500	4.973	8.055
0.194	0.869	4.483	4.953	8.053
0.181	0.831	4.593	5.075	8.066
0.186	0 850	4.563	5.042	8.063
0.188	0.858	4.568	5.047	8.063
			Mean	**8.056**
			SD	**0.008**
Sample 4				
0.189	0.854	4.512	4.986	8.056
0.190	0.858	4.519	4.993	8.057
0.189	0.878	4.655	5.144	8.074
0.187	0.869	4.653	5.141	8.074
0.190	0.874	4.597	5.080	8.067
0.181	0.844	4.651	5.139	8.074
0.187	0.855	4.570	5.050	8.064
0.198	0.918	4.636	5.122	8.072
0.190	0.876	4.617	5.102	8.069
0.190	0.887	4.673	5.163	8.076
0.189	0.882	4.658	5.148	8.075
0.189	0 888	4.709	5.204	8.081
0.195	0.903	4.629	5.115	8.071
0.191	0.872	4.554	5.033	8.062
0.191	0.882	4.628	5.114	8.071
0.183	0.860	4.694	5.187	8.079
0.189	0.870	4.606	5.090	8.068
0.187	0.853	4.563	5.042	8.063
			Mean	**8.070**
			SD	**0.007**
Sample 5				
0.252	1.112	4.412	4.875	8.044
0.195	0.874	4.492	4.964	8.054
0.193	0.870	4.499	4.971	8.055
0.198	0.891	4.508	4.981	8.056
0.191	0.862	4.508	4.981	8.056
0.209	0.938	4.479	4.949	8.052
0.265	1.182	4.455	4.923	8.049
0.206	0.920	4.474	4.944	8.052
0.204	0.921	4.509	4.982	8.056
0.196	0.882	4.491	4.962	8.054
0.210	0.942	4.490	4.961	8.054
0.200	0.901	4.499	4.972	8 055
0.258	1.148	4.448	4.916	8.048
0.200	0.900	4.497	4.969	8.054
0.203	0.909	4.488	4.959	8.053
0.191	0.869	4.543	5.020	8.060
0.195	0.878	4.498	4.970	8.055
0.192	0.864	4.507	4.980	8.056
0.247	1.095	4.438	4.904	8.047
0.192	0.864	4.504	4.977	8.055
0.190	0.854	4.485	4.956	8.053
0.191	0.857	4.492	4.963	8.054
0.189	0.858	4.531	5.007	8.059
			Mean	**8.053**
			SD	**0.004**
		Weighted Mean SD		**0.005**

4.5.1.2. Characterising the temperature dependence of the absorption ratio of phenol red

When using flow injection analysis it is preferable to introduce the solution into the flow cell at the measuring temperature in order to speed analysis. Shipboard chemical analyses are commonly performed under transient local environmental conditions and as solutions carried in PTFE tubing rapidly equilibrate with room temperature there may be circumstances, as experienced during this work, when room temperature and, thus, solution temperature control is not stringent. Molar absorptivity ratios for phenol red have only been determined at 25°C (Robert-Baldo *et al.*, 1985) and as such any deviation of the sample from this temperature will incur an error in the resultant pH when using Equation 4.3. There were times, therefore, when the temperature of the Peltier thermostat was changed to approximate room temperature and it was, therefore, necessary to characterise the temperature dependence of the absorption ratio of phenol red in seawater to account for any such deviation from 25°C. The method of Breland and Byrne (1993) used to characterise the temperature dependence of the absorption ratio of bromocresol green in seawater was adapted. After the cruise, solid phenol red was added to seawater, $S \approx 33.7$, to furnish an absorbance of about 0.8 at 558 nm and 25°C. Absorption measurements were taken at 433, 558 and 730 nm for both a seawater blank and the seawater/indicator solution over the temperature range 18 - 27°C. All measurements were taken at night when the room temperature was the most stable as throughout the day the instrument drifted excessively with extreme changes in room temperature. The absorption ratio is calculated from the equation

$$R = \frac{A_{558}}{A_{433}} \qquad 4.6.$$

after any drift has been accounted for. The temperature relationship of the normalised ratio (R_t/R_{25}), where R_t is the absorption ratio at the temperature of measurement (t°C) and R_{25} is the ratio at 25°C, is illustrated in Figure 4.17. This relationship corresponds to a change in R of 0.7 % for every °C variation, or expressed in mathematical form:

$$R_{25} = R_t(1 - 0.007(25 - t)) \qquad 4.7.$$

where 18 °C < t < 27 °C. The average residual, the difference between the best fit line and the empirical points is 0.005 ± 0.009 R, which for a typical value from the cruise for R of 4.5 corresponds to an error of 0.0006 ± 0.001 pH unit.

4.5.2. At-sea potentiometric pH measurements

For all potentiometric measurements, buffer pH was calculated on the total hydrogen ion scale using Equations 3.11. to 3.15b., taking salinity to be 35. Seawater pH was then calculated from Equation 3.20 assuming a constant residual liquid junction potential for both standard and seawater electrode potential measurements.

The unfiltered surface pH values for a survey across the divergence zone are shown in Figure 4.18. The trace is erratic with large changes in pH not illustrated on a similar profile of spectrophotometric pH (see Figure 4.16). Throughout the cruise there were problems in maintaining consistency between the temperature of the buffer and sample. In addition, there were surges in the electrical circuit from the 'clean' supply resulting in spikes which were also reported on other instruments in the laboratory. Electrode potential may have been affected by the stop/start regime of the seawater flow and also the rate differential between the buffer and sample flow was large and in both cases the flow characteristics were changed from those ascribed as 'optimum' in Section 4.2.2.4.

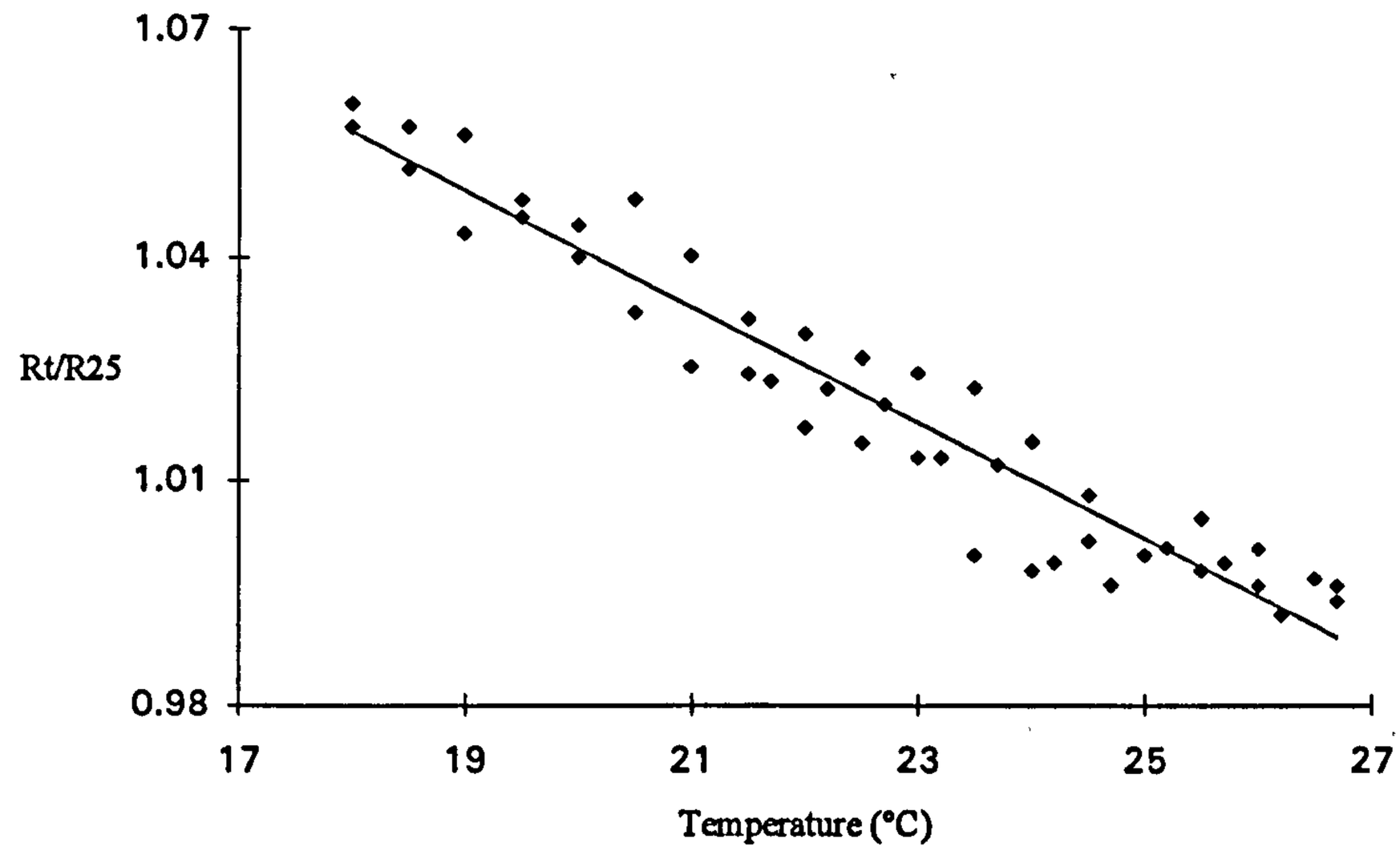

Figure 4.17. Temperature dependence of the normalised absorption ratio of phenol red in seawater.

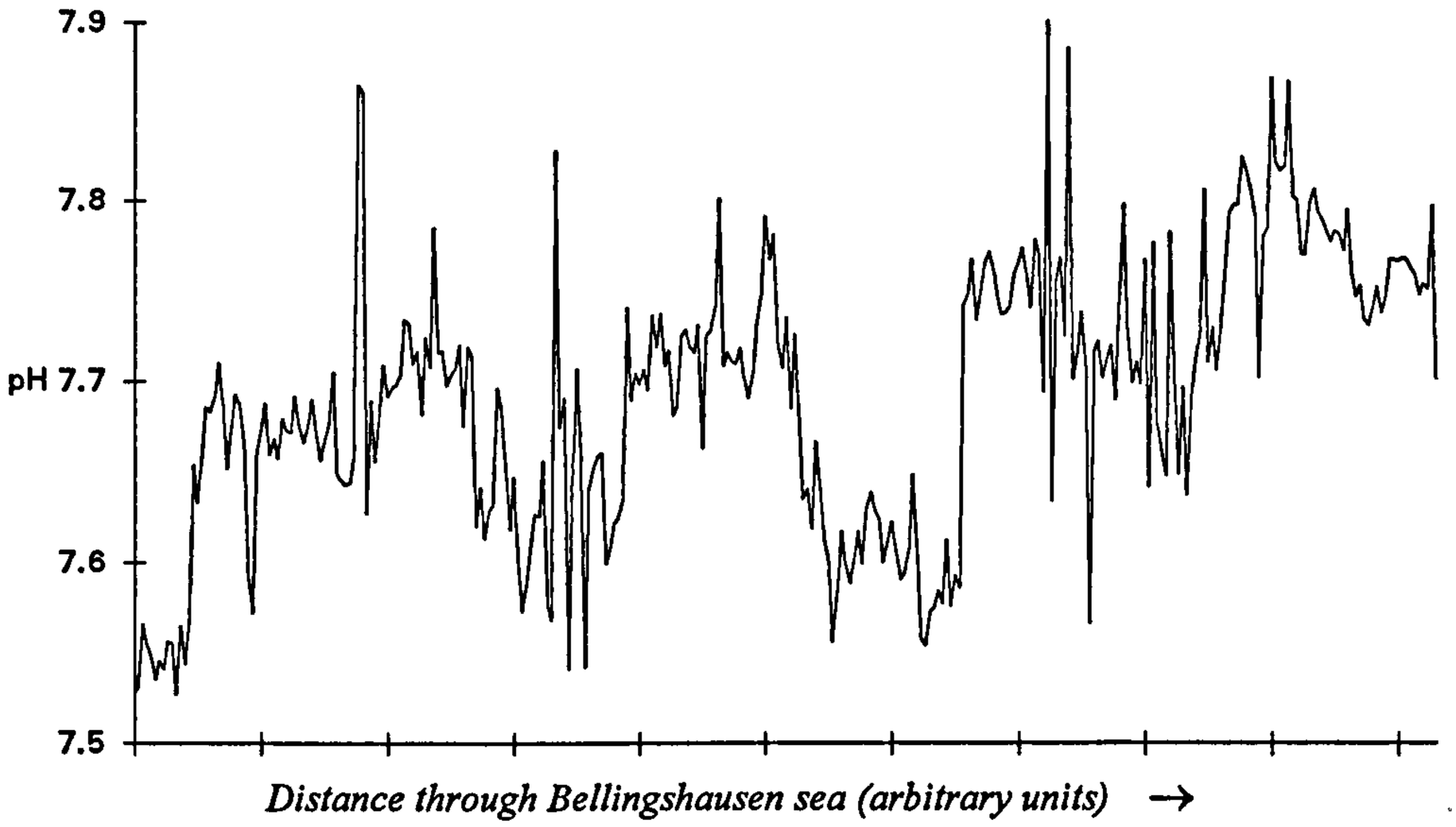

Figure 4.18. Surface potentiometric pH(SWS) (25°C) readings determined during survey 1 across the Antarctic Divergence Zone, Bellingshausen Sea.

4.5.3. Calibration of the spectrophotometric technique

Over-determination of the carbonate system through the concomitant measurement of pH, pCO_2 and TCO_2 allows an assessment of the performance of the spectrophotometric technique via the bilateral determination of total alkalinity. Alkalinity was calculated from pH(SWS) (25°C) and TCO_2, and pCO_2 (*in situ* temperature) and TCO_2 using the carbonic acid dissociation constants of Goyet and Poisson (1989)

$$pK_1 = 812.27/T + 3.356 - 0.00171*S*\ln T + 0.000091*S^2 \qquad 4.8.$$

$$pK_2 = 1450.87/T + 4.604 - 0.00385*S*\ln T + 0.000182*S^2 \qquad 4.9.$$

on the molinity scale. Residual alkalinities (dAlk), the difference in alkalinities determined from the two combinations, are illustrated in Figure 4.19. and correspond to

$$dAlk = 1.3 \pm 7.3\ \mu equiv.kg^{-1}\ seawater \qquad 4.10.$$

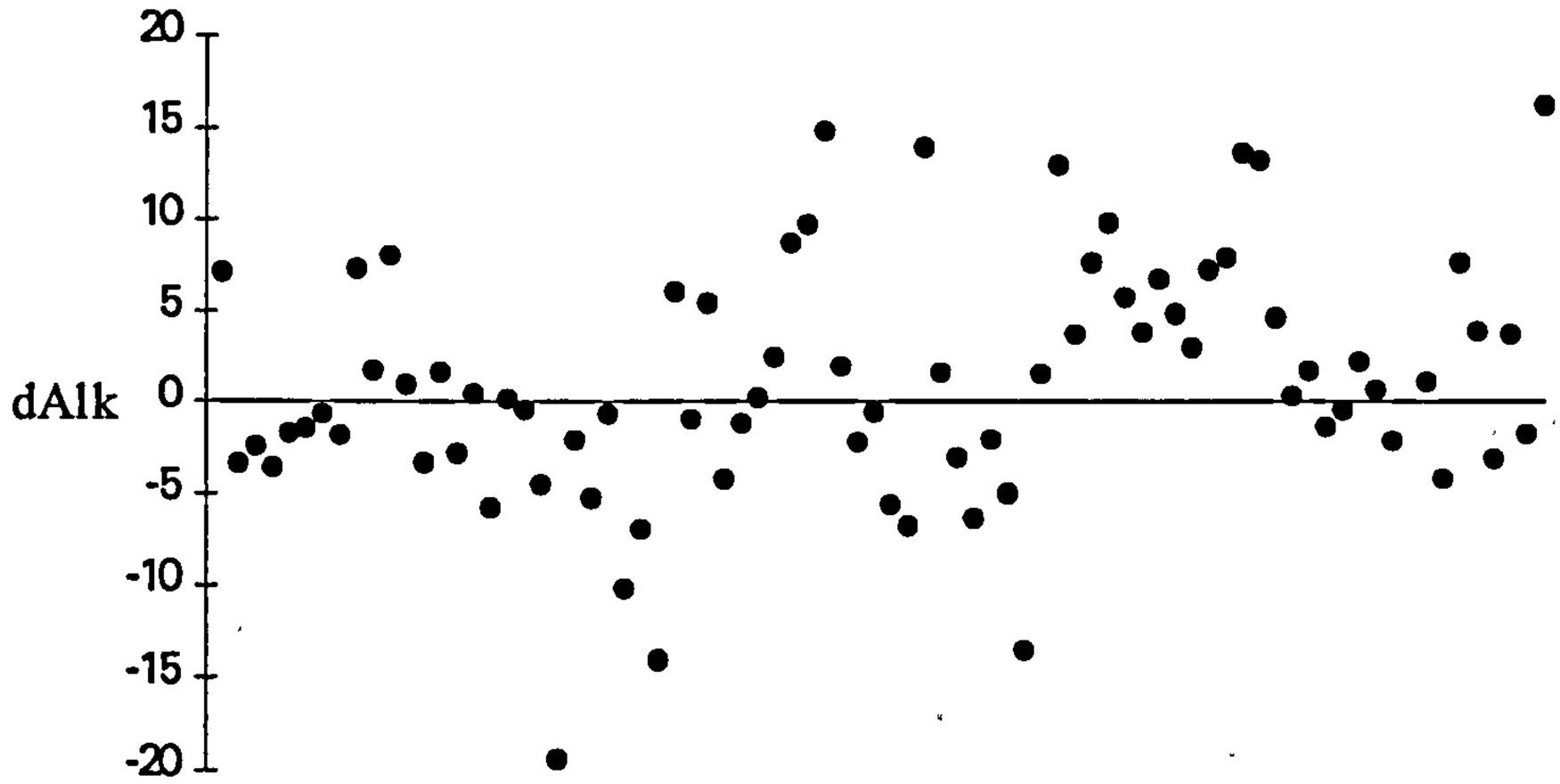

Figure 4.19. Difference between alkalinity calculated from pH(SWS) (25°C) and TCO_2, and pCO_2 (in situ temperature) and TCO_2 using the carbonic acid dissociation constants of Goyet and Poisson (1989) on the molinity scale. dAlk is shown as μequivalents.kg^{-1} seawater

$n = 79$. The average alkalinity for the stations was 2304.9 ± 11.2 μequiv.kg^{-1} seawater and therefore the residual agrees to about 0.32 %.

The specific alkalinity (SA), which is the alkalinity divided by the salinity, for the samples is 68.100 ± 0.281. The residual SA, the difference between the SA calculated from the two pairings used in the alkalinity comparison, has a residual of 0.39 %.

The theoretical precision of the alkalinity comparison was calculated following a method of Dickson and Riley (1978). The change in a derived parameter resulting from a change in the measured variables can be represented by (Dickson and Riley, 1978).

$$\mathrm{var}\left[\frac{(y_j)}{y_j^2}\right] = \sum_i \left[\frac{\delta y_j}{y_j}\right] \Big/ \left[\frac{\delta x_i}{x_i}\right]^2 \mathrm{var}\left[\frac{(x_i)}{x_i^2}\right]. \qquad 4.11.$$

Partial derivatives (δy/y)/(δx/x) corresponding to a 1% increase in the measured parameters are listed in Table 4.5. Using these derivatives and the percentage precision of the measured parameters (listed in Table 4.6.) it is possible to determine the percentage error in the

calculated variable. Percentage errors in the calculated parameter resulting from the use of all carbon dioxide parameter pairings are listed in Table 4.7.

Table 4.5. Partial derivatives corresponding to a 1% increase the measured parameters. Adapted from Dickson and Riley (1978).

Calculated parameter	Measured parameters		Partial Derivatives						
			pH	pCO_2	TCO_2	alk	Kp	K_1	K_1
alk	TCO_2	pCO_2	0.00	-0.09	1.10	0.00	-0.09	-0.08	-0.08
alk	pH	pCO_2	-1.20	1.00	0.00	0.00	1.00	1.00	0.21
alk	TCO_2	pH	-0.10	0.00	1.00	0.00	0.00	0.00	0.09
pH	TCO_2	pCO_2	0.00	0.90	-0.89	0.00	0.90	0.89	0.11
TCO_2	pCO_2	pH	-1.10	1.00	0.00	0.00	1.00	1.00	0.12
pCO_2	TCO_2	pH	1.10	0.00	1.00	0.00	-0.99	-0.98	-0.12
TCO_2	alk	pH	0.10	0.00	0.00	1.00	0.00	0.00	-0.09
pCO_2	alk	pH	1.20	0.00	0.00	1.00	-0.99	-0.99	-0.21
TCO_2	alk	pCO_2	0.00	0.08	0.00	0.92	0.08	0.08	-0.08
pH	alk	pCO_2	0.00	0.82	0.00	-0.82	0.82	0.82	0.18
pH	TCO_2	alk	0.00	0.00	10.80	-9.20	0.00	0.05	0.95
pCO_2	TCO_2	alk	0.00	0.00	13.20	-10.30	-0.99	-0.94	0.94

Table 4.6. Analytical precision and percentage precision of the techniques employed during this study.

Parameter	precision	% precision	Reference
pH	± 0.005 units	1.15	This study (spectrophotometry)
pCO_2	± 2 µatm.	0.56	Robertson *et al.* (1993).
TCO_2	± 1 µmol.kg	0.05	Robinson and Williams (1991)
alkalinity*	± 1 µmol.kg	0.05	Bradshaw and Brewer (1989)

* - alkalinity precision is included for completeness in Table 4.7.

Table 4.7. Percentage errors in the calculated parameter resulting from the use of carbon dioxide parameter pairings and the partial derivatives listed in Table 4.5. The analytical precisions used in the calculation of the errors are listed in Table 4.6.

Calculated parameter	Measured parameters		% error in calculation	% error in calculation - observed
alk	TCO_2	pCO_2	0.23	0.23
alk	pH	pCO_2	2.10	2.10
alk	TCO_2	pH	0.24	0.25
pH	TCO_2	pCO_2	1.37	1.79
TCO_2	pCO_2	pH	1.99	1.99
pCO_2	TCO_2	pH	1.88	1.97
TCO_2	alk	pH	0.24	0.25
pCO_2	alk	pH	2.01	2.09
TCO_2	alk	pCO_2	0.22	0.23
pH	alk	pCO_2	1.30	1.74
pH	TCO_2	alk	2.30	2.57
pCO_2	TCO_2	alk	2.67	2.73

With most relevance to this study, the combination of TCO_2 and pCO_2 results in an error of 0.23 % in the calculation of total alkalinity whilst the combination of TCO_2 and pH has an error of 0.24 %. The total error incurred when comparing the derived alkalinities is thus

$$\% \text{ error} = \sqrt{0.23^2 + 0.24^2} = 0.34\ \% \qquad 4.12.$$

which indicates that the actual combined imprecision of the analytical techniques is similar to that which their individual imprecisions would suggest, and the methodologies employed to measure the carbonate system during this cruise exhibit excellent internal consistency.

Although it is preferable to report pH at *in situ* conditions, the analysis of seawater

under these situations is not always practical and it is generally the case that pH is reported at the temperature of measurement. pH measured on an ionic medium (pH(SWS) or pm_H) scale at 25°C is corrected to the *in situ* pH for surface waters, *i.e.* with no pressure effects, using the relationships of Millero (1979):

$$pH_t = pH_{25} + A(t - 25) + B(t-25)^2 \qquad 4.13.$$

where t is the *in situ* temperature, and

$$A = (-9.296 - 32.505(pH_{25} - 8) + 63.806(pH_{25} - 8)^2)/1000 \qquad 4.14.$$

$$B = (3.916 - 23.000(pH_{25} - 8) + 41.637(pH_{25} - 8)^2)/10000. \qquad 4.15.$$

Equations 4.13. to 4.15. were used to calculate *in situ* pH values for the samples used in the alkalinity comparison. pH(SWS) was calculated using varying relationships for the formation constant of hydrogen sulphate according to Khoo *et al.* (1977), Millero (1986) and Dickson (1990b). The resultant pH values are shown in Figure 4.20. with *in situ* pH(SWS) calculated from TCO_2 and alkalinity (calculated from pCO_2 and TCO_2).

Problems with biofouling of the flowcell were encountered after the completion of the first survey, when air bubbles were frequently seen to stick in the aperture. Values of pH(SWS) calculated from alkalinity and TCO_2 (alkalinity calculated from TCO_2 and pCO_2) have been overlaid on the pH(SWS) profile (Figure 4.21.) from a leg from the second survey to illustrate the offsets produced by the detritus and bubbles. No long term improvement was evident after flushing the system with DECON or 0.1 M HNO_3. This problem of biofouling has recently been noted by researchers at Scripps Institute of Oceanography (A.G. Dickson, personal communication) and they have reduced the problem employing regular flushing of sample tubing and flow cells with *aqua regia*. It may also be desirable to filter the seawater before it enters the instrument though this will incur additional problems with filter blockage in highly productive waters.

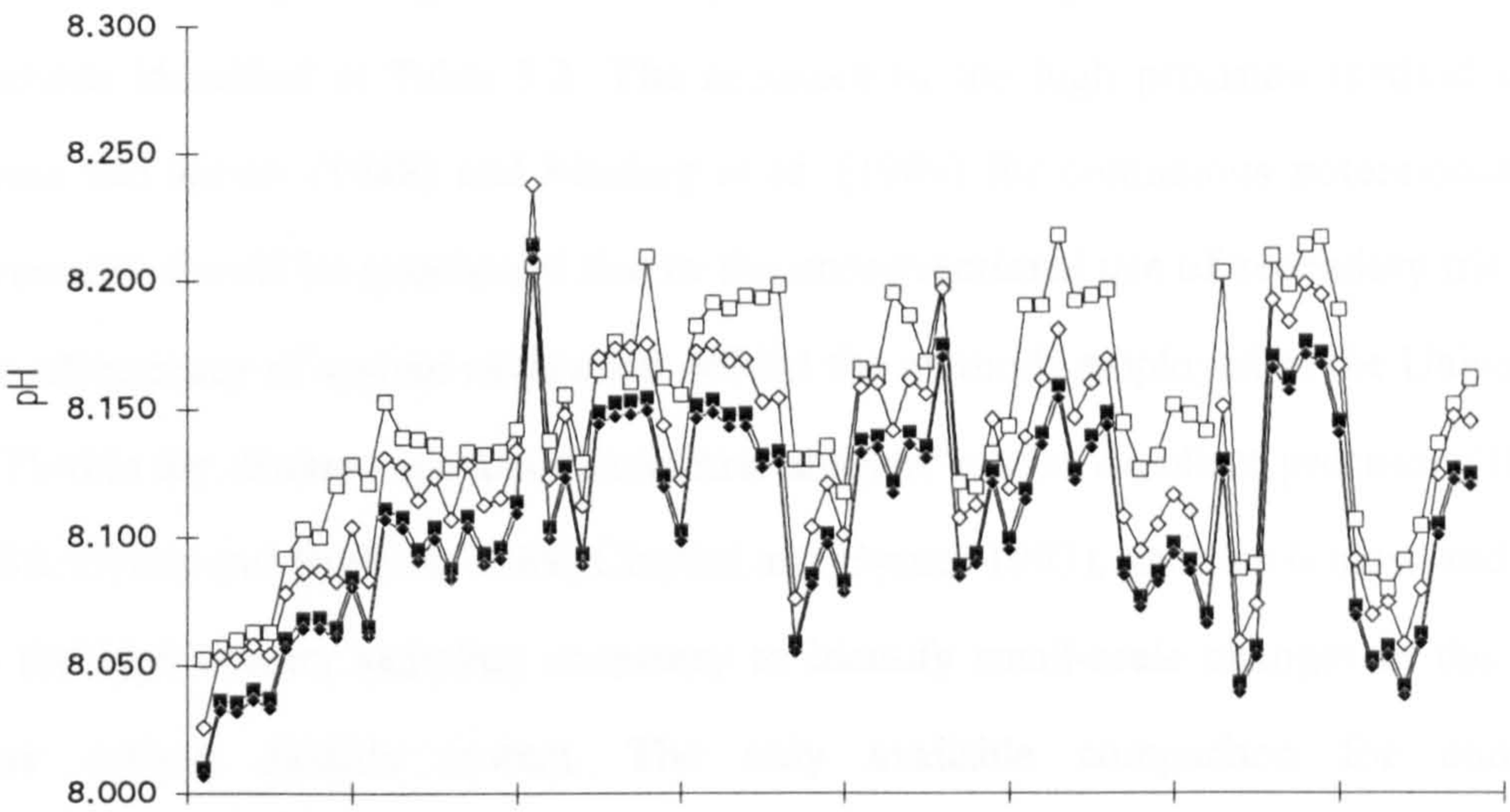

Figure 4.20. Comparison of in situ pH(SWS) calculated from TCO_2 and alkalinity (- □ -) and measured spectrophotometric pH. pm_H values have been first converted to the pH(SWS) scale using sulphate formation constants calculated from: (1) - ◊ - Dickson (1990b), (2) - ■ - Khoo et al. (1977) and (3) - ♦ - Millero (1986) and the fluoride formation constant of Dickson and Riley (1979) and then to in situ temperature using the equations of Millero (1979).

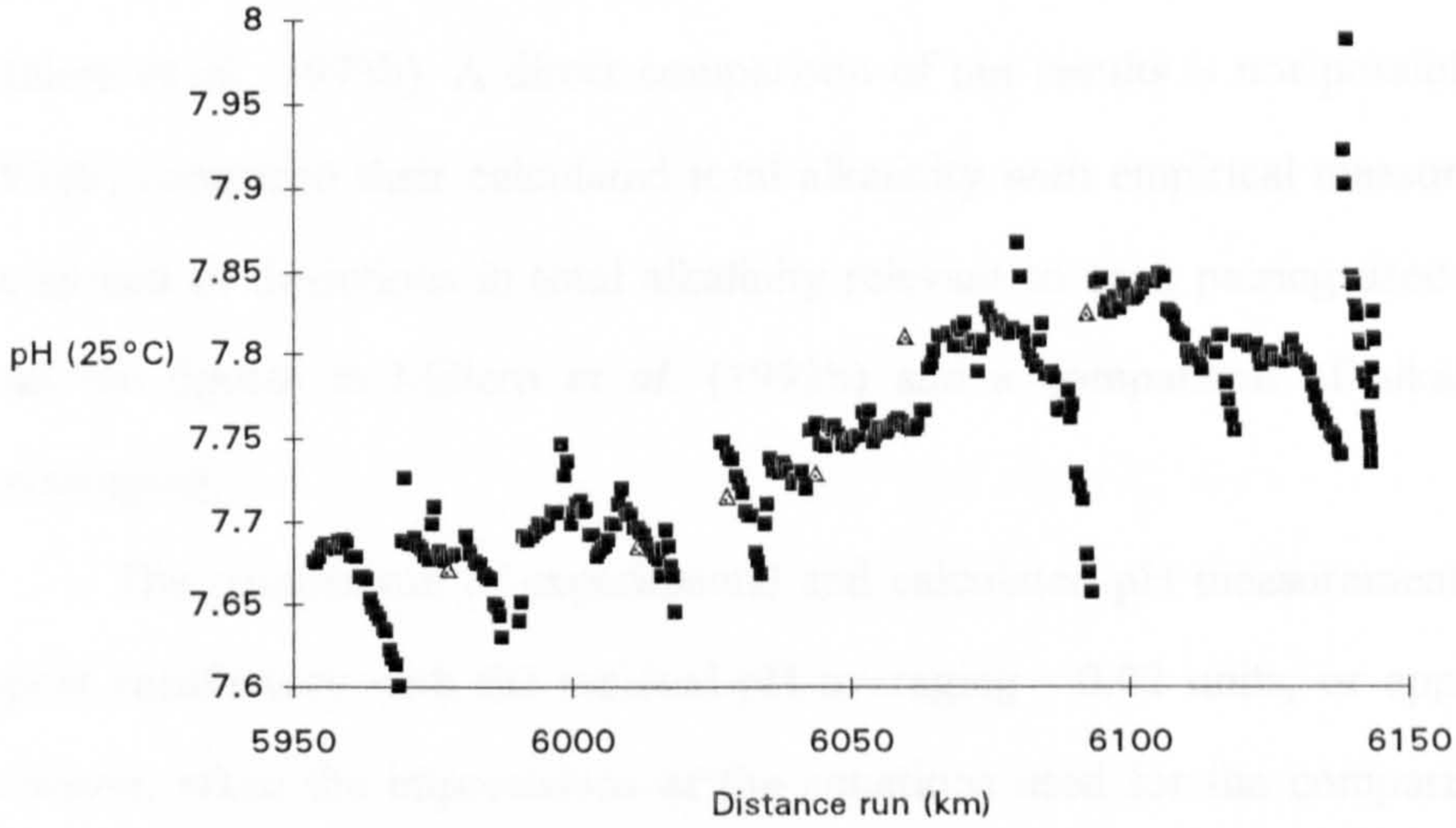

Figure 4.21. Example of a pH profile from the second survey. The drifting due to bubbles can be seen on the trace. Calculated pH values (triangles) are overlaid.

4.6. Discussion

The precision shown by the spectrophotometric method as verified by replicate measurements on single samples is ± 0.005 pH unit. This compares favourably with many of the methods identified in Table 3.2. The accuracy of the high precision method used by Fuhrmann and Zirino (1988) and Mackey *et al.* (1989) for continuous potentiometric pH measurements should be questioned due to the unconventional use of secondary tris buffers and the infrequency of system calibration. Whilst the methods employed at the University of South Florida for discrete spectrophotometric analysis exhibit excellent precision (Byrne *et al.*, 1988; Byrne and Breland, 1989; Clayton and Byrne, 1993), analysis is slow and cannot supply the high density sampling necessary to identify small-scale changes in the surface seawater carbon dioxide system. The only available comparison for continuous spectrophotometric measurements is with the work of Pia *et al.* (1990) who, analysing poorly buffered, low ionic strength solutions using a flow injection technique, attained a precision of only ± 0.2 pH unit.

The internal consistency of the carbon dioxide parameters measured on the cruise has been shown to be greater than that expected from the individual precisions of the methods employed. Total alkalinity calculated from the pairings of pH(SWS) and TCO_2, and pCO_2 TCO_2 agree with a precision of 0.32 %. This is good and compares well with work done recently in the Equatorial Pacific measuring all the carbon dioxide parameters (Millero *et al.*, 1993b). A direct comparison of our results is not possible as Millero *et al.* (1993b) compared their calculated total alkalinity with empirical measurements. However, the spread of deviations in total alkalinity relevant to each pairing used above is available from the figures in Millero *et al.* (1993b) and a comparison of alkalinity variations is encouraging.

The comparison of experimental and calculated pH measurements does not at first appear satisfactory with the residual pH averaging - 0.02 units, or approximately 4.6 %. However, when the imprecisions of the equations used for the comparison are taken into account there is an inherent error estimated at 4 % which rises to 5 % when the imprecision of the temperature conversion equations are accounted for. It should also be noted that in developing the pH/temperature relationships, Millero (1979) used the carbonic acid

constants of Hansson (1973a) where as this study has calculated the *in situ* pH from alkalinity and TCO_2 using the constants of Goyet and Poisson (1989). Also, Millero (1979) assumed a specific alkalinity (alkalinity/salinity) of 68.57 and from the alkalinity comparison it is apparent that the specific alkalinity was about 68.10.

There are some necessary comments on the spectrophotometric method and in particular the choice of indicator and its application. It is preferable to employ an indicator with a pK_2 close to the pH of the measured solution, the absorption ratio will then be near unity and any drift or deviation from the true absorption value at either wavelength will have a reduced effect on the final pH. Deviations may have been incurred directly through the use of phenol red as the indicator, with a pK_2 of 7.491 at 25°C (Robert-Baldo *et al.* (1985), when measuring seawater of approximately 7.65 - 7.85 pH units. Table 4.8. lists the changes in calculated pH from assumed errors in absorbance readings at both wavelengths (433 and 558 nm) for all pm_H measurements made during the alkalinity pH comparisons. It can be seen that significant errors are associated with changes in absorption measurements. The use of a spectrophotometer measuring one wavelength at a time does not allow for an assessment of the extent of drift between blank and indicator measurements, and indeed between wavelength changes. This problem would be reduced through instantaneous multiwavelength measurements afforded by diode array spectrophotometry.

The concentration of indicator solution and the mixing ratio, *i.e.* the dilution of the sample through addition of the indicator solution, for reviewed spectrophotometric techniques are listed in Table 4.9. The effect of the addition of indicator solution on the pH of the sample has been studied by Clayton and Byrne (1993) and was found to change the final pH by < 0.005 unit. Their method, however, used a stock solution of indicator (*m*-cresol purple) dissolved in deionised water. This water has a pH of ~ 5.8, adjusted to ~ pH 6.65 with NaOH (Clayton and Byrne, 1993) and will therefore involve a more significant change in pH than that suggested by this study where the indicator was dissolved in seawater of a similar pH to the test seawater.

Inconsistencies amongst workers studying the formation of hydrogen sulphate in seawater and the subsequent problems with the use of the free hydrogen ion scale are highlighted in this work. The difference in pH encountered when using the formation constant determined from Dickson (1990b) and those constants reported by Khoo *et al.*

(1977) and Millero (1986) amounts to about 0.02 units after pH values have been converted to *in situ* pH(SWS) values. To avoid using the free hydrogen ion scale it is preferable to define the pK_2 of phenol red on the total hydrogen ion scale which includes implicitly the effect of hydrogen sulphate. This is in line with current thinking on pH scales (Clayton and Byrne, 1993; Dickson, 1993). Millero *et al.* (1993a) has characterised the pK_2 - temperature relationship for salinity of 35. The deficiency of any salinity relationship has precluded the use of the Millero *et al.* (1993a) pK_2 values in this work.

The low temperatures encountered during the cruise are not covered in some of the empirical equations used in this study. The carbonic acid dissociation constants (Equations 4.8. and 4.9.) have been determined for $-1°C < t < 40°C$ (Goyet and Poisson, 1989) and Millero (1979) reports that the equations expressing the pH - temperature relationship are valid from $0°C < t < 40°C$. Seawater temperatures were often less than -1.5°C and thus data obtained through extrapolation of the fit afforded to each equation are assumed to be true.

Table 4.8. Errors in calculated pm_H incurred from deviations in absorbance readings averaged over all the absorbance values used in the calibration of the spectrophotometric technique.

	Error in absorbance					
Wavelength(s)	0.001	0.002	0.003	-0.001	-0.002	-0.003
A_{558}	0.001	0.002	0.003	-0.001	-0.002	-0.003
A_{433}	-0.002	-0.008	-0.011	0.005	0.009	0.013
A_{558} and A_{433}	-0.003	-0.007	-0.011	0.004	0.007	0.001

Table 4.9. Indicator properties employed for the measurement of pH used by selected authors for the spectrophotometric determination of solution pH

Study	Indicator	Mixing ratio	cell pathlength (cm)	Final indicator concentration (moles.L^{-1})
Robert-Baldo *et al.*,1985.	PR.	< 1:600	10	$2x10^{-6}$
Acker *et al.*, 1987.	PR.	not given	variable‡	$8x10^{-6}$
Byrne, 1987.	PR, TB, BTB.	not applicable†	1	$\leq 7x10^{-5}$
Byrne *et al.*, 1988.	PR.	1:125 and 1:400	10 and 2.75±0.3‡	not given
Byrne and Breland,1989.	CR.	1:600	10	$3x10^{-6}$
King and Kester,1989.	TB,BPB,BCG BCP,PR.	~1:1000	10	$1\text{-}2x10^{-6}$
Pia *et al.*, 1990.	MR, MY, NR	1:50	1	not given
Yamazaki *et al.*, 1992.	TB,BCG.	1:6	not given	$2x10^{-5}$
Clayton and Byrne,1993.	*m*-CP	1:375	10	$5x10^{-6}$
This study.	PR.	1:120	1	~ $8x10^{-5}$ ‡‡

PR - Phenol red
TB - Thymol blue
BTB - Bromothymol blue
CR - Cresol red
MR - Methyl red
MY - Methyl yellow
NR - Neutral Red
m-CP - *m*-Cresol Purple

‡ -variable pathlength used
† -indicator added in solid from
‡‡ -apparent concentration required to furnish A_{558} values of ~ 0.8 using mixing ratio and final indicator concentrations according to Robert-Baldo *et al.* (1985).

4.7. Conclusions

During this study a continuous potentiometric pH system has been optimised for laboratory pH measurement and a novel flow injection spectrophotometric method has been introduced and its performance evaluated. Both systems are fully automated for instrument control and data acquisition. A new flow cell has improved the performance of the potentiometric system through the reduction in bubble entrapment and increasing the temperature control over the tubing, buffer reservoirs, liquid junction and reference electrode has reduced the potential drift. The optimum response time of the glass electrode when switching from one solution to another has been determined and is achieved by flushing the electrode for 60 seconds with the new solution at 1.84 $mL.min^{-1}$ from a standing flow of 0.44 $mL.min^{-1}$.

The spectrophotometric method has shown an encouraging precision of better than ± 0.02 pH unit using phenol red on freshwater samples which is an order of magnitude better than found in the literature for low ionic strength solutions. The effect of pulsing apparent from the peristaltic nature of the indicator pump on the absorbance signal has been reduced by adopting an injection time of 5 seconds and adjusting the mixing coil length to 1m. This was also seen to avoid problems with lateral movement of the plug once the pump had stopped. The dilution by the indicator solution was assumed not to affect the pH of the sample.

Shipboard potentiometric studies on seawater pH have illustrated erratic results which are not in agreement with the spectrophotometric method operated simultaneously from the same seawater source. Problems with maintaining consistency of solution temperature, as well as a comparable flow across the glass electrode, between potential measurements in buffer and sample were encountered. In addition, there were inconsistencies in the electrical circuit resulting in spikes from the 'clean' supply.

The spectrophotometric method developed as part of this study has exhibited good precision (± 0.005 pH unit) concordant with the stated aims of the research. The internal consistency of the CO_2 parameters successfully measured during the cruise is excellent and lies within the expected imprecision afforded by the comparison of calculated alkalinities. Although large discrepancies exist between calculated pH values at *in situ* temperatures, these also rest on or within the inherent imprecision of the comparison when the sulphate formation constant of Dickson (1990b) is used. Greater residuals are found when the constants of Khoo *et al.* (1977) and Millero (1986) are used. Uncertainties with the extent of this dissociation will be overcome through the universal adoption of the total hydrogen ion concentration scale for pH measurements. The error afforded by the temperature conversion equations could be avoided if pH was analysed at *in situ* temperature.

CHAPTER 5.

CARBON DIOXIDE CHARACTERISTICS OF THE SURFACE WATERS OF THE BELLINGSHAUSEN SEA, SOUTHERN OCEAN

5.1. Introduction to the Southern Ocean

The Southern Ocean is the only body of water circumnavigating the globe. It is also in contact with, and mutually influenced by, three of the world's oceans. Wind stress is the dominant forcing agent of the surface ocean currents around Antarctica and there is generally a deep mixed layer. The extremes in solar radiation witnessed by the area generate an environment where ice formation has a dominant role in controlling both physical and biogeochemical features of the ocean. The Ocean is approximately 47 x 10^6 km^2 and the maximum and minimum ranges of ice cover indicate that about 19 x 10^6 km^2 of the surface waters are traversed by the ice edge (Gloerson *et al.*, 1992).

The transient ice response to changes in solar input is a major factor controlling the biogeochemical properties of the Southern Ocean. Ice cover constrains primary productivity through reductions in the amount of photosynthetically available radiation in the surface waters, and acts as a barrier to gas exchange between the atmosphere and the ocean. This latter point has significant implications for the role of the formation of deep waters as conduits for gas transfer to the deep oceans. Stabilisation of the surface waters through the release of fresher water during ice-melt leads commonly to the formation of plankton blooms.

This first section describes the main hydrographical features of the Southern Ocean and the influence of ice cover on the physical environment and the importance of the marginal ice zone is discussed with respect to biological activity. A review of work done on the carbon dioxide system and the importance of the Southern Ocean as a sink for atmospheric CO_2 is given.

5.1.2. Physical Characteristics

5.1.2.1. Hydrography

The currents around Antarctica are mainly the result of wind stress, with additional localised topographical forcing which may be terrestrial or submarine in origin. Density currents result from the downwelling of cold, saline waters which are the product of ice formation at the sea surface. Intrusions of 'warm', saline waters at middle depths originating from high latitudes in the northern hemisphere are seen to upwell.

Disregarding any mesoscale events, the hydrography of the Southern Ocean has historically been divided into three latitudinal sections, with markedly contrasting thermohaline properties, separated by distinct transitional zones. From the Antarctic mainland heading north these are the *East Wind Drift* which is separated from the *Antarctic Circumpolar Current* (ACC) by the *Antarctic Divergence Zone* (ADZ) now termed the *Continental Water Boundary* (CWB) (Read *et al.*, 1994). The ACC is partitioned by the *Polar Front* with Antarctic water to the south and Subantarctic water to the north, which is bounded itself to the north by the *Subtropical Convergence Zone*. The main currents and frontal positions are shown in Figure 5.1.

The Continental Water Boundary

High atmospheric pressure over the Antarctic mainland causes a semi-permanent, anti-clockwise wind circulation over and around the extremities of the continent. Consequently, this creates an ocean current close to the mainland, the East Wind Drift, which flows against the typical easterly flow of the waters to the north in the ACC. Coriolis forcing results in Ekman transport to the left of the respective currents and thus upwelling occurs to conserve mass in the area. Additionally, the zone is characterised by localised upwelling events with isopycnals sloping both to the north and south. Surface water to the South of the CWB is the coldest of the Southern Ocean with temperatures from -0.5 °C to as low as - 1.9 °C - the freezing point of seawater at the salinities found in the East Wind Drift - and the salinity is generally less than 34.5 (Pickard and Emery, 1982).

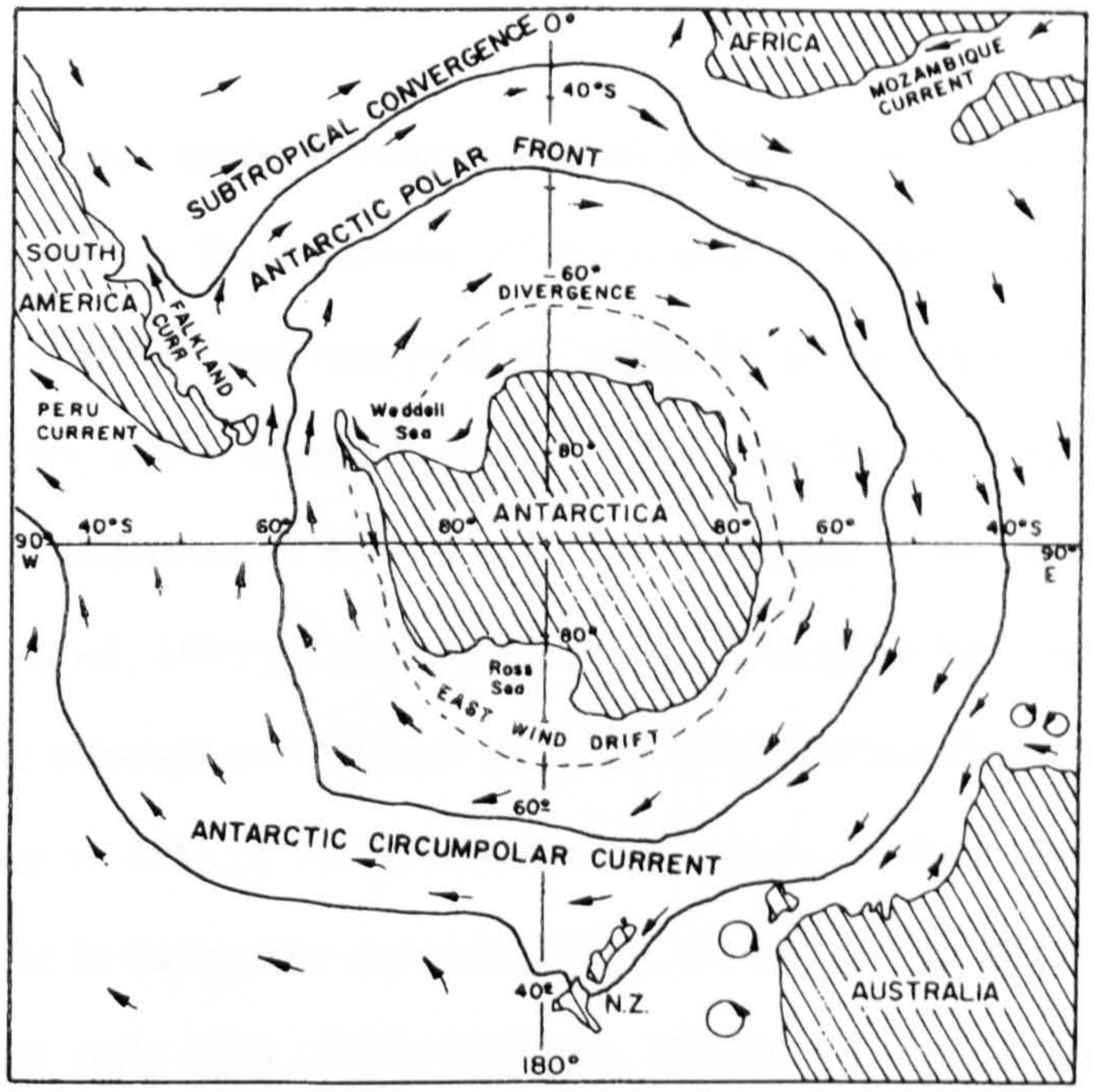

Figure 5.1. Principle water masses and frontal zones in the Southern Ocean (from Pickard and Emery, 1982)

The Polar Front

The ACC is not the movement of a homogeneous water type. It has been divided into two distinct masses each characterised by definitive thermohaline properties - the Antarctic and Subantarctic Zones (Pickard and Emery, 1982). North from the CWB, under the line of average strongest west wind, lies the Polar Front, where Antarctic surface water, with a temperature of about 0.5 °C and a salinity less than 34.5, flows under Subantarctic water to the north with a temperature of about 1 to 4 °C, and a salinity of between 33.9 and 34.9. The position of the Polar Front is predictable at about 50°S in the Atlantic and Indian sectors and 60°S in the Pacific.

The Subtropical Convergence

This zone forms the northern boundary of the Southern Ocean (Whitworth, 1988). Subantarctic waters with temperatures between 10 and 14 °C and salinity 33 to 34.9 meet the warmer, more saline waters from the north.

5.1.2.2. Ice Cover

The low incidence angle of solar radiation at high latitudes creates an environment for ice formation both on the mainland of Antarctica and the surrounding waters. The seasonality of the radiation input results in variability in the extent of the oceanic ice cover (Comiso and Sullivan, 1986; Gloerson *et al.*, 1992). Sea-ice coverage for the months of January and July is illustrated in Figure 5.2. The coverage is an average over the years 1978-85 (Gloerson *et al.*, 1992). There is a transient relationship between heat lost from the surface ocean to the atmosphere and heat supplied to the surface from the waters below. In the austral winter up to 60% of the Southern Ocean south of the Polar Front is under ice. Heating from the sun in the austral summer swings the balance towards ice melting and the ice recedes to cover only 12% of the Southern Ocean. Ice cover retards gas, heat and momentum exchange between the ocean and the atmosphere. Deacon (1982) suggested that this retardation in slowing summer warming of the surface waters would have effects on the physiological response of phytoplankton. However, El-Sayed and Taguchi (1981) state that phytoplankton in Antarctic waters are psychrophilic, and thus temperature effects may be insignificant.

Of more significance to planktonic activity is the influence of ice in shading of the water column thus reducing the photosynthetically available radiation (PAR) for the phytoplankton.

The ice is not a complete blanket and ventilation holes are common. These holes fall into two categories; *leads* which are crack in the ice, and *polynas* which are larger breaks in the ice and are themselves of two types - coastal latent heat polynas and open-ocean sensible heat polynas (Gordon, 1988). Latent heat polynas are formed by ice forming along the shoreline and being blown offshore. The resulting polyna then allows latent heat transport from the ocean to the atmosphere via ice formation. Sensible heat polynas are formed when upwelling warm water melts through the ice. These polynas can grow to 100's of kilometers across and persist for a long time. The *Weddell Sea Polyna* lasted for over three years (Gordon, 1988).

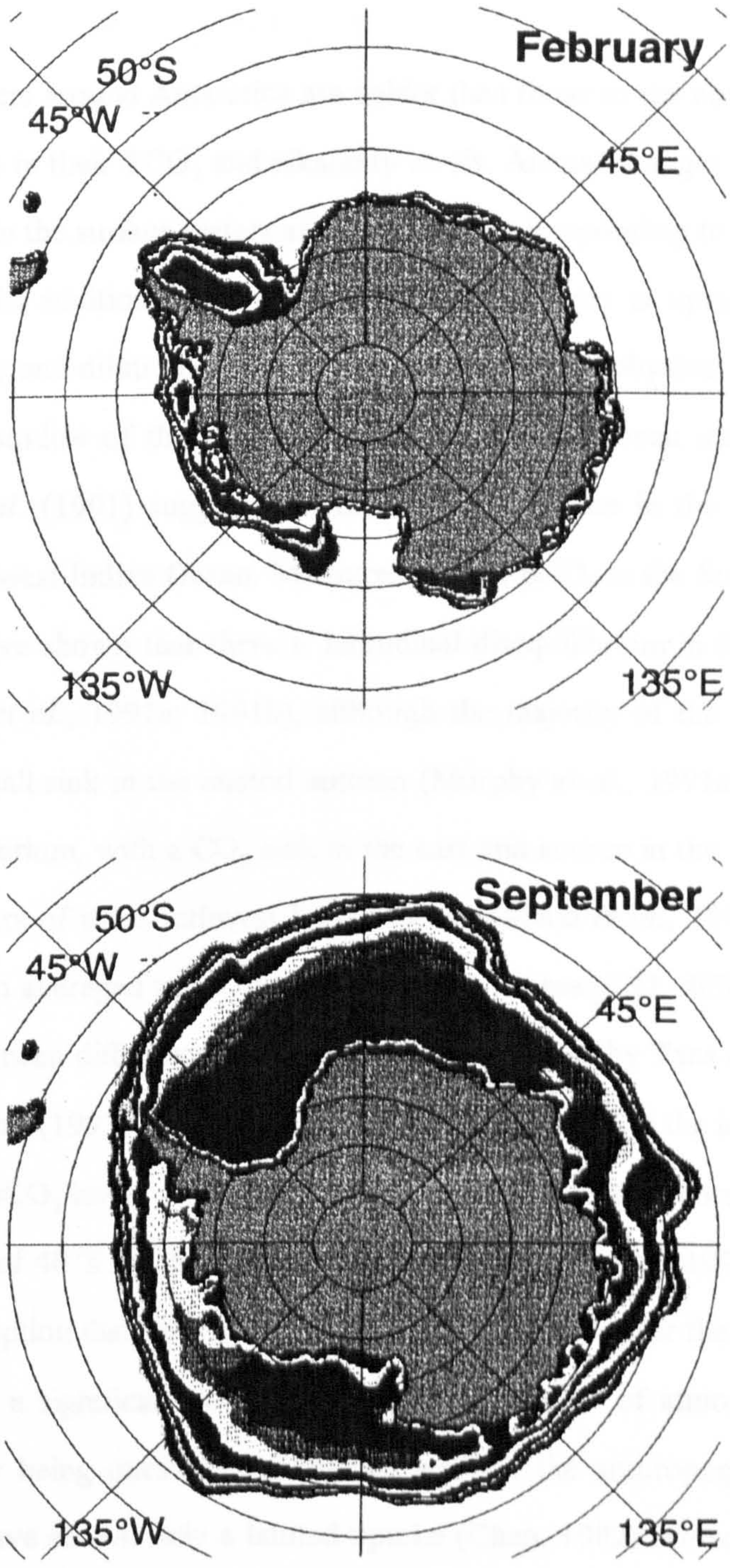

Figure 5.2. Contrasting ice coverage over the Southern Ocean between February (top) and September (bottom). Ice cover is determined from satellite data between 1979 - 1986/7. (from Gloerson et al., 1992)

5.1.3. Carbon dioxide and biogeochemistry

As the waters around Antarctica are colder than those to the north there is a general increase polewards in their TCO_2 and alkalinity levels. Annual changes in the concentration of carbon dioxide in the surface waters are significant, corresponding to shifts in the amount of solar heating. In addition to this annual 'breathing' there is uptake of CO_2 through autotrophic activity and dilution of the surface waters through physical mixing events.

Very few studies of the carbon dioxide system have been made in the Southern Ocean. Goyet *et al.* (1991) suggest a significant CO_2 source in the Subantarctic region south of the Southwest Indian Ocean. Measurements of pCO_2 in the South Pacific down to the Polar Front have shown that there is latitudinal disequilibrium in the direction of CO_2 transfer (Murphy *et al.*, 1991a; 1991b), although the majority of the Subantarctic region appears to be a small sink in the austral autumn (Murphy *et al.*, 1991a; 1991b). A reverse latitudinal disequilibrium, with a CO_2 sink in the east and source in the west, was identified in the surface waters of the Southwest Indian Ocean (Metzl *et al.*, 1991). Broecker *et al.* (1986) described an averaged zonal distribution of the air-sea pCO_2 difference of - 20 μatm south of 50 °S. A mean difference of -17 μatm was attributed by Tans *et al.* (1990) to this area. Takahashi *et al.* (1993) identified a significant sink for CO_2 in the ice-free Weddell Sea around 65°S with pCO_2 levels 100 μatm below atmospheric Furthermore, they highlighted a general sink south of 40°S for the austral summer (Takahashi *et al.*, 1993).

The presumption that, as a major source of bottom water for the world's oceans, the Southern Ocean is a significant conduit for the sequestration of atmospheric CO_2 to the deep ocean is now being questioned. Measurements of the anthropogenic CO_2 signal in Antarctic waters have shown only a limited uptake (Chen, 1982; Poisson and Chen, 1987; Chen, 1993). During the period of greatest bottom water formation pack ice inhibits gas exchange between the surface ocean and the atmosphere. As the ice recedes, the formation of bottom water decreases and consequently only the top few hundred meters of the ocean have been influenced by the anthropogenic signal (Poisson and Chen, 1987).

The *quasi*-infinite fetch of the Southern Ocean in association with highly active meteorological conditions over the region result in a deep oceanic mixed layer, often throughout the water column. Critical depth theory for phytoplankton growth (Sverdrup,

1953; Smith and Nelson, 1985) suggests that in such areas of high wind stress, productivity is limited by low net irradiance availability for the photosynthetic cells. Thus, productivity in the Southern Ocean has generally been thought to be low, even under high macro-nutrient and light environments, only increasing when conditions prevail favouring increased stability.

Such increased stability of the upper water column is apparent in the marginal ice zone during the retreat of the ice edge during periods of ice-melt (Smith and Nelson, 1985; Sullivan *et al.*, 1988) and additionally in the locality of islands resulting from freshwater run-off (Perissinotto *et al.*, 1990). Hydrographic features common to marginal ice zones are shown in Figure 5.3. The meltwater forms a stable layer over the more dense seawater below. Additionally, ice-edge upwelling (Johannessen *et al.*, 1983) may counteract sinking and thus 'hold' organisms in the surface water. The reduction in vertical mixing determines that the phytoplankton may then remain in the euphotic zone for a sufficient length of time to grow and reproduce to levels far in excess of those found in surrounding waters. Sakshaug and Holm-Hansen (1984) proposed that the maximum depth of this vertical stability was about 50m to sustain prolonged phytoplankton growth. The plankton often form dense mesoscale blooms of comparable intensity to those found in the North Atlantic.

The receding ice-edge release epontic phytoplankton (Brightman and Smith, 1989) and bacterioplankton (Kottmeier and Sullivan, 1990) from their overwintering in the ice to serve as inocula providing the initial building blocks for bloom formation. Antarctic ice edge blooms are not, however, confined to periods where the ice is in retreat. High productivity (El-Sayed and Taguchi, 1981; Comiso *et al.*, 1990) and phytoplankton standing stocks (El-Sayed and Taguchi, 1981; Nelson *et al.*, 1989) have been measured in late austral summer and autumn when the ice was stationary or advancing. Dieckmann (1987) reported augmented levels of phytoplankton in the austral winter. Highest levels of productivity are possibly limited to a very short part of the year. Wefer *et al.* (1988) found that 97% of the particle flux caught in sediment traps in the Bransfield Strait was associated with only 2 months of the year. Smith *et al.* (1988) suggest that open ocean blooms persist for up to 2 months, the length of a bloom depends on the continuation of the vertical stability, the availability of trace nutrients and the extent of heterotrophic grazing on the bloom.

Proximity to land masses controls primary productivity in the Weddell Sea (El-Sayed and Taguchi, 1981). Comiso *et al.* (1990) suggested that this proximity relationship was due to the shallow waters (<500m) enhancing residence times, water column stratification and micro-nutrient flux.

Nutrient studies in the Southern Ocean have illustrated that although total productivity is not defined by the availability of macro-nutrients, as is generally the case, Antarctic phytoplankton may be limited by low micronutrient concentrations (De Baar *et al.*, 1990; Martin *et al.* , 1990). Martin *et al.* (1990) have shown that there are enhanced iron concentrations in neritic waters close to the land, where as the waters in Drake Passage are low in iron and thus autotrophic activity is only able to utilise <10 % of the available macro-nutrients.

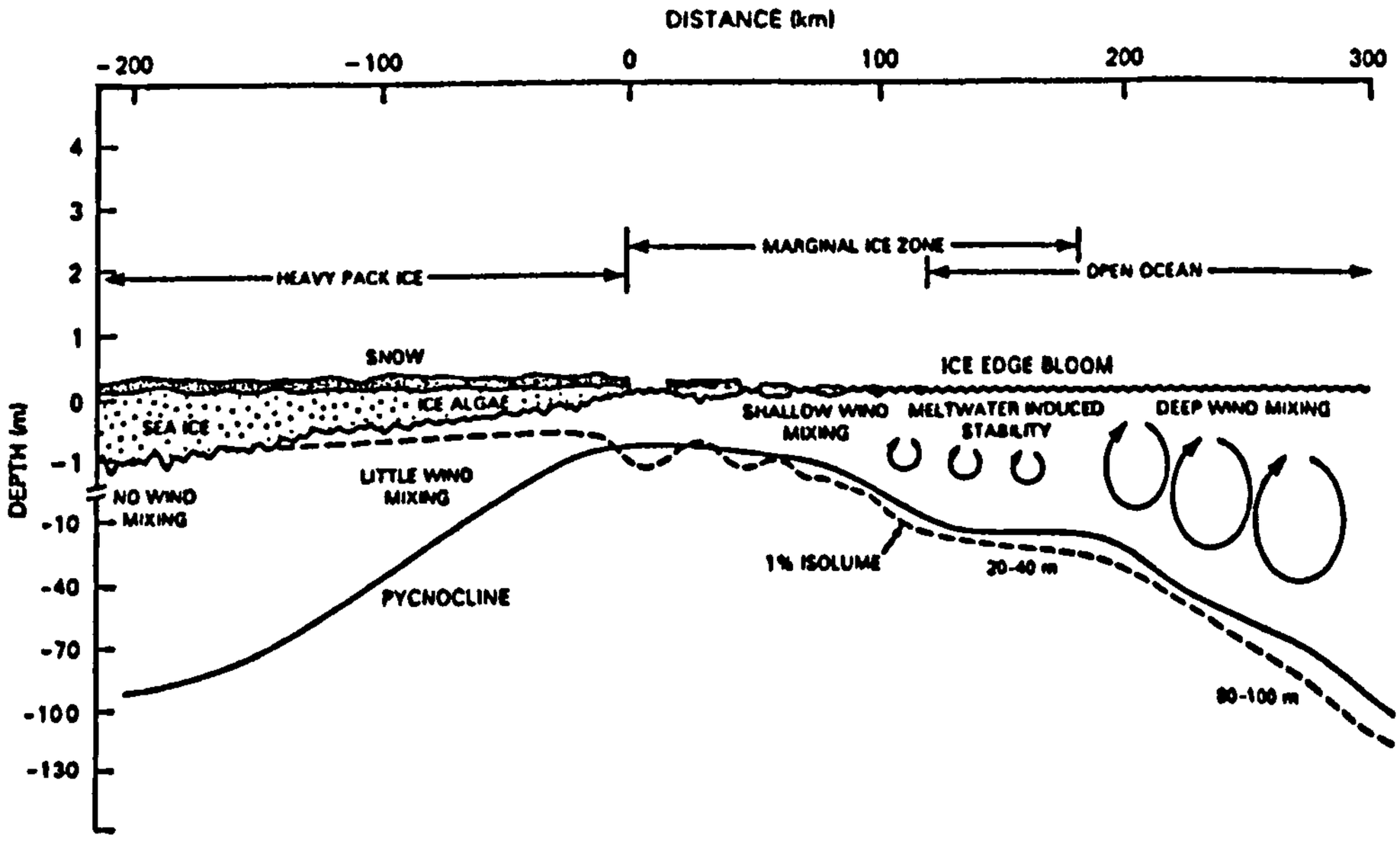

Figure 5.3. Some hydrographical properties of a retreating marginal ice zone(from Sullivan et al. (1988)).

5.2. Introduction to Cruise D198

As highlighted in Section 5.1. previous studies of the carbon dioxide system in the Southern Ocean, including the Subantarctic waters, have concentrated on the Weddell Sea (Chen, 1982; Poisson and Chen, 1987), the South-West Indian Ocean (Goyet *et al.*, 1991; Metzl *et al.*, 1991) and the South Pacific, north of 60°S (Murphy *et al.*, 1991a: 1991b). An opportunity arose to participate in a scientific cruise to the Southern Ocean as part of the Biogeochemical Ocean Flux Study (BOFS), the U.K. contribution to the Joint Geochemical Ocean Flux Study (JGOFS). The main objective of the programme, involving both the R.R.S. *Discovery* and the R.R.S. *James Clarke Ross*, was identified in the cruise proposal (Owens *et al.*, 1991) as to:

> *"Evaluate the magnitude and variability of biogeochemical fluxes (particularly carbon and nitrogen) during early summer in the South East Pacific sector of the Southern Ocean, with emphasis on rates and processes in the marginal ice zone."*

Within this main objective recognised four main aims were identified (Owens *et al.*, 1991):

> *"To determine ocean-atmosphere exchanges of radiatively active gases, and the factors influencing such fluxes over a wide latitude range.*
>
> *To investigate the interactions between the biological, chemical and physical processes that control carbon fluxes in the euphotic zone.*
>
> *To assess the impact of sea-ice on biogeochemical fluxes, in order to estimate the importance of climatic feedback effects.*
>
> *To determine the export of biogenic material from the upper ocean and its subsequent fate."*

The Bellingshausen Sea was chosen as a survey area both because of the sparsity of scientific information in the South-East Pacific, Southern Ocean and the comparative predictability of the position of the retreating ice-edge afforded by the region (Enomoto and Ohmura, 1990; Gloerson *et al.*, 1992).

The particular aim of this work was linked to the former two aims of the cruise: - to measure the degree of intimacy between seawater pH and other carbon dioxide characteristics, and the biology and hydrography of the surface waters of the Bellingshausen Sea using the newly developed spectrophotometric system and other state of the art instrumentation employed at the Plymouth Marine Laboratory. The results would be used to assess whether the region was a source or sink for CO_2 during the austral summer and evaluate the influence of the marginal ice zone on CO_2 properties of the surface waters. The use of high precision instrumentation would enable the internal consistency of the carbon dioxide system to be determined with regard to the accuracy of calculating a carbon dioxide parameter from the measurement of another pair (see Section 4.5.3.).

5.2.1. The cruise track

The R.R.S. *Discovery* left Stanley, Falkland Islands, on the 11th November 1992, and sailed south across Drake Passage and through Bransfield Strait. The ship headed west across the Bellingshausen Sea at approximately 65°S, and after intensive box surveys around 67°S 85°W the ship headed north along 88°W arriving in Punta Arenas, Chile on the 17th December 1992. The cruise track is shown in Figure 5.4. A close up of the first survey is illustrated in Figure 5.5. To ease analysis of the information gained throughout the cruise, the cruise track has been divided into sections:

Bransfield Strait		321 00 00 - 322 23 59
Bellingshausen Sea		323 00 00 - 325 10 07
Survey 1	V	327 23 01 - 329 05 59
	W	329 06 00 - 329 19 59
	X	329 20 00 - 330 07 59
	Y	330 08 00 - 330 20 59

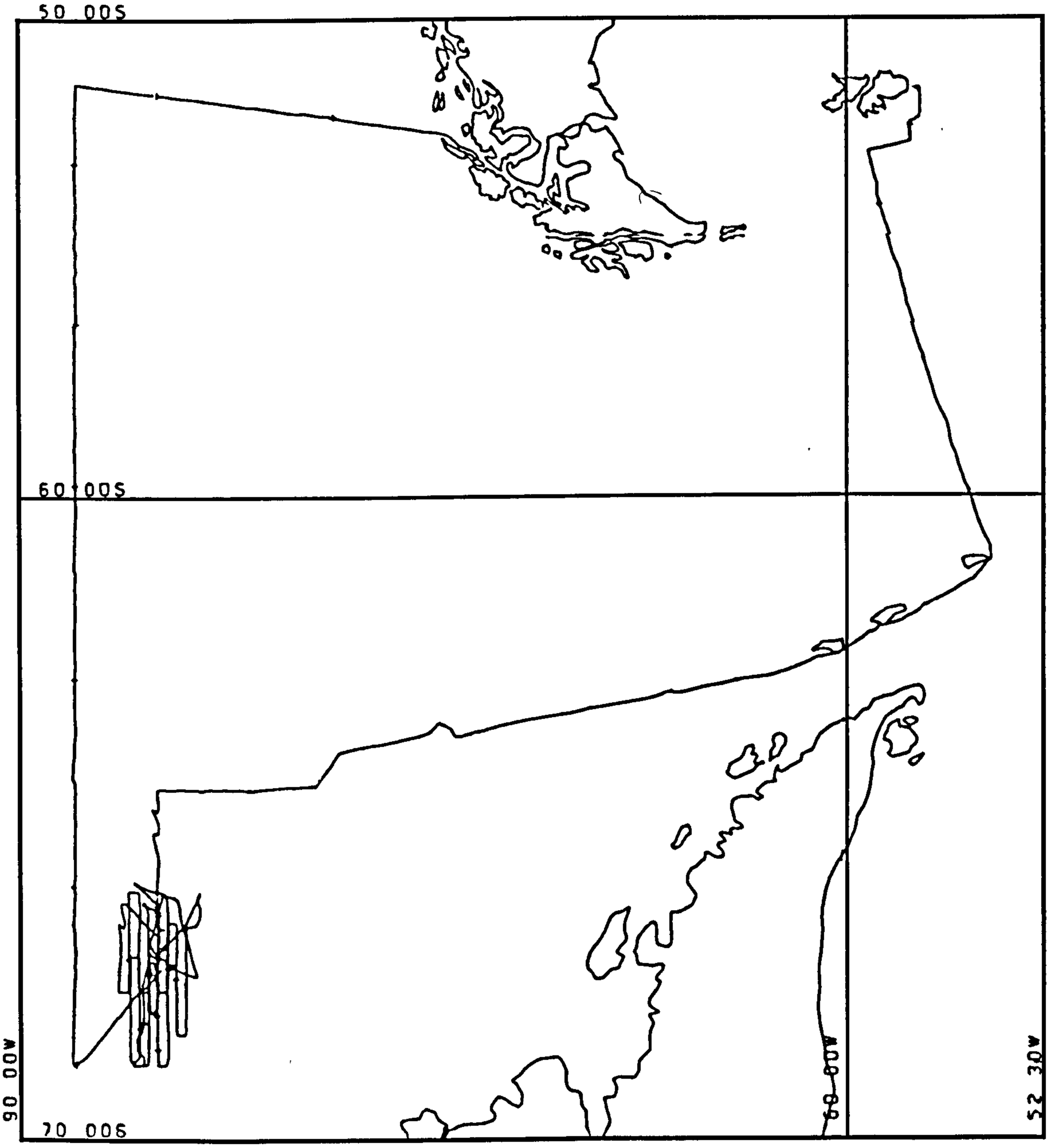

Figure 5.4. Cruise track of the R.R.S. Discovery during the Sterna Cruise to the Bellingshausen Sea, Southern Ocean, 11th November 1993 to 17th december 1993.

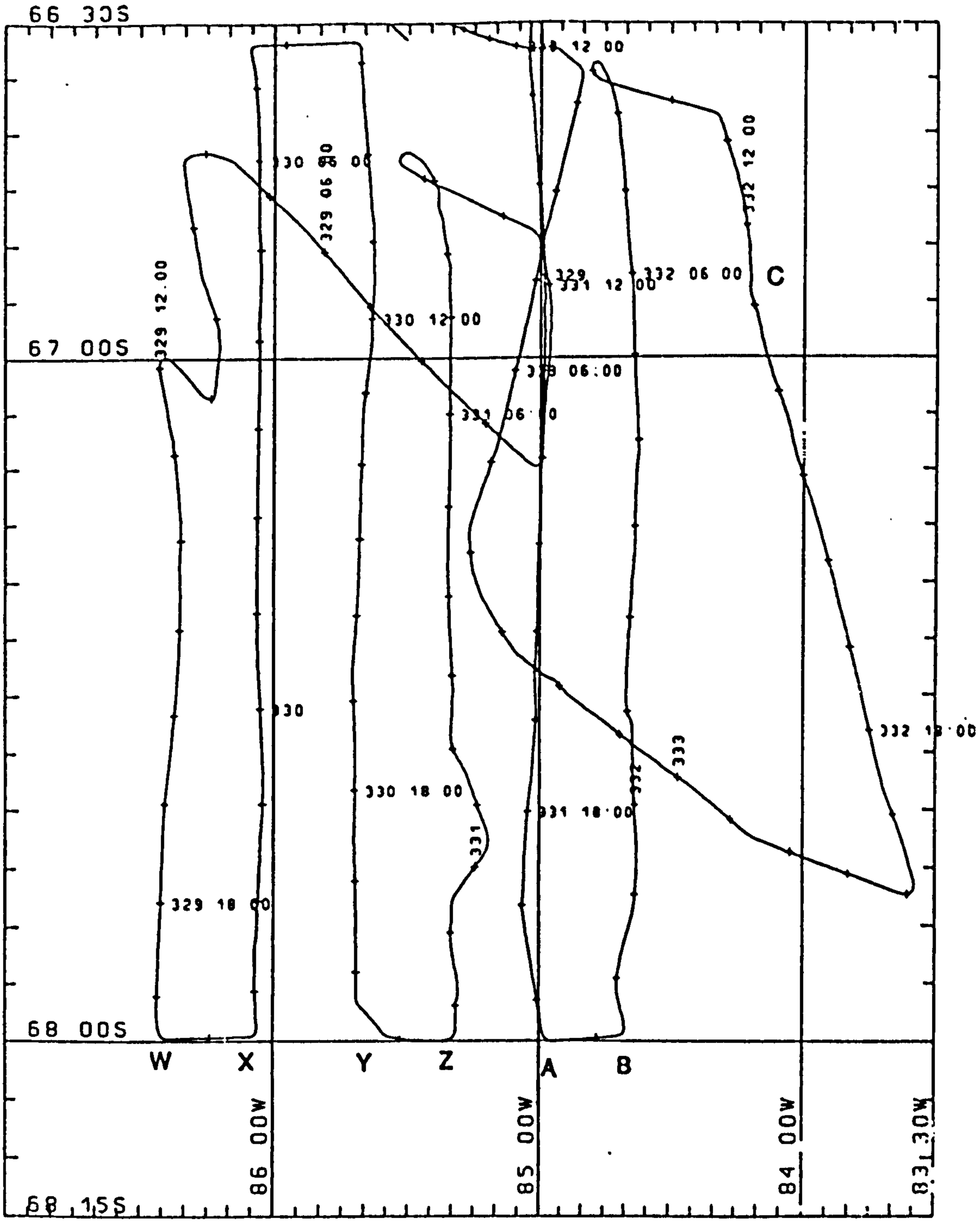

Figure 5.5. Cruise track of R.R.S. Discovery during the 1st survey across the South Polar Front, Bellingshausen Sea.

Z	330 21 00 - 331 09 59
A	331 10 00 - 331 20 59
B	331 21 00 - 332 08 59
C	332 09 00 - 332 19 59
D	332 20 00 - 333 11 59

The rough positions of the start and stop times for each transect can be obtained from the date markings on Figures 5.4. and 5.5. The latter track is also marked at hourly intervals.

5.3. Method

The methodology for the spectrophotometric determination of pH was explained in Chapter 4. pCO_2 was measured every 17 minutes using a GC and showerhead equilibrator (Robertson *et al.*, 1993). Chlorophyll concentrations were estimated using a Turner Designs fluorometer (model 10-005) calibrated hourly from discrete samples from the on-line supply measured on a Turner Designs fluorometer (model 10AU) (Head and Miller, 1993). Temperature and salinity were measured using a thermosalinograph system mounted in the hull at the non-toxic supply intake (Morrison and Miller, 1993).

5.4. Results

Spectrophotometric pH values are reported both at 25°C and *in situ* temperatures, however, they are discussed mainly at 25°C, not through convention, although this is usually the case, but because of the uncertainty in the accuracy of the *in situ* values expressed in Chapter 4. All correlation coefficients are expressed as r at the 95 % confidence level unless otherwise indicated. Data gaps evident in the profiles are due mainly to the nature of the data analysis as all data points are 5 minute averages around times of pH measurement. Therefore where pH measurements were in error (*i.e.* they had high S.D.) or no measurements were taken there are concurrent gaps in the reporting of the other variables. Other data gaps are due to respective inoperation in measurements of the variable concerned.

5.4.1. Southern Bransfield Strait

Surface seawater pH was measured from Potter Cove along the Bransfield Strait into the Bellingshausen Sea. Profiles of temperature, salinity, pCO_2, chlorophyll, pH(25°C) and *in situ* pH are illustrated in Figure 5.6. The pH profile is essentially in two parts. From the north, values decrease from 7.68 units to about 7.65, which were the lowest found during the whole survey, and then rise rapidly to about 7.73 out into the Bellingshausen Sea. The rise is associated with the Continental Water Boundary (Read *et al.*, 1994) at about 1800 km where salinity and temperature, after an initial short rise, fall rapidly. Also identified with this front is a decrease in pCO_2 from about 370 to 340 μatm and a very small rise in chlorophyll from 0.6 to 0.8mg.m^{-3}. For the whole transect there are good negative correlations between pH and pCO_2 (r = - 0.86, n = 90), pH and temperature (r = - 0.73, n = 189) and pH salinity (r = - 0.77, n = 189) and there is no correlation between pH and chlorophyll. The profiles to the east of the CWB correlate poorly. From the CWB westwards, biological activity, represented here by chlorophyll, although low has a significant influence on the carbon dioxide system. pH is reasonably correlated with chlorophyll (r = 0.78, n = 58) which in turn has a strong inverse relationship with pCO_2 (r = - 0.92, n = 26). pH and pCO_2 show a good correlation (r = 0.87, n = 26) although pH exhibits a poor relationship with the physical parameters when pCO_2 correlates strongly with both salinity (r = 0.82, n = 26) and temperature (r = 0.82, n = 26).

5.4.2. Bellingshausen Sea transect

Figures 5.7. to 5.9. show the observed temperature, salinity, pCO_2, chlorophyll and pH values for a transect across the Bellingshausen Sea from the west of the Bransfield Strait to 85°W, north of the survey area. The hydrography of the Bellingshausen Sea, as depicted by the transect, is characterised by small-scale heterogeneity with respect to both temperature and salinity. However, there is a general trend for salinity to decrease from 34 to 33.8, and temperature, whilst exhibiting significant small-scale changes, lies most commonly between - 0.8 and -1.0 °C. pH variations throughout the transect are closely related with pCO_2 (r = - 0.83, n = 408) and salinity (r = - 0.76, n = 805).

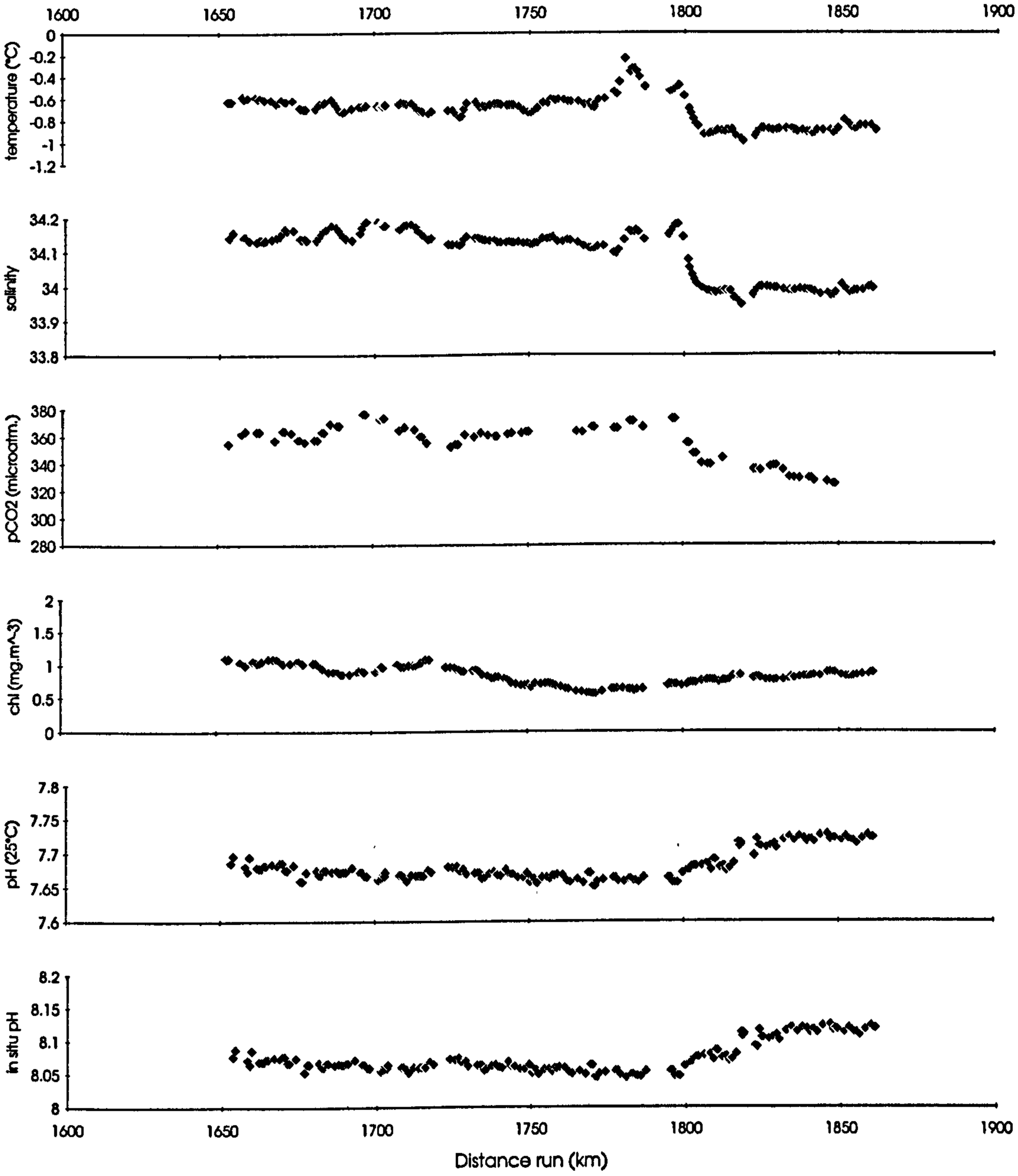

Figure 5.6. Surface profiles of temperature, salinity, pCO2, chlorophyll, pH(25°C) and in situ pH for the Southern Bransfield Strait - Potter Cove to the Bellingshausen Sea

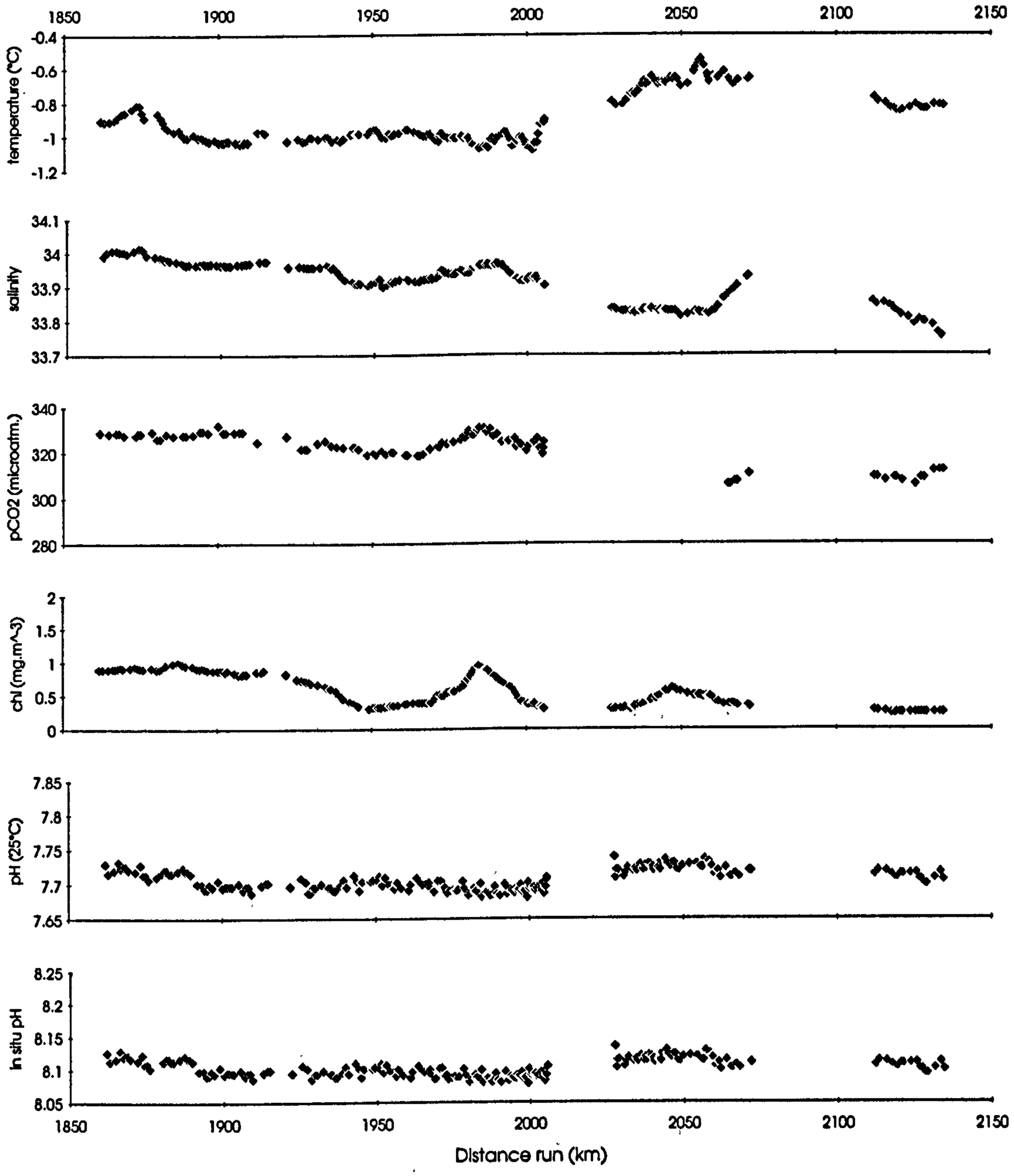

Figure 5.7. Surface profiles of temperature, salinity, pCO2, chlorophyll, pH(25°C) and in situ pH - Bellingshausen Sea transect, 1st leg

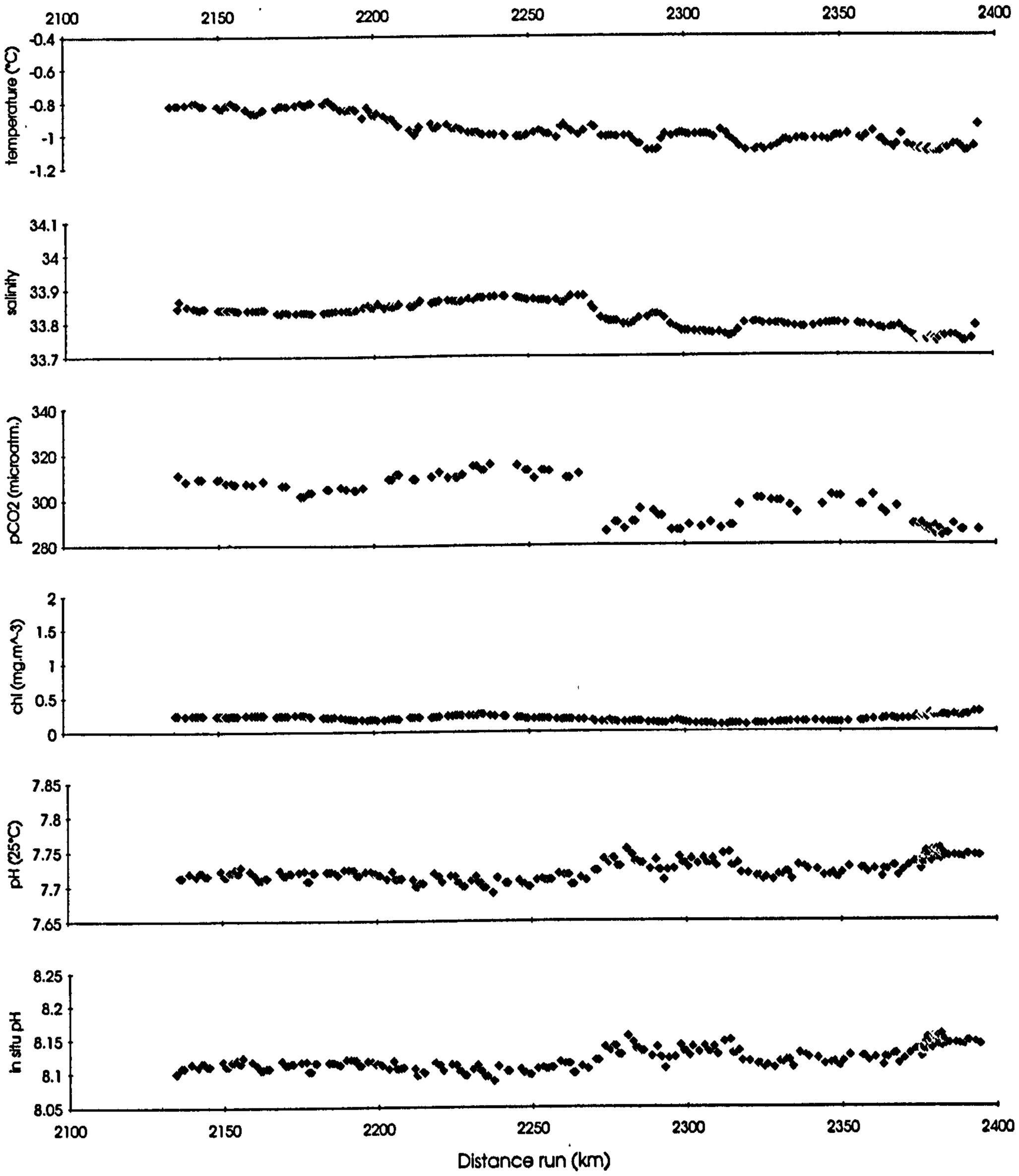

Figure 5.8. Surface profiles of temperature, salinity, pCO2, chlorophyll, pH(25°C) and in situ pH - Bellingshausen Sea transect, 2nd leg

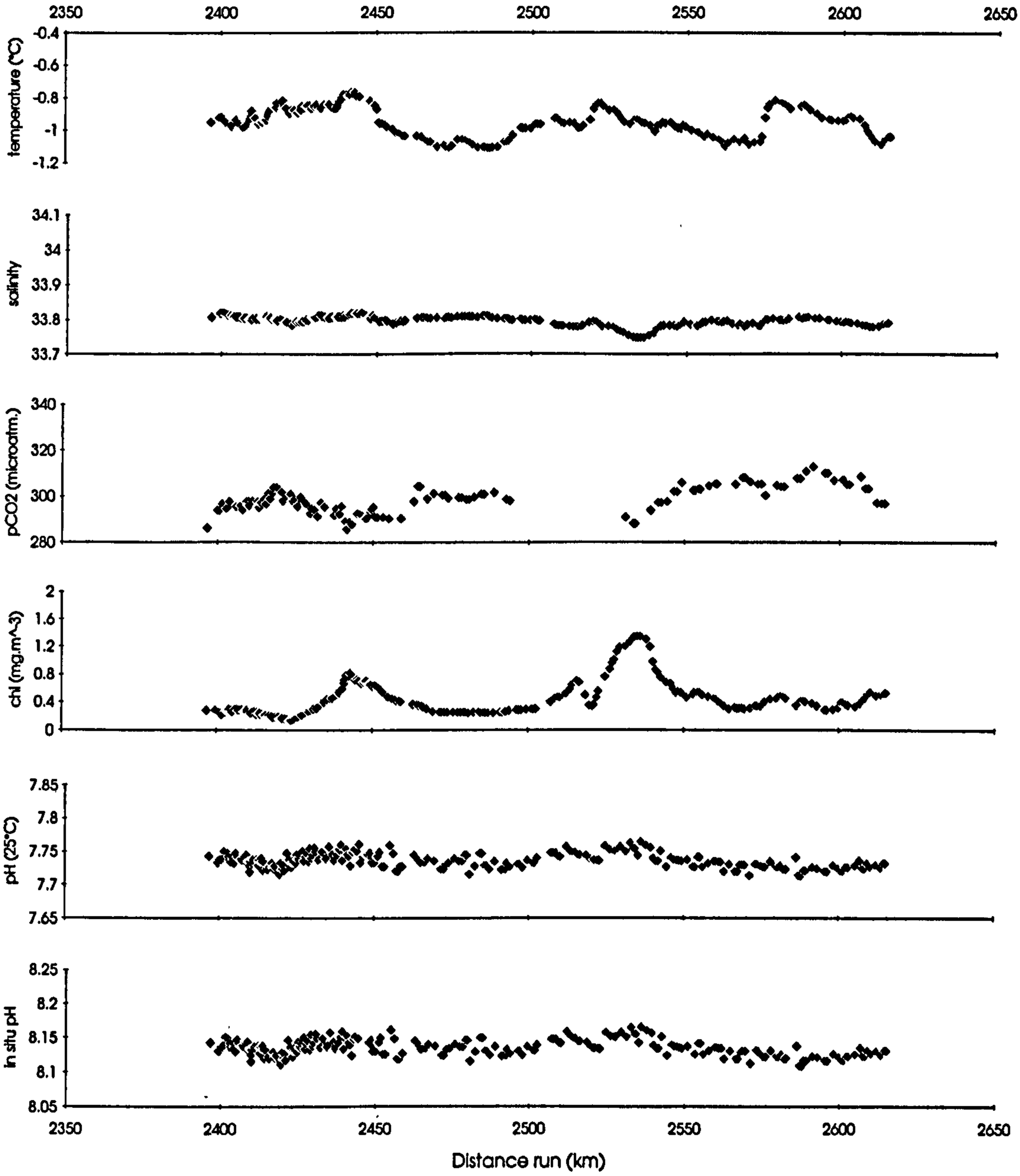

Figure 5.9. Surface profiles of temperature, salinity, pCO2, chlorophyll, pH(25°C) and in situ pH - Bellingshausen Sea transect, 3rd leg

There is no correlation between pH and either temperature or chlorophyll. Salinity is strongly correlated with pCO_2 ($r = 0.98$, $n = 408$).

Westwards across the Bellingshausen Sea, pH decreases gradually from about 7.73 to 7.68 at 2000 km. However, there is a small, but rapid, drop in pH of about 0.04 units at about 1885 km which is linked to a temperature front, although there is no discernible change in pCO_2. A small plankton bloom at approximately 1980 km is associated, paradoxically, with an increase in pCO_2 and a small decrease in pH of about 0.01 unit. For this first sector (Figure 5.7.) pH is not correlated with pCO_2 or chlorophyll, however, there is a good *positive* correlation between pCO_2 and chlorophyll ($r = 0.79$, $n = 122$), and salinity ($r = 0.84$, $n = 122$), and a negative correlation with temperature ($r = -0.72$, $n = 122$). pH is correlated with temperature ($r = 0.79$, $n = 266$).

The second leg of the transect (Figure 5.8) found very low concentrations of chlorophyll (< 0.3 $mg.m^{-3}$) which did not correlate with the other measured parameters. Temperature decreased gradually from - 0.8 °C to - 1.1 °C. pCO_2 was relatively constant (305 - 315 µatm) upto 2270 km until dropping to 285 µatm, in association with a sharp salinity front, the South Polar Front (Read *et al.*, 1994). A large rise in pH from 7.71 to 7.75 was associated with this front. pH and pCO_2 followed the salinity very closely throughout the transect and accordingly correlated well ($r = 0.95$, $n = 128$; $r = -0.82$, $n = 128$; respectively) as did pCO_2 and pH ($r = -0.84$).

The features identified during the final segment of the transect (Figure 5.9.) suggest that physical and biological interactions have inter-mixed such that there are no correlations between any of the measured parameters. There are two noticeable chlorophyll peaks, the latter with a concentration of ~ 1.4 $mg.m^{-3}$, associated with small hydrological changes. Increases in pH of about 0.02 units accompany these peaks and a decrease in pCO_2 of 20 µatm is observed for the first peak.

The survey 'V' (Figure 5.10.), depicts the passage south from 65°S to the survey area. The temperatures at the start of the transect are the highest of the survey, ranging from 0.3 to - 0.1°C. This water is also more saline than the waters analysed during the

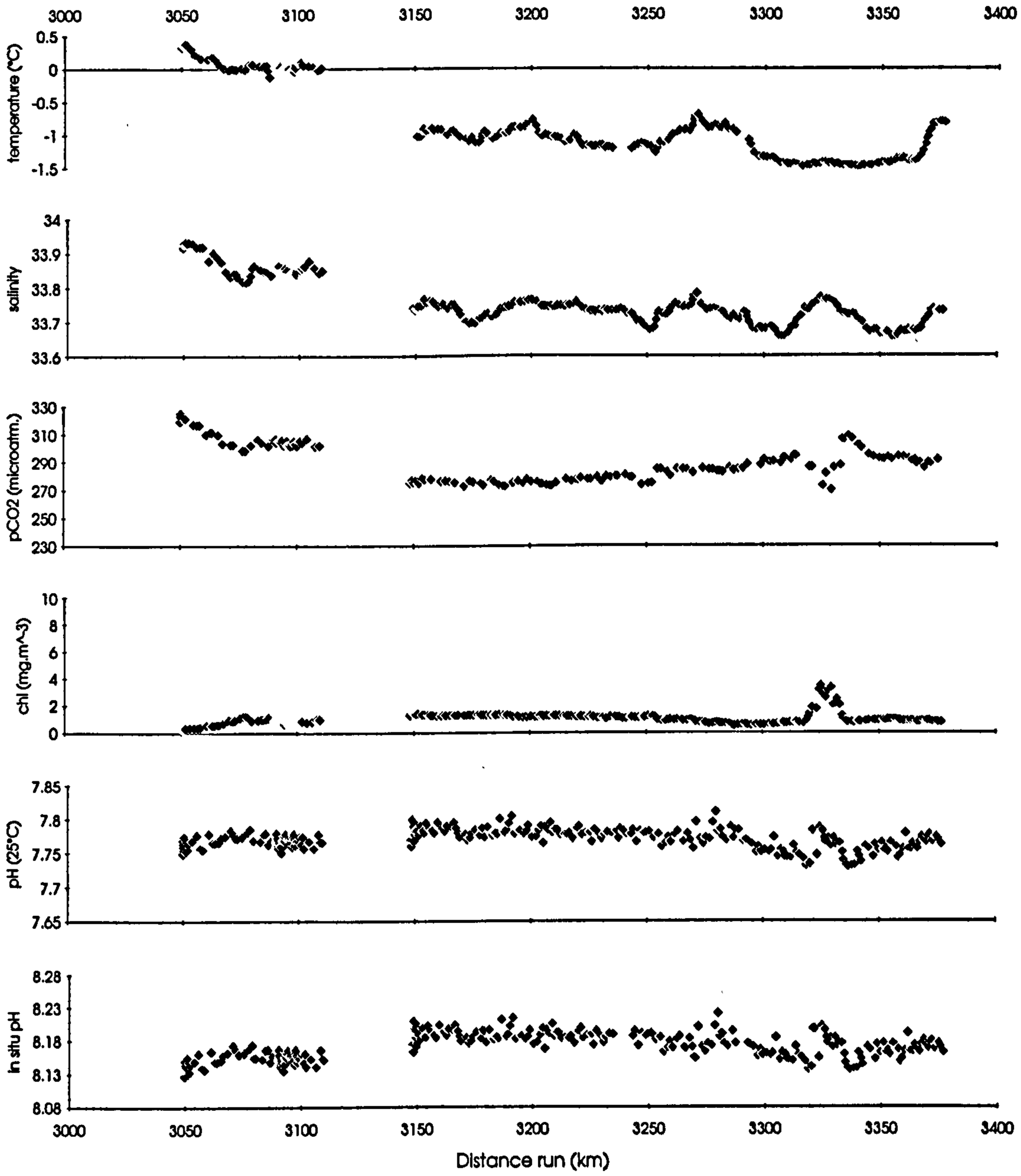

Figure 5.10. Surface profiles of temperature, salinity, pCO2, chlorophyll, pH(25°C) and in situ pH for leg V, survey 1, Bellingshausen Sea

westerly transect and density depth profiles show isopycnals reaching the surface from 200m (Read *et al.*, 1994). pH values are higher (7.75 - 7.77 units) than for the transect, however, *in situ* pH values show little departure from those of the transect. Chlorophyll concentrations are slightly elevated, although pCO_2 levels (300 - 330 µatm) are also higher. Further south a sharp chlorophyll peak (~ 3.5 $mg.m^{-3}$) was located at about 3325 km with attendant increases in pH to about 7.78 units, and decreases in pCO_2 to 280 µatm. The ship turned northwest on reaching this bloom and started the intensive survey. During the final passage pH levels were seen the rise with temperature and salinity, although there was no discernible change in chlorophyll or pCO_2.

5.4.3. Bellingshausen Sea survey 1

Contour plots for pH, pCO_2 and chlorophyll in the survey area are shown in Figures 5.11 to 5.13. Initial comparisons of the profiles illustrate the intimate relationship between the three variables particularly the correspondence between the chlorophyll and pH highs, and pCO_2 lows, and *vice versa*. The individual transects W to D, as defined in Section 5.2.1., are illustrated in Figures 5.14. to 5.21. The survey area is divided by a sharp salinity front, the South Polar Front (Read *et al.*, 1994) running at the surface from 67.1°S 86.5°W to 67.05°N 83.5°W across the survey area. This front is the southern zone of concentrated eastward transport of the Antarctic Circumpolar Current 3° north of the Continental Water Boundary (Read *et al.*, 1994).

To highlight the differences between the two water masses, all data from the survey transects have been divided into the area to the north and the area to the south of the salinity front. The northern, low salinity area has little chlorophyll, with generally less than 2 $mg.m^{-3}$. The pCO_2 levels, although all are lower than atmospheric, are the highest readings for the survey area (280 - 320 µatm). There is a general trend for pH and chlorophyll to fall, and pCO_2 to rise, towards the front. However, there are poor correlations between all variables. South of the front, in the high salinity area, chlorophyll levels are generally greater than to the north with concentrations ranging from 0.5 to 8 $mg.m^{-3}$. pH levels vary significantly throughout the area with the range throughout a transect commonly

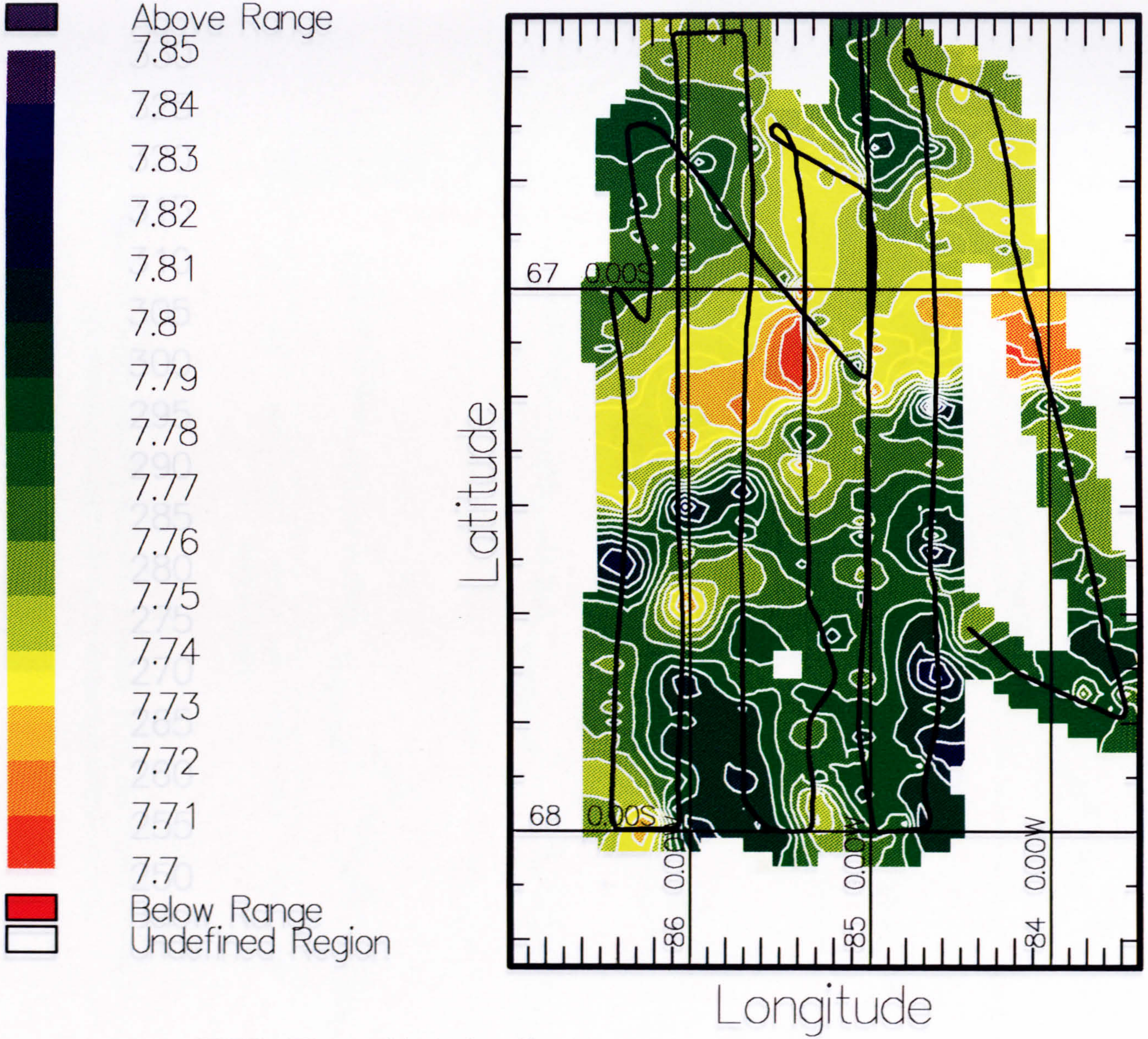

Figure 5.11. Contour plot of pH (25°C) for surface waters near and on the South Polar Front, Bellingshausen Sea. The latter part of leg V through to the end of leg C are represented in the plot.

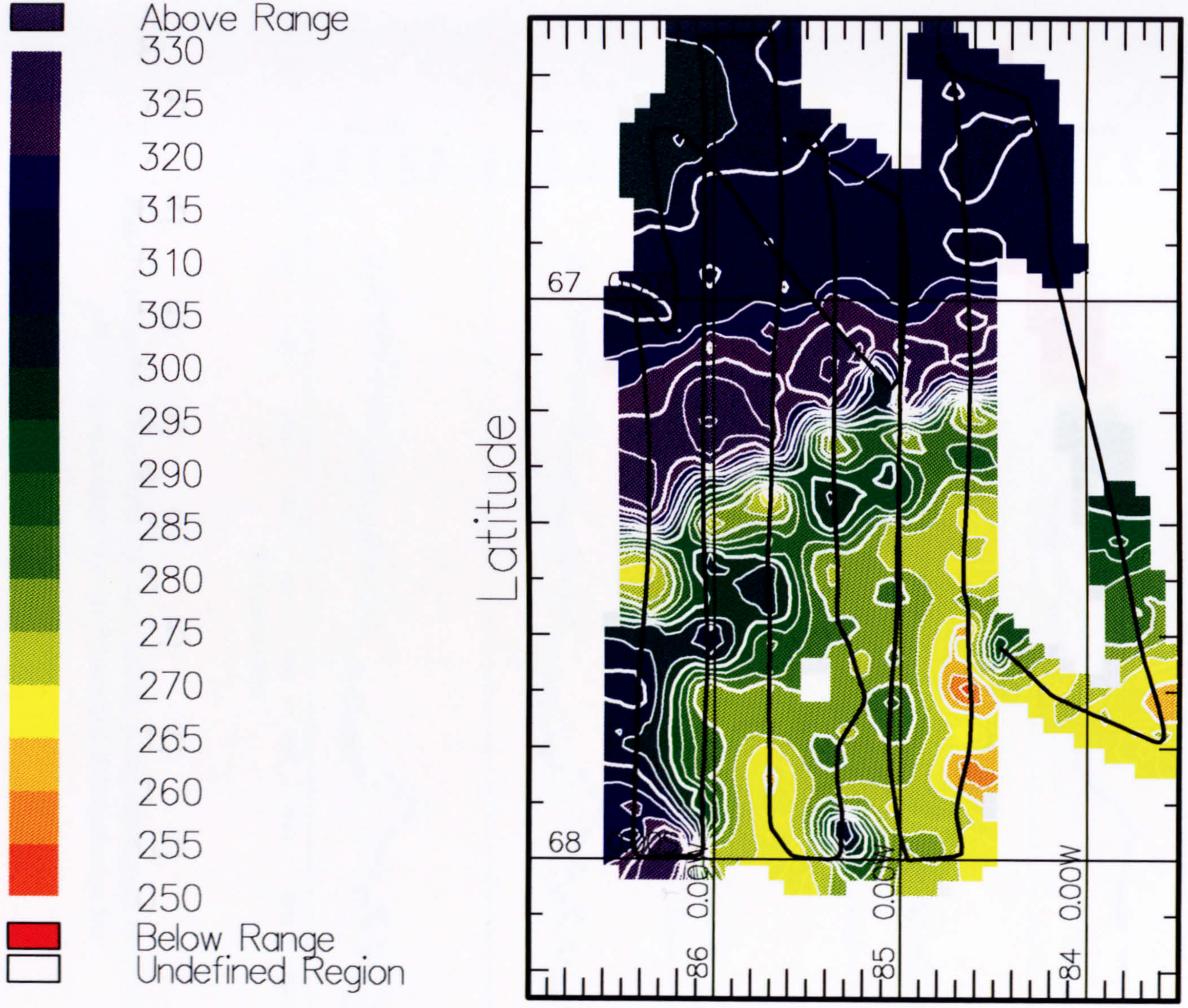

Figure 5.12. Contour plot of pCO_2 (µatm.) for surface waters near and on the South Polar Front, Bellingshausen Sea. The latter part of leg V through to the end of leg C are represented in the plot.

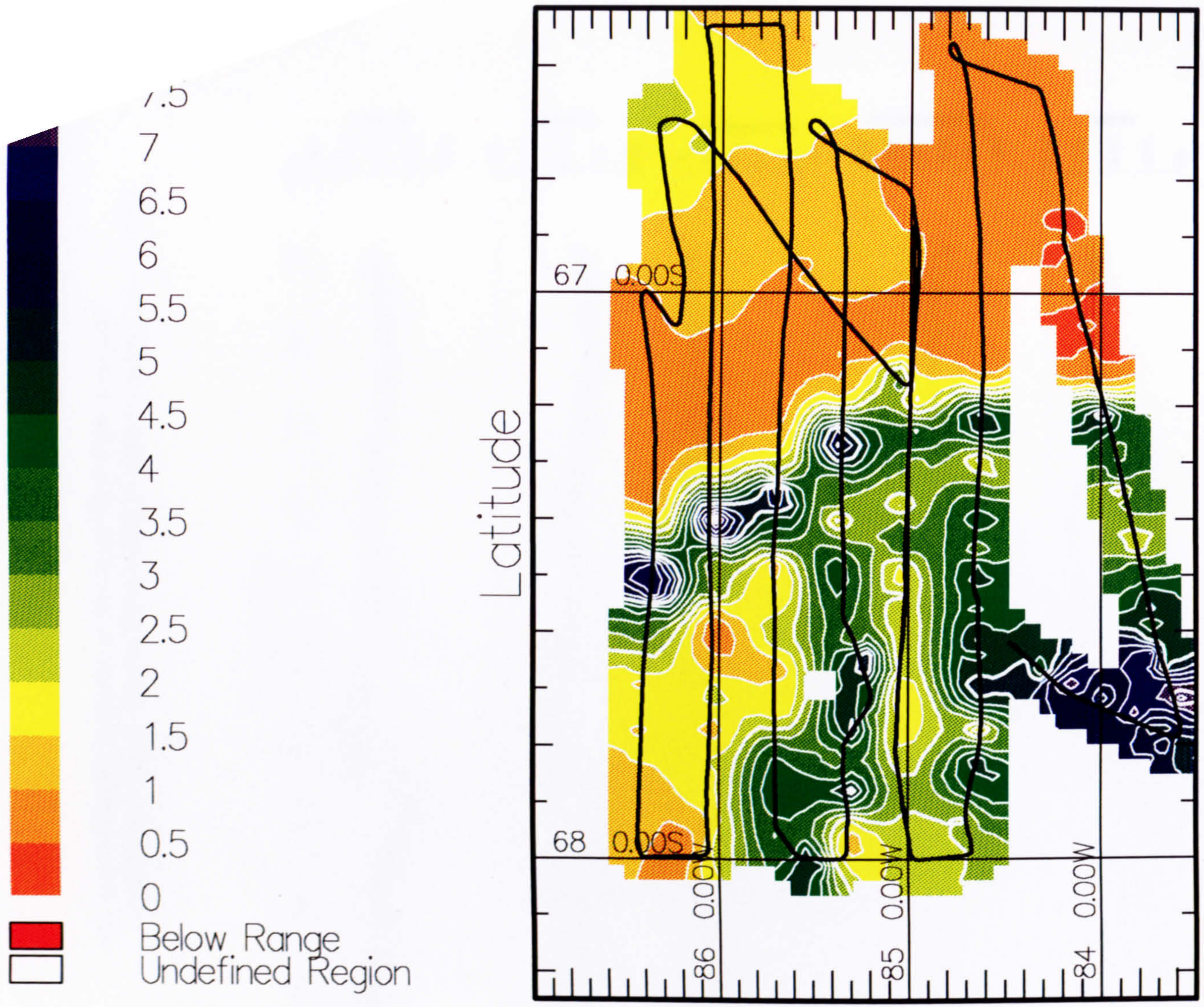

ure 5.13. Contour plot of chlorophyll (mg.m^{-3}) for surface waters near and on the South Polar Front, Bellingshausen Sea. The latter part of leg V through to the end of leg C are represented in the plot.

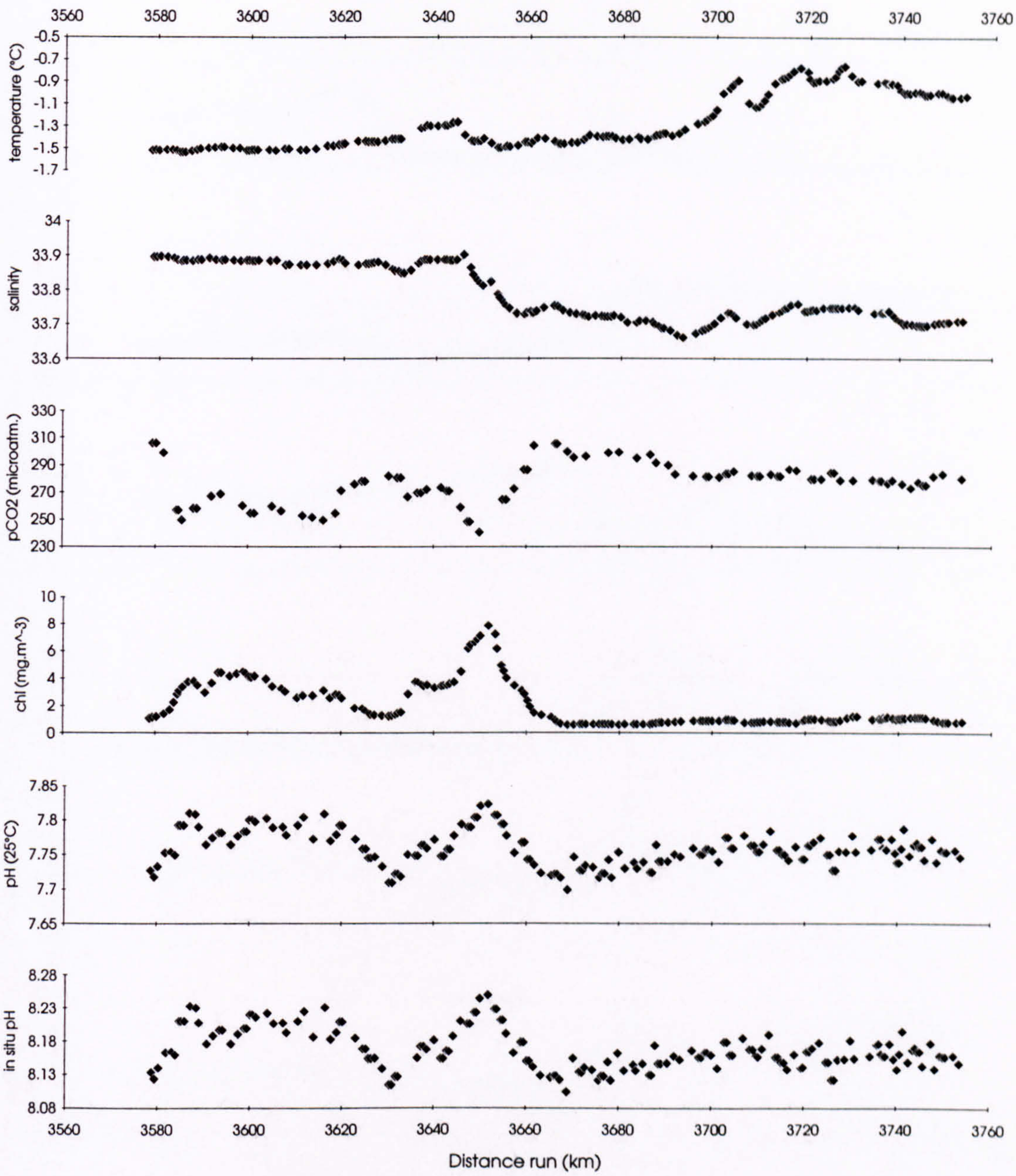

Figure 5.15. Surface profiles of temperature, salinity, pCO2, chlorophyll, pH(25°C) and in situ pH for leg X, survey 1, Bellingshausen Sea

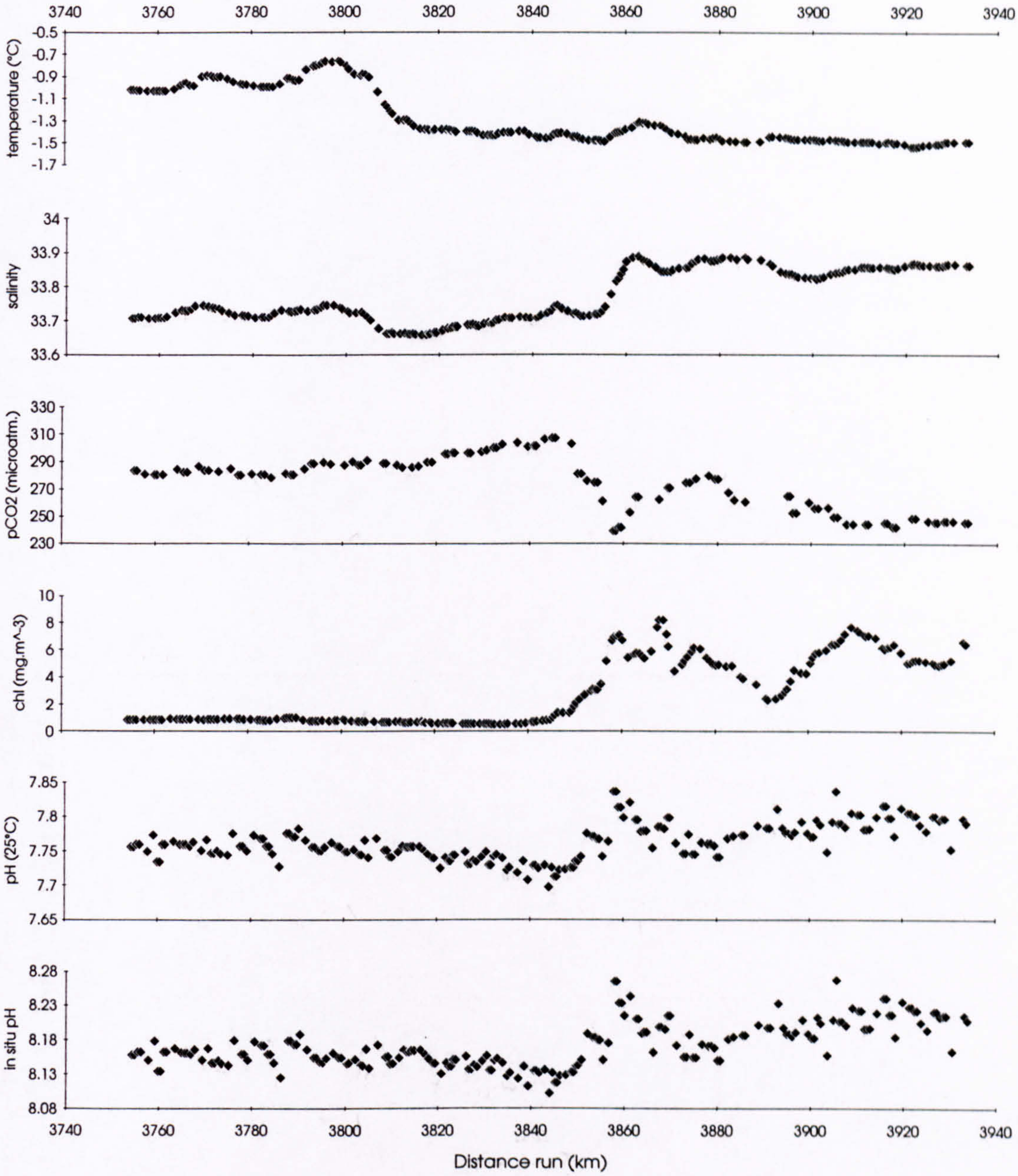

Figure 5.16 Surface profiles of temperature, salinity, pCO2, chlorophyll, pH(25°C) and in situ pH for leg Y, survey 1, Bellingshausen Sea

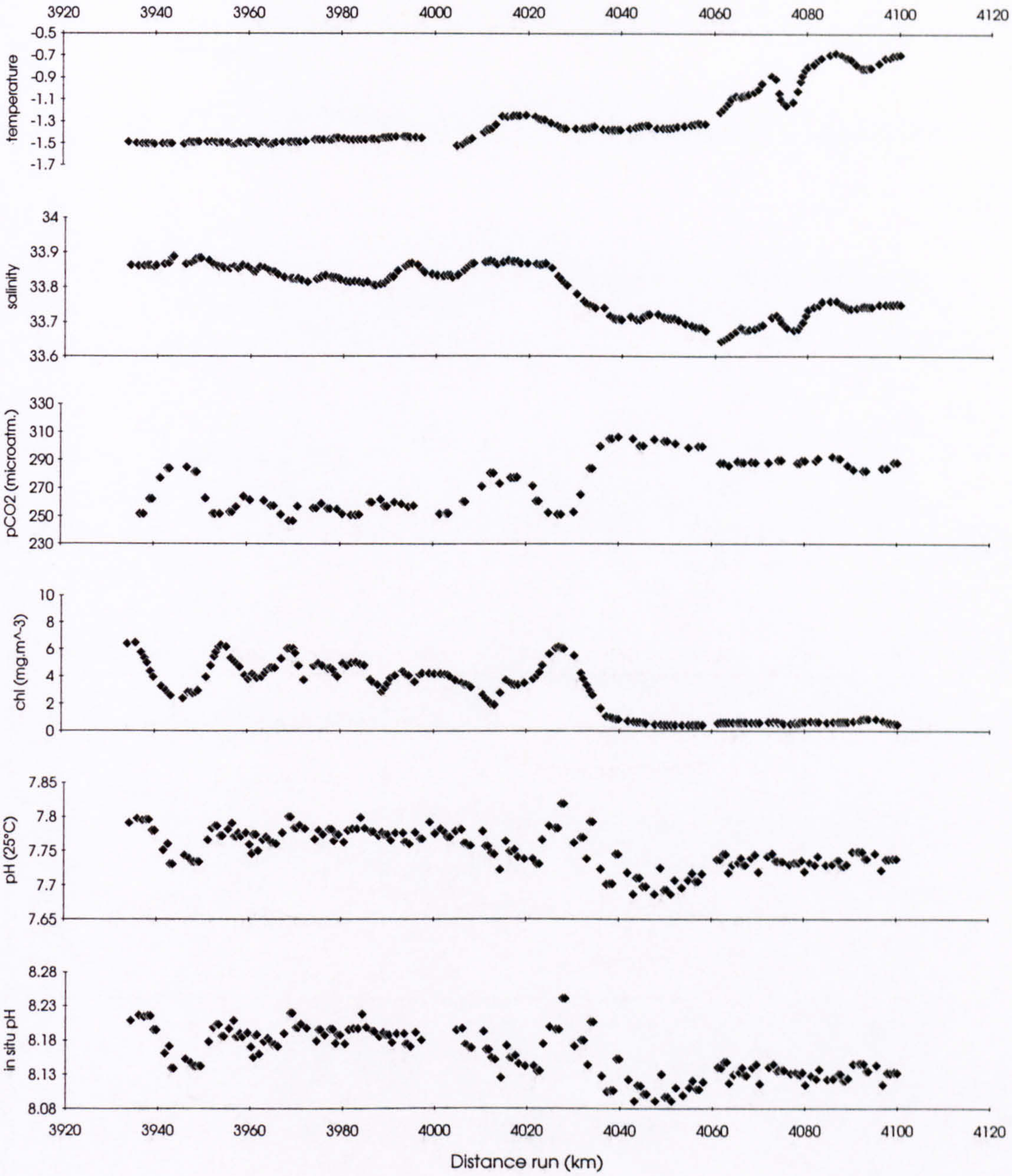

Figure 5.17. Surface profiles of temperature, salinity, pCO2, chlorophyll, pH(25°C) and in situ pH for leg Z, survey 1, Bellingshausen Sea

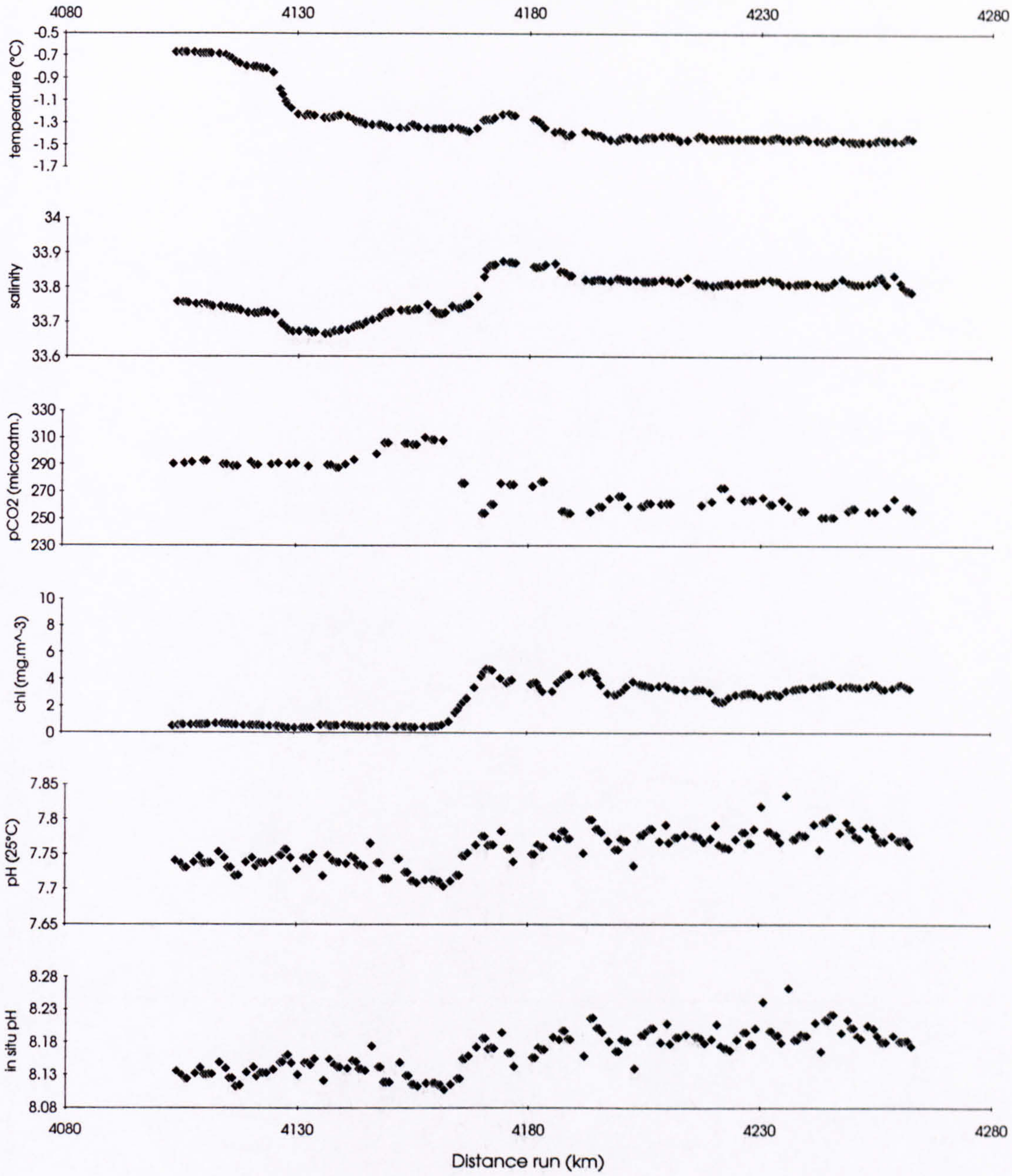

Figure 5.18. Surface profiles of temperature, salinity, pCO2, chlorophyll, pH(25°C) and in situ pH for leg A, survey 1, Bellingshausen Sea

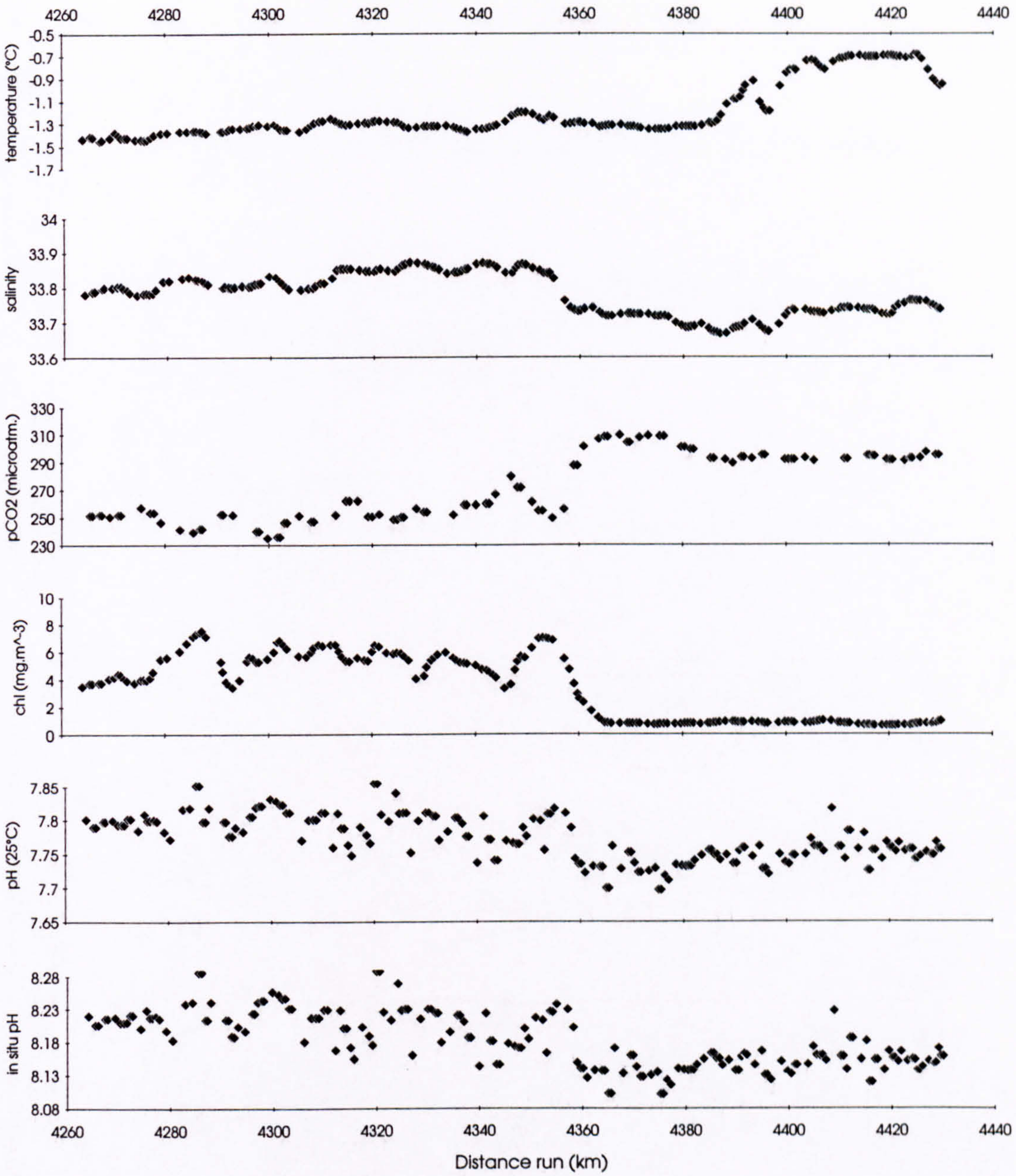

Figure 5.19. Surface profiles of temperature, salinity, pCO2, chlorophyll, pH(25°C) and in situ pH for leg B, survey 1, Bellingshausen Sea

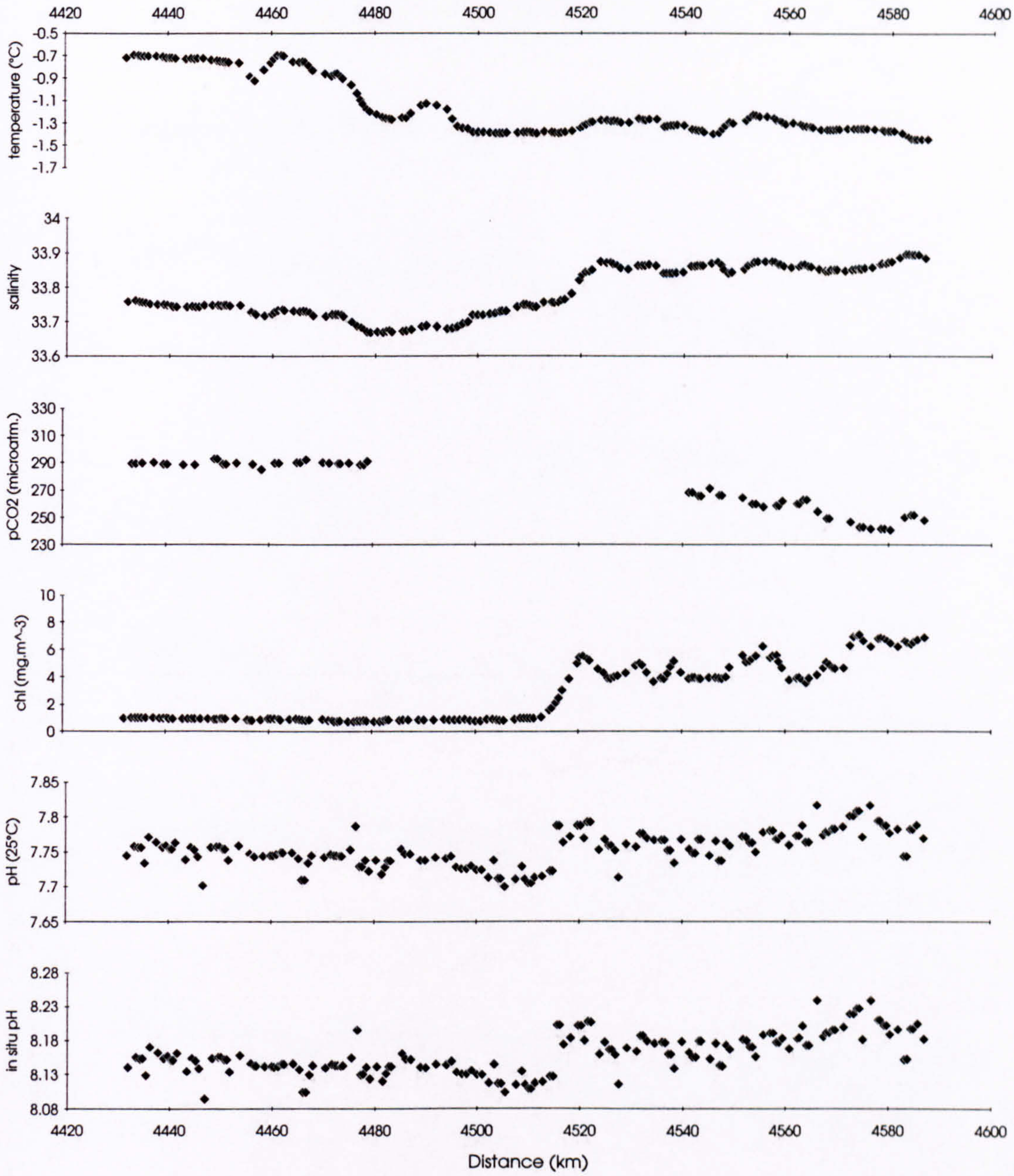

Figure 5.20. Surface profiles of temperature, salinity, pCO2, chlorophyll, pH(25°C) and in situ pH for leg C, survey 1, Bellingshausen Sea

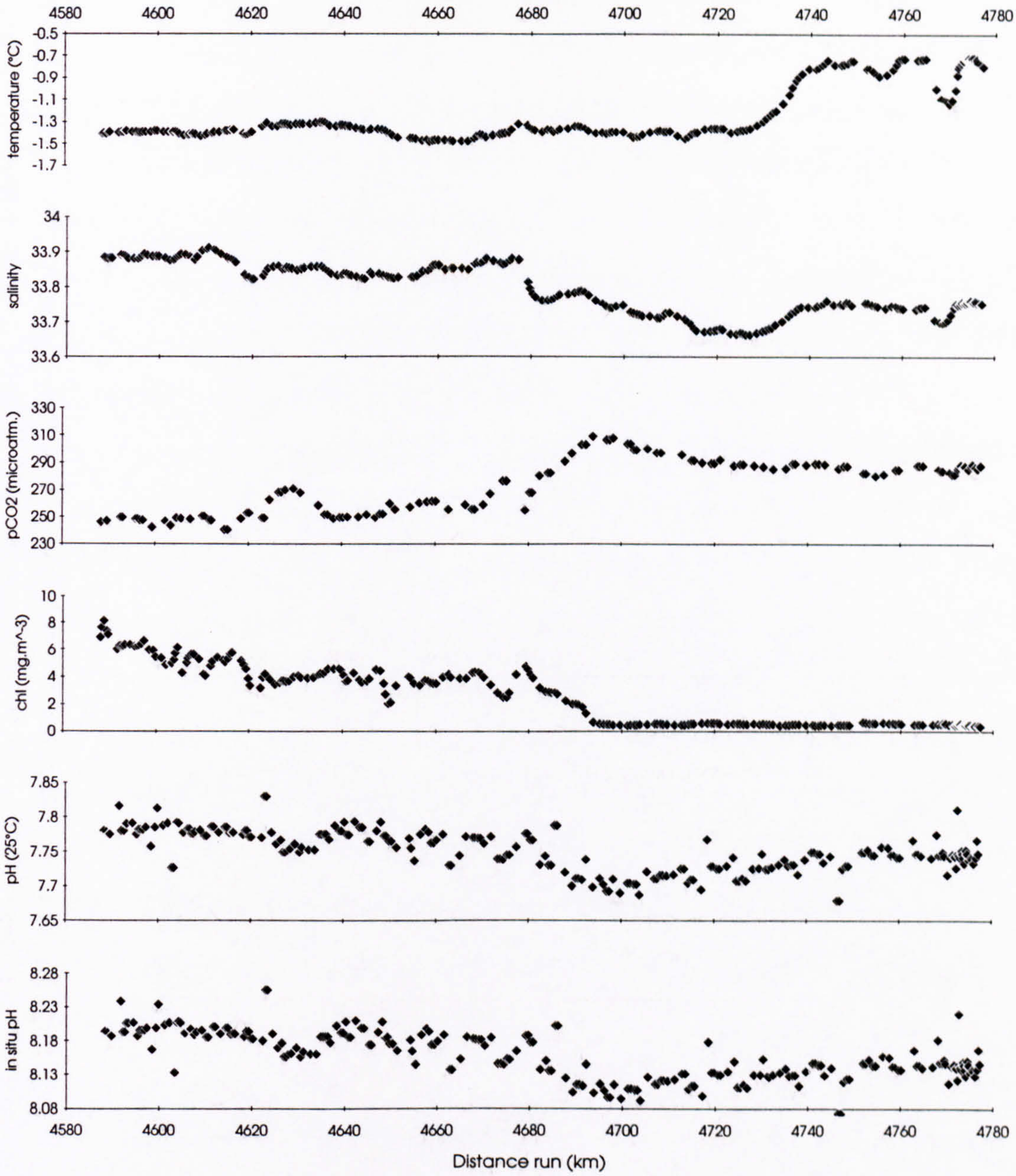

Figure 5.21. Surface profiles of temperature, salinity, pCO2, chlorophyll, pH(25°C) and in situ pH for leg D, survey 1, Bellingshausen Sea

exceeding 0.1 pH units. The highest pH values (~ 7.83 - 7.85) were associated with the highest chlorophyll concentrations immediately to the south of the salinity front, at the end of leg C - beginning of leg D, and also with a longitudinal band of high chlorophyll (> 4 $mg.m^{-3}$) measured on leg Z. pCO_2 levels drop to about 240 μatm in areas of intense chlorophyll production concurrent with the areas of highest chlorophyll and pH. The carbon dioxide parameters, pH and pCO_2 are negatively correlated (r = - 0.73, n = 445) and there is a slightly lower positive correlation between pH and chlorophyll (r = 0.65, n = 809). pCO_2 and chlorophyll exhibit a good negative correlation (r = - 0.78, n = 445). There is no correlation between salinity and temperature and the other parameters.

For the whole survey there is a good negative correlation between pH and pCO_2 (r = - 0.76, n = 831), and a reasonable positive correlation between pH and chlorophyll (r = 0.68, n = 1525). Commensurably, a good negative correlation exists between chlorophyll and pCO_2 (r = - 0.88, n = 831). Chlorophyll is also correlated well with salinity (r = 0.79, n = 1525). There are examples of excellent intimacy between the carbon dioxide system and the biological activity during selected legs throughout the survey. In the high chlorophyll area during leg W pH is strongly correlated with chlorophyll (r = 0.93, n = 80) and pCO_2 (r = - 0.91, n = 47) with a good relationship between pCO_2 and chlorophyll (r = - 0.89, n = 47). The most significant relationships for a whole leg were found during leg Z with good correlations between pH and chlorophyll (r = 0.83, n = 183) and pH and pCO_2 (r = - 0.86, n = 109).

5.4.4. Application to Remote Sensing

In terms of the monitoring of the evolution of the global CO_2 system, it is essential that regional algorithms are developed relating remotely sensed synoptic mapping of ocean colour, temperature and windspeed (from sea surface roughness) to the carbon flux across the air-sea interface and the biological and physical characteristics of surface waters. Towards this objective, this study has established the relationship between the carbon dioxide parameters pCO_2 and pH, and the remotely sensed parameters - chlorophyll and temperature. The *in situ* pH values, pH(is), have been used as, although they possibly

contain an offset of 0.02 pH units (see Chapter 4), they reflect more closely changes in the ambient sea surface conditions, and thus those related to satellite imagery, than the pH values at 25 °C. The relationships for the whole grid survey, the low chlorophyll area north of the front and the high chlorophyll area south of the front are as follows:

Whole grid survey

$pCO_2 = 311 + 28.56(\pm 2.29).t$ ($r = 0.40$, $n = 823$, $p < 0.001$)

$pCO_2 = 296 - 8.03(\pm 0.15).chl$ ($r = -0.88$, $n = 831$, $p < 0.001$)

$pH(is) = 8.115 - 0.042(\pm 0.003).t$ ($r = -0.32$, $n = 1510$, $p < 0.001$)

$pH(is) = 8.137 + 0.012(\pm 0.000).chl$ ($r = 0.74$, $n = 1510$, $p < 0.001$)

Low chlorophyll

$pCO_2 = 274 - 15.22(\pm 1.26).t$ ($r = -0.53$, $n = 383$, $p < 0.001$)

$pCO_2 = 302 - 16.74(\pm 1.69).chl$ ($r = -0.45$, $n = 386$, $p < 0.001$)

$pH(is) = 8.166 - 0.018(\pm 0.003).t$ ($r = -0.22$, $n = 711$, $p < 0.001$)

$pH(is) = 8.103 + 0.060(\pm 0.004).chl$ ($r = 0.52$, $n = 711$, $p < 0.001$)

High chlorophyll

$pCO_2 = 244 - 12.74(\pm 10.26).t$ ($r = -0.06$, $n = 445$, $p = 0.215$)

$pCO_2 = 296 - 8.13(\pm 0.31).chl$ ($r = -0.78$, $n = 445$, $p < 0.001$)

$pH(is) = 8.171 - 0.010(\pm 0.014).t$ ($r = -0.02$, $n = 799$, $p = 0.494$)

$pH(is) = 8.133 + 0.012(\pm 0.001).chl$ ($r = 0.64$, $n = 799$, $p < 0.001$)

In every case there is a weak pH - temperature relationship with negative correlation coefficients (r) ≤ -0.32. Similarly, pCO_2 correlates poorly with temperature. There is a reasonable relationship between pH and chlorophyll throughout the survey area ($r = 0.74$) although correlations are lower for the low and high chlorophyll regions ($r = 0.52$ and 0.64). The standard error of 0.004 for the former algorithm is significant. pCO_2 correlates well with chlorophyll over the survey area ($r = -0.88$) and similarly, there is a significant correlation in the high chlorophyll area ($r = -0.78$). The algorithms for this study are

compared with other published relationships in Section 5.6.1.

5.5. Discussion

5.5.1. CO_2 system properties

The refinement of spectrophotometric techniques has allowed for very precise pH measurements at sea (Robert-Baldo *et al.*, 1985; Byrne *et al.*, 1988; Byrne and Breland, 1989; Clayton and Byrne, 1993; Bellerby *et al.*, 1993) free from the problems associated with potentiometric techniques (Bellerby *et al.*, 1993). Spectrophotometric measurements are internally calibrated during the determination of the dissociation constant and molar absorptivities of the indicator thus obviating the requirement for regular calibration against standard solutions whilst at sea. The overall accuracy of the method depends on the accuracy of (i) the potentiometric determination of the indicator dissociation constant, and (ii) the accuracy of the solution absorbance and temperature measurements. The internal consistency of the pH and pCO_2 measurements reported here is shown by the significant negative correlation between them (r = - 0.88, n = 1524; Figure 5.22). More detailed calculations which take advantage of concomitant TCO_2 measurements show that the results are consistent with accuracies of 2 μatm. (pCO_2) and 0.005 pH unit (see Chapter 4).

5.5.2. Comparison of Bellingshausen Sea pH with other pH observations in the Southern Ocean

The number of pH observations in this area of the World's oceans is very limited and values have been collected using potentiometry, the problems of which are discussed in Section 3.3. Hence, this study has compiled not only the first pH data for the Bellingshausen Sea, but has also obtained the first reliable pH data in the Southern Ocean. The range of pH values found on this survey was from 7.65 to 7.85 units at 25°C, and at *in situ* temperatures from 8.04 to 8.28 units, with a general increase from the Bransfield Strait across the Bellingshausen Sea through the survey area. The latitudinal variation of pH between 55°N and 70°S reviewed by Skirrow (1975) shows *in situ* values also generally increasing

between 60°S and 68°S (the latitudes of this study) although the *in situ* pH values are more tightly constrained between 8.05 and 8.15 units.

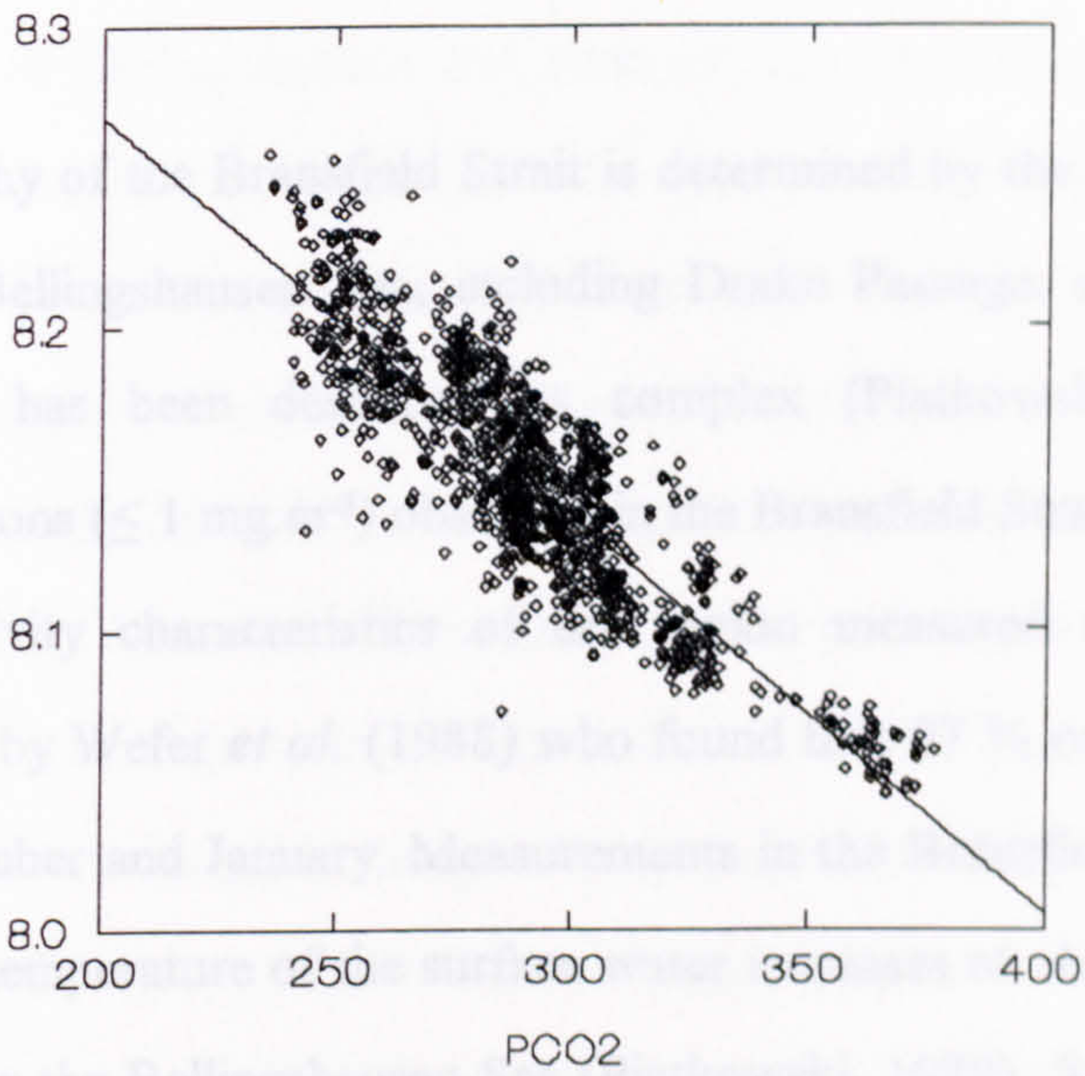

Figure 5.22. Relationship between in situ pH and pCO_2 (µatm.) throughout the whole cruise (r = - 0.88, n = 1524)

Sea surface pH values for November in the Weddell Sea measured potentiometrically by Poisson and Chen (1987) were higher than for any of the values reported in this study, even in the highest chlorophyll areas. Their pH(25°C) values for waters with temperatures between 0 and - 2.0 °C range from about 7.88 to 7.92 units. Whereas, for similar temperatures during this study, pH did not exceed 7.85 units. The degree of disagreement is due to the different calibration scales used in the studies. Chen and co-workers measure pH on the NBS scale which has been shown to be about 0.15 units higher than measurements on the total hydrogen ion scale at 25 °C (Hansson, 1979c; Millero, 1979) but is ultimately dependent on the residual liquid junction potential between buffer and seawater (See Section 3.3.). Full details of the apparent activity coefficient are required before comparisons with the results from this study can be made. Similarly, Catalano *et al.* (1991a; 1991b) measured pH potentiometrically in the Southern Ocean using NBS buffers according to the method of Zirino (1975) but did not document their

results sufficiently well to enable comparison.

5.5.3. Processes controlling CO_2 system in the Bellingshausen Sea area

Bransfield Strait

The hydrography of the Bransfield Strait is determined by the relative influences of the waters from the Bellingshausen Sea, including Drake Passage, and the Weddell Sea (Deacon, 1937) and has been described as complex (Piatkowski, 1989). The low chlorophyll concentrations ($\leq$ 1 mg.m^{-3}) observed in the Bransfield Strait are consistent with the temporal productivity characteristics of the region measured during a time-series sediment trap exercise by Wefer *et al.* (1988) who found that 97 % of the total particulate flux occurred in December and January. Measurements in the Bransfield Strait in February 1982 suggest that the temperature of the surface water increases to about 1 °C in the inner strait to over 2°C out in the Bellingshausen Sea (Piatkowski, 1989). Salinity decreases to a minimum of 33.3 in the inner strait and to 33.7 out into the Bellingshausen Sea/North West Drake Passage (Piatkowski, 1989). The temperature of surface water at a mid-strait station in winter has been reported as - 1.6 °C, with very low chlorophyll concentrations of ~ 0.1 mg.m^{-3} (Brightman and Smith, 1989). The waters of the Strait are part of the East Wind Drift and are a mixture of water upwelled from the Circumpolar Deep Water and that from ice-melt and runoff. Warming of the surface waters apparent at this time of year may have increased the pCO_2 levels to above atmospheric levels and thus the pH has decreased through shifts in the equilibrium of the carbon dioxide species.

In this region, low chlorophyll concentrations have a marked relationship with pCO_2 and pH. Under conditions of *quasi*-constant temperature and salinity a 120 km stretch of the Bransfield Strait (Figure 5.6), the combination of minor hydrographical changes combined with low autotrophic activity appears to be responsible for changes in surface pCO_2 of about 20 μatm and a change in pH of upto 0.03 pH units.

Across the CWB hydrographic properties dominate the CO_2 system although chlorophyll correlates well with pH and pCO_2. The small rise in surface chlorophyll concentration from the front westwards cannot be responsible for the apparent increase in

pH and decrease in pCO_2 and must in part be due to the increasing influence of the CO_2 undersaturated waters of the open ACC.

Bellingshausen Sea transect

The whole of the Bellingshausen Sea transect was undersaturated with respect to CO_2 with little indication of any significant biological activity to account for the CO_2 deficit. Other possibilities are discussed in the following paragraphs.

Upwelling of deep water under the ice during the austral winter in the Weddell Sea has been shown to dilute the anthropogenic CO_2 signal in both the surface and deep waters (Poisson and Chen, 1987). The waters in the Bellingshausen Sea during the transect and the survey had recently been covered with ice and therefore it is conceivable that the surface waters had been influenced through mixing with upwelled low-CO_2 waters. This was not the case during the austral spring in the Weddell Sea as Bakkar *et al.* (1994) found that seawater pCO_2 under the ice was higher than atmospheric which agrees with values measured by Takahashi *et al.* (1993).

Although kinetic rate constants for CO_2 equilibration in seawater are on the order of 100 seconds, equilibration of CO_2 in the surface mixed layer with the atmosphere is slow and may take up to a year (Broecker and Peng, 1982). It is, therefore, possible that the seawater is undersaturated with respect to CO_2 because of cooling once the ice had formed. To reach a pCO_2 of 300 μatm this would have required a reduction in temperature of about 4°C, assuming the waters were initially at equilibrium with the atmosphere, as the change in pCO_2 with temperature ($\delta \ln pCO_2/\delta t$) has been shown to approximate 4.23 % per °C (Takahashi *et al.*, 1993). Temperatures in the Bellingshausen Sea in summer reach about 2°C (Piatkowski, 1989), a cooling from such temperatures to present conditions would account for the deficit between the CWB and the SPF.

The pCO_2 values in the Subantarctic waters have been shown to exhibit a 25 μatm reduction in surface concentrations resulting from biological activity during the summer months (Goyet *et al.*, 1991). The Polar Front is about 10° further north in the Indian Ocean sector compared to the Pacific Ocean sector (Deacon, 1982) so the waters of the study area in this work and the Goyet *et al.* (1991) survey are comparable. Robertson and Watson

(1994) suggested that the low pCO_2 levels found during the Bellingshausen Sea transect may be a consequence of previous biological activity. Again the incongruity between pCO_2 and chlorophyll concentrations may be due to the slow equilibrium response of the carbon dioxide system in the whole of the mixed layer. Nutrient uptake properties in this region indicate low f-ratio values which are characteristic of a post-bloom scenario in temperate northern latitudes (H. Waldron personal communication, 1994).

Chlorophyll concentrations are characteristically low (< 1 mg.m^{-3}) for the Southern Ocean (*e.g.* Nelson *et al.*, 1989; Sullivan *et al.*, 1990) during both the Bellingshausen Sea transect and the area to the north of the SPF. Except for the second leg of the transect chlorophyll profile exhibits prominent peaks often associated with changes in the hydrographic nature of the surface waters. There is no high chlorophyll bloom associated with the SPF during the Bellingshausen Sea transect as is the case at 85°W. The low chlorophyll levels during the second leg allow the significance of the hydrography on the CO_2 system to be assessed. At the SPF a decrease in salinity of 0.1 is associated with a rise in pH of 0.05 unit and a decrease in pCO_2 of 25 μatm. The CO_2 system is strongly controlled by the salinity (hydrography) in this region and it is this overriding influence that is responsible for the paradoxical positive relationship between chlorophyll and pCO_2 during the 1st leg of the transect.

Mean monthly ice concentration maps for 1979-86 produced by Gloersen *et al.* (1992) show that the most of the transect generally has significant ($\geq 40\%$) ice coverage up until October. The ice edge commonly retreats anti-clockwise, partially hinged near the tip of the Antarctic Peninsula. As such, the waters to the east of the Bellingshausen sea retain their ice cover longer than that in the open ocean. Partial ice coverage is common throughout November over the first third of the transect (Gloersen *et al.*, 1992). It is not possible to ascertain the reasons for the changes in hydrography without a full knowledge of the upper ocean physical characteristics. Changes may be due to upwelling or downwelling, or resulting from localised ice-melt from floes or icebergs. Nevertheless, the Bellingshausen Sea transect has illustrated the limited productivity of the area signified by low chlorophyll concentrations which are common to open-waters in the Southern Ocean throughout the year (El-Sayed and Taguchi, 1981). The whole of the transect is a sink for atmospheric CO_2

with seawater pCO_2 levels generally 30 - 60 μatm below atmospheric. This is a major finding of this study and fits recent thinking on the uptake of CO_2 in the Southern Ocean (see Section 5.6.1).

The South Polar Front

The intensive survey area at around 66.5 - 68°S straddled the SPF. The waters immediately to the north of the front have been described as 'extremely fresh' (Read *et al.*, 1994) with salinities less than 33.8 to a minimum of 33.6. This is Antarctic Surface Water and its character results from the relative mixing of meltwater and terrestrial runoff and the upwelling of Circumpolar Deep Water (Read *et al.*, 1994). South across the front salinity increases rapidly to more than 33.8 due to the upwelling of warmer, more saline Circumpolar Deep Water from 1000m inducing isopycnal surface outcropping at about 67°S. South of this low salinity region was again found Antarctic Surface Water.

The appearance of surface eddies immediately south of, and parallel to, the salinity front is possibly an artefact of the contour plotting procedure (Figures 5.11. to 5.13.) although eddy structures further to the south are probably real (R.T. Pollard, personal communication, 1994). It is nevertheless apparent that there is a significant relationship between all three variables throughout the survey with considerable agreement between expected highs and lows for each parameter.

Causal factors for the high chlorophyll concentrations measured during STERNA did not follow common theories of meltwater induced stability and subsequent bloom formation. Areas of low salinity supported the lowest chlorophyll levels, and it was the narrowing of the mixed layer through a strengthening of the pycnocline due to upwelling at the front of warm, high salinity Circumpolar Deep Water that supported bloom formation.

5.6. CO_2 processes in the Bellingshausen Sea and global implications

The pCO_2 levels reported in this study are consistently lower than those described by Takahashi and Chipman (1982) for similar latitudes in the Southern Ocean during the GEOSECS cruises. Added to this difference should be the present day increased

atmospheric loading of carbon dioxide increasing the apparent disequilibrium between the two studies. Conversely, Metzl *et al.* (1991) identified significantly low pCO_2 values in the southwest sector of the Indian Ocean with levels down to 310 μatm. Interspersed between these readings existed significant sources of CO_2 (Metzl *et al.*, 1991). Autotrophic activity corresponded well with pCO_2 sinks, and chlorophyll levels between the Polar Front and the Antarctic Divergence were similar to those in the Bellingshausen Sea transect in this study.

Conventional processes of bloom formation in the marginal ice zone in the wake of retreating ice cover has not been witnessed during this study. The low salinity surface waters responsible for the stability in the surface layers were generally present for all waters north of the Continental Water Boundary with exceptions above the low salinity front and immediately to the north of the intensive survey area. In these stabilised areas were found the lowest chlorophyll levels. Conversely, upwelling of high salinity Circumpolar Deep Water pushing water above it to the surface was linked to the areas of highest chlorophyll and pH levels and lowest pCO_2 values. Here was found the steepest halocline where upwelling water had compressed the isohalines creating intense stability in the surface waters.

Surface waters throughout the survey, except waters of the East Wind Drift, had pCO_2 values less than atmospheric. The CO_2 flux for the region has been calculated to be 0.02 Gt C. area^{-1}. month^{-1} based on an area of 3 million km^2 using the Tans *et al.* (1990) approximation for gas exchange rates (J.E. Robertson, personal communication). Robertson and Watson (1994) have calculated, using data from this cruise and another in the Southwest Indian Ocean during the Summer of 1992, that the Southern Ocean may be a sink of between 0.25 - 0.40 Gt C during the spring and summer months. The range of this estimate is due to the present discrepancies in estimating the CO_2 transfer velocity discussed in Section 2.4. This sink is consistent with recent work by Conway *et al.* (1994), based on atmospheric measurements, showing that the CO_2 sink in the Southern Ocean has increased sharply between 1989 and 1992 from 0 to 1.5 Gt C. yr^{-1}.

The algorithms developed relating the carbon dioxide parameters with temperature and chlorophyll have illustrated the complex association between the hydrography and biology on determining the carbonate system in seawater. The relationships with

temperature with both pH and pCO_2 are poor. pH shows an encouraging relationship with chlorophyll over the whole survey area, and the slope is similar for the high chlorophyll area, although the fit is not as good. pCO_2 correlates well with chlorophyll over of the whole survey area and the high chlorophyll area and the slopes of the algorithms are very similar to that determined by Watson *et al.* (1991b) for low pCO_2 values. Watson *et al.* (1991b) characterised the relationship between pCO_2 and temperature and chlorophyll in the North Atlantic. These relationships were;

$$pCO_2 = 427 - 10.74(\pm 0.16).t \qquad (r = -0.91)$$

$$pCO_2 = 299 - 6.60(\pm 0.57).chl \qquad (r = -0.70)$$

$$pCO_2 = 332 - 10.60(\pm 0.64).chl \qquad (r = -0.61)$$

$$pCO_2 = 358 - 16.80(\pm 0.60).chl \qquad (r = -0.79)$$

where, the three regressions are representative of a senescent or secondary bloom, peak bloom stage and a bloom of recent history respectively (Watson *et al.*, 1991b). During this study, the slope of the pCO_2/chlorophyll relationship in the low chlorophyll area, although less significant, is similar to that developed by Watson *et al.* (1991b) for waters with higher pCO_2 values. Murphy *et al.* (1991a) calculated the additional relationships for the Southeast Pacific:

$$pCO_2 = 334 + 1.72.t \qquad (r = 0.88)$$

and the Southwest Pacific:

$$pCO_2 = 312 - 0.388.t \qquad (r = -0.48).$$

which can be compared with those found by Watson *et al.* (1991b) and this study, respectively;

$$pCO_2 = 427 - 10.74(\pm 0.16).t \qquad (r = -0.91)$$

$$pCO_2 = 311 + 28.56(\pm 2.29).t \qquad (r = 0.40)$$

It is important to note that although the slopes of the chlorophyll/pCO_2 algorithms show considerable congruity, there is a significant disagreement between the temperature/CO_2

algorithms in the three separate studies. This implies that relationships with temperature are regional in nature and may therefore have to be determined on a smaller scale than the basin-wide chlorophyll/pCO_2 interrelations.

The correlation coefficient for pH/chlorophyll relationships is generally lower than for pCO_2/chlorophyll relationships. This is probably because the changes in surface pH are smaller than can be detected using this method and, therefore, even better precision is required - although uncertainties in the temperature correction to *in situ* conditions may also contribute.

The short period over which the Bellingshausen Sea was surveyed does not allow for a determination of the annual CO_2 flux for the area. Although the survey showed that the area was a net sink in the austral spring/summer, it is essential to repeat the survey at other times of the year in order to ascertain whether the area is a net annual sink or source for CO_2. It is possible that the gas is released back to the atmosphere during summer warming of the seawater, or through respiration in the surface layers. The introduction of the ocean colour Sea-Viewing Wide Field-of-view Sensor (SeaWiFS) will enable, through the use of algorithms such as those given in Sections 5.4.4 and 5.6.1, gas transfer rates to be estimated for distant areas, such as the Southern Ocean, from remotely sensed chlorophyll, sea surface and sea surface roughness readings.

CHAPTER 6.

CONCLUSIONS AND FUTURE WORK

6.1. Analytical development and future applications of pH analysis

A continuous potentiometric technique has been refined with a flow regime producing the optimum electrode response characteristics and strict temperature control over the buffer reservoirs, tubing and electrodes. A novel stopped-flow injection spectrophotometric technique for the semi-continuous determination of seawater pH using phenol red has been designed, implemented and validated. Both instruments have been automated for control and data acquisition. The two techniques were employed concurrently during an oceanographic cruise to the Bellingshausen sea, Southern Ocean, whose objective was the investigation of the flux of carbon in this area. The potentiometric technique exhibited very low precision due to problems with irreproducible electrode responses and electrical interference probably from the on-line seawater supply and the ship's electrical supply. The spectrophotometric method illustrated a precision of ± 0.005 pH unit, which is over an order of magnitude more precise than previous continuous spectrophotometric methods and concordant with the aims of this research. Sampling frequency for the spectrophotometric technique was about 20 h^{-1} whilst the system was operating simultaneously with the potentiometric method and about 25 h^{-1} in isolation.

This study has identified the great potential for very precise continuous spectrophotometric measurements at sea, and it is recommended that the spectrophotometric technique becomes the method of choice for future investigations. It is, however, noticeable that the correlations of pH with chlorophyll and salinity are generally a little poorer than those of pCO_2 with the same properties. This is possibly due to the lower accuracy of the pH measurements (0.005 pH is equivalent to 1.2%, compared with 0.6% for pCO_2) and highlights the need for further improvements in the accuracy of pH measurement. A major limitation in this work was the spectrophotometer, which was only able to measure absorption at one wavelength at a time. The use of a diode array spectrophotometer would reduce errors associated with unknown instrument drift. The measurement of more than two wavelengths will allow greater confidence in the pH reading if the spectral dependence of the indicator with varying pH is characterised. This will enable each measurement to be checked for cell fouling, interfering absorbents, *etc*.

pH measurements by indicator spectrophotometry offer perhaps the best possibility for monitoring of the marine CO_2 system from unmanned platforms. It is anticipated that micro-miniaturisation of the technique through the use of wavelength specific diodes and fibre optics, and possibly the introduction of charge-coupled detectors, will be the future mode of *in situ* seawater pH measurement. These techniques will be employed remotely on buoys, autonomous submarines such as the NERC Autosub, and additionally will take advantage of ships of opportunity. The pH system may be used in conjunction with pCO_2 sensors to determine the CO_2 system, or if the specific alkalinity of the water mass has been determined then pH may be used alone. The increased global coverage of CO_2 measurements, on spatial and temporal scales, will provide a more accurate constraint on carbon cycle models and provide information which is currently too expensive to collect using conventional methods, *i.e.* research cruises

6.2. pH in the Bellingshausen Sea and suggestions for future research in the Southern Ocean

A unique data set has been obtained describing the surface water pH characteristics of the Southern Bransfield Strait and the Bellingshausen Sea. These are the first reliable documented pH measurements to be made anywhere in the Southern Ocean. Values of alkalinity calculated from firstly pH and pCO_2, and then pCO_2 and TCO_2, agree to 1.3 ± 7.3 $\mu equiv.kg^{-1}$ seawater, $n = 79$, or about 0.32 %. The imprecision of the comparison arising from the precision of the analytical methods and the carbonic acid dissociation constants is approximately 0.34 % suggesting that the methodologies employed exhibit excellent internal consistency.

When measured pH values are compared with *in situ* values calculated from alkalinity and TCO_2 the standard deviation is $\pm$ 0.016 pH unit with a standard error ranging from 0.02 to 0.04 dependent on the chosen formation constant for hydrogen sulphate used to convert pH values from the free to total hydrogen ion concentration scale. The Dickson (1990b) constants give the smallest standard error which was within the precision of the *in situ* pH comparison if the standard deviation associated with the pH-temperature

relationship is included.

The carbon dioxide properties of the surface waters in the Bellingshausen Sea are mainly controlled by the hydrography, although in regions of increased biological activity there is considerable intimacy illustrated between biological activity and the carbonate system. In areas of low productivity in the Eastwind Drift through the Bransfield Strait the pH(25°C) levels were the lowest of the cruise down to 7.65 associated with waters supersaturated with carbon dioxide. Across the Bellingshausen Sea at about 55-60°S current pH features were generally related to hydrographical features. The intense phytoplankton bloom surveyed at about 65°S illustrated the significant relationship between the biological properties and the pH and pCO_2 of the surface waters in the area. Here, pH values were the highest for the cruise reaching a maximum of 7.85.

The ACC is a *quasi*-continuous body of water with predictable latitudinal thermohaline properties. The chlorophyll distribution of the Southern Ocean have also been shown to be predictable, on a seasonal basis, via ocean colour measurements (Sullivan *et al.*, 1994). It is, therefore, reasonable to suggest relationships between different areas of the Southern Ocean with similar water types and colour characteristics. This study has identified a significant CO_2 sink in the Bellingshausen Sea during the early austral summer. If the processes causing this drawdown are present throughout the Southern Ocean, then the area will be an important control on atmospheric CO_2 concentrations. For this to be consistent with the results of Conway *et al.* (1994), biological and thermodynamic processes occurring throughout the year must result in a net sink for CO_2 of about 1.5 Gt C $year^{-1}$.

Further work in the Southern Ocean should identify: (1) the processes promoting the bloom associated with the SPF and determine its duration; (2) the processes in the Bellingshausen Sea leading to the low pCO_2 levels found throughout the survey and whether CO_2 is released to the atmosphere in the austral autumn; (3) whether the variability in surface CO_2 determined by Metzl *et al.* (1991), Goyet *et al.* (1991) and Poisson *et al.* (1993) is typical of the Southern Ocean, or is the relatively predictable phytoplankton distribution identified by Sullivan *et al.* (1994) indicative of more orderly CO_2 characteristics.

It is necessary to further study the processes controlling the carbonate system in the Southern Ocean in order to ascertain the net CO_2 flux. Future studies will be facilitated through the use of pH systems such as those discussed in section 6.1. The large data sets compiled from such *in situ* systems will provide excellent ground-truthing for remotely sensed algorithms which will enable annual, basin wide measurements of biogeochemical properties of surface waters using SeaWiFS.

REFERENCES

Acker J.G., Byrne R.H., Ben-Yaakov S., Feely R.A. and Betzer P.R., 1987. The effect of pressure on aragonite dissolution rates in seawater. *Geochim. Cosmochim. Acta*, **51**, 2171-2175.

Almgren T., Dyrssen D. and Strandberg M., 1975. Determination of pH on the moles per kg seawater scale (M_W). *Deep-Sea Res.*, **22**, 635-646.

Bakkar D.C.E., De Baar H.J.W. and Bathmann U., 1994. Surface water CO_2 changes in a southern spring. ASLO/AGU 1994 Ocean Sciences Meeting, San Diego, 177-178. (Abstract).

Balch W.M., Holligan P.M. and Kilpatrick K.A., 1992. Calcification, photosynthesis and growth of the bloom forming coccolithophore *Emiliania huxleyi*. *Cont. Shelf Res.*, **12**, 1353-1374.

Barnola J. -M., Raynaud D., Korotkevich Y.S. and Lorius C., 1987. Vostock ice-core provides 160,000 year record of atmospheric CO_2. *Nature*, **329**, 408-414.

Bates R.G., 1973. *Determination of pH: Theory and Practice*, John Wiley and Sons, New York, 479pp.

Bates R.G. and Calais J.G., 1981. Thermodynamics of the dissociation of $BisH^+$ in seawater from 5 to 40°C. *J. Sol. Chem.*, **10**, 269-279.

Bates R.G. and Hetzer H.B., 1961. Dissociation constant of the protonated acid form of 2-amino-2-(hydroxymethyl)-1,3-propanediol [TRIS-hydroxymethyl-aminomethane] and related thermodynamic quantities from 0 to 50°C. *J. Phys. Chem.*, **65**, 667-671.

Bates R.G. and Macaskill J.B., 1975. Acid-base measurements in seawater. In: *Analytical Methods in Oceanography* (Ed: T.R.P. Gibb), A.C.S. Advances in Chemistry Series, **147**, American Chemical Society, p110-123.

Bellerby R.G.J., Millward G.E., Turner D.R. and Worsfold P.J., 1993. Approaches to the continuous monitoring of seawater pH and its role in the global carbon cycle. *Trends Anal. Chem.*, **12**(9), 382-386.

Ben-Yaakov S. and Lorch Y., 1983. Alkalinity determinations in hypersaline solutions: a method for overcoming glass electrode errors. *Mar. Chem.*, **13**, 293-304.

Berger R. and Libby W.F., 1969. Equilibration of atmospheric carbon dioxide with seawater: possible enzymatic control of the rate. *Science*, **164**, 1395-1397.

Berner 1991. A model for atmospheric CO_2 over Phanerozoic time. *Am. J. Science*, **291**, 339-376.

Boyle E.A., 1986. Paired carbon isotope and cadmium data for benthic foraminifera: implications for changes in oceanic phosphorous, oceanic circulation and atmospheric carbon dioxide. *Geochim. Cosmochim. Acta*, **50**, 2655-2657.

Bradshaw A.L. and Brewer P.G., 1989. High precision measurements of alkalinity and total carbon dioxide in seawater by potentiometric titration. 2. Measurements of standard solutions. *Mar. Chem.*, **24**, 155-162.

Breland J.A. and Byrne R.H., 1993. Spectrophotometric procedures for determination of seawater alkalinity using bromocresol green. *Deep-Sea Res.*, **40**(3), 629-641.

Brezinski D.P., 1983. Kinetic, static and stirring errors of liquid junction reference electrodes. *Analyst*, **108**, 425-442.

Brightman R.I. and Smith W.O. Jr., 1989. Photosynthesis-irradiance relationships of Antarctic phytoplankton during austral winter. *Mar. Ecol. progr. Ser.*, **53**, 143-151.

Broecker W.S., 1982. Glacial to interglacial changes in ocean chemistry. *Prog. Oceanog.* **11**, 151-197.

Broecker W.S., 1991. Keeping global change honest. *Global Biogeochem. Cycles*, **5**(3), 191-192.

Broecker W.S., Ledwell J.R., Takahashi T., Weiss R., Merlivat L., Memery L., Peng T-H., Jähne B. and Munnich K.O., 1986. Isotopic versus micrometeorological ocean CO_2 fluxes: a serious conflict. *J. Geophys. Res.*, **91**, C9, 10,517-10,527.

Broecker W.S. and Peng T-H., 1974. Gas exchange rates between air and sea. *Tellus*, **24**, 21-35.

Broecker W.S. and Peng T-H., 1982. *Tracers in the Sea*. Eldigo Press, Palisades, New York, 690pp.

Broecker W.S. and Peng T-H., 1989. The cause of the glacial to interglacial atmospheric CO_2 change: a polar alkalinity hypothesis. *Global Biogeochem. Cycles*, **3**(3), 215-239.

Butler C.V. and Mackey D.J., 1992. Continuous shipboard measurement of the pH of surface seawaters, and derivation of the corresponding record of pCO_2. *Sci. Total Environ.*, **112**, 165-175.

Butler J.N., 1992. Alkalinity titration in seawater; how accurately can the data be fitted by an equilibrium model? *Mar. Chem.*, **38**, 251-282.

Butler R.A., Covington, A.K. and Whitfield, M., 1985. The determination of pH in estuarine waters. II: Practical considerations. *Oceanol. Acta*, **8**(4),433-439.

Byrne R.H., 1981. Inorganic lead complexation in natural seawater determined by UV spectroscopy. *Nature*, **290**, 487-489.

Byrne R.H., 1987. Standardisation of standard buffers by visible spectroscopy. *Anal. Chem.*, **59**, 1479-1481.

Byrne R.H., Acker J.G., Betzer P.R., Feely R.A. and Cates M.H., 1984. Water column dissolution of aragonite in the Pacific Ocean. *Nature*. **312**, 321-326.

Byrne R.H. and Breland J.A., 1989. High precision multiwavelength pH determinations in seawater using cresol red. *Deep-Sea Res.*, **36**(5), 803-810.

Byrne R.H. and Kester D.R., 1978. Ultraviolet spectroscopic study of ferric hydroxide complexation. *J. Sol. Chem.*, **7**, 373-383.

Byrne R.H., Robert-Baldo G., Thompson S.W. and Chen C.T.A., 1988. Seawater pH measurements: an at-sea comparison of spectrophotometric and potentiometric methods. *Deep-sea Res.*, **35**(8), 1405-1410.

Catalano G., Benedetti F., Goffart A. and Iorio M., 1991a. Distribution of dissolved oxygen, pH, total alkalinity and nutrients in the Southern Ocean and Ross Sea (R/V "Cariboo" 1989-90 cruise). *Nat. Sci. Com. Ant. Ocean Camp. 1989-90. Data Rep.*, **1**, 11-23.

Catalano G., Benedetti F. and Iorio M., 1991b. Coastal oceanography from Cape Russel to Campbell Ice Tongue (Terra Nova Bay). Dissolved oxygen, nutrients, pH, total alkalinity and total inorganic distribution. *Nat. Sci. Com. Ant. Ocean Camp. 1989-90. Data Rep.*, **1**, 25 - 32.

Chen C-T. A., 1982. On the distribution of anthropogenic CO_2 in the Atlantic and Southern Oceans. *Deep-Sea Res.*, **29**(5A), 563-580.

Chen C-T. A., 1993. The oceanic anthropogenic CO_2 sink. *Chemosphere*, **27**(6), 1041-1064.

Chen C.T.A., Feely R.A. and Gendron J.F., 1988. Lysocline, calcium compensation depth, and calcareous sediments in the North Pacific Ocean. *Pacific. Sci.*, **42**(3-4), 237-252.

Clayton T.D. and Byrne R.H., 1993. Spectrophotometric seawater pH measurements: total hydrogen ion concentration scale calibration of *m*-cresol purple and at-sea results. *Deep-Sea Res.*, **40**(10), 2115-2129.

Clegg S.L. and Whitfield M., 1991. Activity coefficients in natural waters. In *Activity Coefficients in Electrolyte Solutions*, 2nd Edition (Ed: K.S. Pitzer), CRC Press, p279-434.

Comiso J.C., Maynard N.G., Smith W.O. and Sullivan C.W., 1990. Satellite ocean colour studies of Antarctic ice edges in summer and autumn. *J. Geophys. Res.*, **95**, C6, 9481-9496.

Comiso J.C. and Sullivan C.W., 1986. Satellite microwave and *in situ* observations of the Weddell Sea ice cover and its marginal ice zone. *J. Geophys. Res.*, **91**, C8, 9663-9681.

Conrad R. and Seiler W., 1988. Influence of the surface microlayer on the flux of non-conservative trace gases (CO, H_2, CH_4, N_2O) across the ocean interface. *J. Atmos. Chem.*, **6**, 83-94.

Conway T.J., Tans P.P., Waterman L.S., Thoning K.W., Kitzis D.R., Masarie K.A. and Zhang N., 1994. Evidence for interannual variability of the carbon cycle from the NOAA/CMDL global air sampling network. *Journal of Geophysical Research*, submitted.

Covington A.K., Whalley, P.D., Davidson, W., 1983. Procedures for the measurement of pH in low ionic strength solutions including freshwater. *Analyst*, **108**, 1528-1532.

Covington A.K., Whalley, P.D., Davidson, W. and Whitfield, M., 1988. In: *The determination of trace metals in natural waters* (Ed: T.S.West), Blackwell scientific Publ., pp162-178.

Covington A.K. and Whitfield, M., 1988. Recommendations for the determination of pH in seawater and estuarine waters. *Pure Appl. Chem.*, **60**(6), 865-870.

Culberson C.H., 1981. Direct Potentiometry. In: *Marine electrochemistry: a practical introduction* (Eds: M. Whitfield and D. Jagner), John Wiley and Sons, Chichester, p187-261.

Culberson C.H., Pytkowitz R.M. and Hawley J.E., 1970. Seawater alkalinity determination by the pH method. *J. Mar. Res.*, **28**, 15-21.

Culberson C.H. and Pytkowicz, R.M., 1973. Ionization of water in seawater. *Mar. Chem.*, **1**, 309-316.

Deacon E.L., 1977. Gas transfer to and across an air-water interface. *Tellus*, **29**, 363-374.

Deacon G.E.R., 1937. The hydrology of the Southern Ocean. *Discovery Reports*, **15**, 1-124.

Deacon G.E.R., 1982. Physical and biological zonation in the Southern Ocean. *Deep-Sea Res.*, **29**(1A),

De Baar H.J.W., Buma A.G.J., Nolting R.F., Cadée G.C., Jacques G. and Tréguer P.J., 1990. On iron limitation of the Southern Ocean: experimental observations in the Weddell and Scotia Seas. *Mar. Ecol. Prog. Ser.*, **65**, 105-122.

Debney S. and Robertson J.E., 1993. BOFS '*STERNA 92*' cruise report (Ed: D.R. Turner), Plymouth Marine Laboratory.

Diamond D. and Walsh, S., 1991. Automatic pH titration curves. *Educ. Chem.*, **28**, 2, 47-48.

Dickson A.G., 1981. An exact definition of total alkalinity and a procedure for the estimation of alkalinity and total inorganic carbon from titration data. *Deep-Sea Res.*, **28A**(6), 609-623.

Dickson A.G., 1984. pH scales and proton-transfer reactions in saline media such as seawater. *Geochim. Cosmochim. Acta*, **48**, 2299-2308.

Dickson A.G., 1990a. Thermodynamics of the dissociation of boric acid in synthetic seawater from 273.15 to 318.15 K. *Deep-Sea Res.* **37**(5), 755-766.

Dickson A.G., 1990b. Standard potential of the reaction: $AgCl(s) + ½H_2(g) = Ag(s) + HCl(aq)$, and the standard acidity constant of the ion HSO_4^- in synthetic seawater from 273.15 to 318.15 K. *J. Chem. Thermodynamics*, **22**, 113-127.

Dickson A.G., 1993. pH buffers for seawater media based on the total hydrogen ion concentration scale. *Deep-Sea Res.*, **40**, 107-118.

Dickson A.G. and Millero, F.J., 1987. A comparison of the equilibrium constants for the dissociation of carbonic acid in seawater media. *Deep-Sea Res.*, **34**(10), 1733-1743.

Dickson A.G. and Riley J.P., 1978. The effect of analytical error on the evaluation of the components of the aquatic carbon-dioxide system. *Mar. Chem.*, **6**, 77-85.

Dickson A.G. and Riley, J.P., 1979. The estimation of acid dissocation constants in seawater media from potentiometric titrations with strong base. I. The ionic product of water - K_w. *Mar.Chem.*, 7, 89-99.

Dickson A.G. and Whitfield, M., 1981. An ion-association model for estimating acidity constants (at 25°C and 1 atm. total pressure) in electrolyte mixtures related to seawater (ionic strength < 1 mol.kg^{-1} H_2O). *Mar. Chem.*, **10**, 315-333.

Dieckmann G., 1987. High phytoplankton biomass at the advancing edge in the Northern Weddell Sea during winter. *EOS*, **68**, 1765.

Echeto J. and Merlivat L., 1988. Satellite determination of the carbon dioxide exchange coefficient at the ocean-atmosphere interface. *J. Geophys. Res.*, **93**, C12, 15,669-15678.

El-Sayed S. Z. and Taguchi S., 1981. Primary production and standing crop of phytoplankton along the ice-edge in the Weddell Sea. *Deep-Sea Res.*, **28A**(9), 1017-1032.

Emerson S., 1975. Chemically enhanced CO_2 gas exchange in a eutrophic lake: A general model. *Limnol. Oceanogr.*, **20**, 5, 743-753.

Enomoto H. and Ohmura A., 1990. The influences of atmospheric half-yearly cycle on the sea ice extent in the Antarctic. *J. Geophys. Res.*, **95**, C6, 9497-9511.

Eppley R.W. and Peterson B.J., 1979. Particulate organic flux and planktonic new production in the deep ocean. *Nature*, **282**, 677-680.

Erickson D.J., 1993. A stability dependent theory for air-sea gas exchange. *J. Geophys. Res.*, **98**, C5, 8471-8488.

Falkowski P.G., Ziemann D., Kolber Z. and Bienfang P.K., 1991. Role of eddy pumping in enhancing primary production in the ocean. *Nature*, **352**, 55-58.

Fuhrman R. and Zirino A., 1988. High-resolution determination of the pH of seawater with a flow-through system. *Deep-Sea Res.*, **35**(2), 197-208.

Gloerson P., Campbell W.J., Cavalieri D.J., Comiso J.C., Parkinson C.L. and Zwally H.J., 1992. Arctic and Antarctic sea ice, 1978-1987: satellite passive microwave observations and analysis. NASA Scientific and Technical Information Program, National Aeronautics and Space Administration, Washington D.C., 290pp.

Goldman J.C. and Dennet M.R., 1983. Carbon dioxide exchange between air and seawater: no evidence for rate catalysis. *Science*, **220**, 199-201.

Goldman J.C., Dennet M.R. and Frew N.M., 1988. Surfactant effects on air-sea gas exchange under turbulent conditions. *Deep-Sea Res.*, **35**(12), 1953-1970.

Gordon A.L., 1988. The Southern Ocean and global climate. *Oceanus*, **31**, 2, 39-46.

Goyet C., Beauverger C., Brunet C. and Poisson A., 1991. Distribution of carbon dioxide partial pressure in surface waters of the Southwest Indian Ocean. *Tellus*, **43B**, 1-11.

Goyet C. and Poisson A., 1989. New determination of carbonic acid dissociation constants in seawater as a function of temperature and salinity. *Deep-Sea Res.*, **36**(11), 1635-1654.

Hansson I., 1973a. A new set of acidity constants for carbonic acid and boric acid in sea water. *Deep-Sea Res.* **20**, 461-478.

Hansson I., 1973b. Determination of the acidity constant of boric acid in synthetic sea water media. *Acta Chem. Scand.*, **27**, 924-930.

Hansson I., 1973c. A new set of pH-scales and standard buffers for seawater. *Deep-Sea Res.*, **20**, 479-491.

Hansson I., Ahrland S., Bates R.G., Biedermann G., Dryssen D., Högfeldt E., Martell A.E., Morgan J.J., Schindler P.W., Warner T.B. and Whitfield M., 1975. Conventions for seawater equilibria. Group report. In: *The Nature of Seawater* (Ed: E.D. Goldberg), *Physical and Chemical Sciences Research Report*, **1**, Dahlem Konferenzen, p263-280.

Hasse L. and Liss P.S., 1980. Gas exchange across the air-sea interface. *Tellus*, **32**, 470-481.

Head R.N. and Miller W., 1993. BOFS '*STERNA 92*' cruise report (Ed: D.R. Turner), Plymouth Marine Laboratory.

Howson M.R., House W.A. and Pethybridge A.D., 1986. Automated procedure for pH measurement using a flow cell. *Analyst*, **111**, 1215-1218.

IPCC, 1990. *Scientific Assessment of Climate Change*. (Eds: Houghton J.T., Jenkins G.J. and Ephraums J.J.) The IPCC Scientific Assessment, Cambridge Univ. Press. 26 pp.

Jähne B., Munnich K.O. Bosinger R., Dutzi A., Huber W. and Libner P., 1987. On the parameters influencing air-water gas exchange. *J. Geophys. Res.*, **92**, C2, 1937-1949.

Jenkins W.J. and Goldman J.C., 1985. Seasonal oxygen cycling and primary production in the Sargasso Sea. *J. Mar. Res.*, **43**, 465-491.

Johannessen O.M., Johannessen J.A., Morison J., Farrely B.A. and Svendsen E.A.S., 1983. *J. Geophys. Res.*, **88**, 2755.

Johnson K.S., Voll R., Curtis C.A. and Pytkowicz R.M., 1977. A critical examination of the NBS pH scale and the determination of titration alkalinity. *Deep-Sea Res.*, **24**, 915-926.

Johnson K.S., Coale K.H. and Jannasch H.W., 1992. Analytical chemistry in oceanography. *Anal. Chem.*, **64**(22), 1065-1075.

Jones E.P. and Smith S.D., 1977. A first measurement of sea-air CO_2 flux by eddy correlation. *J. Geophys. Res.*, **82**, 5990-5992.

Jones C., Williams D.R. and Marsicano F., 1987. Surface water pH measurements - theory and practice. *Sci. Total Environ.*, **64**, 211-230.

Keeling C.D., 1973. Industrial production of carbon dioxide from fossil fuels and limestone. *Tellus*, **25**(2),174-198.

Khoo K.H., Ramette R.W., Culberson C.H. and Bates R.G., 1977. Determination of hydrogen ion concentrations in seawater from 5 to 40°C: standard potentials at salinities from 20 to 40‰. *Anal. Chem.*, **49**, 29-34.

King D.W., and Kester D.R., 1989. Determination of seawater pH from 1.5 to 8.5 using colorimetric indicators. *Mar. Chem.* **26**, 5-20.

Knox S., 1993. BOFS '*STERNA 92*' cruise report (Ed: D.R. Turner), Plymouth Marine Laboratory.

Kottmeir S.T. and Sullivan C.W., 1990. Bacterial biomass and production in pack ice of Antarctic marginal ice zones. *Deep-Sea Res.*, **37**(8), 1311-1330.

Kristensen H B., Salomon A. and Kokholm G., 1991. International pH scales. *Anal. Chem.*, **63**(18), 885-891.

Kroopnick, P.M., 1985. The distribution of ^{13}C of SCO_2 in the world oceans. *Deep-Sea Res.* **32**(1), 57-84.

Kuo C., Lindberg C. and Thompson D.J., 1990. Coherence established between atmospheric carbon dioxide and global temperature. *Nature*, **343**, 709-714.

Lampitt R.S., 1985. Evidence for the seasonal deposition of detritus to the deep-sea ocean floor and its subsequent resuspension. *Deep-Sea Res.*, **32**(8), 885-897.

Lashof D.A. and Ahuja D.R., 1990. Relative contributions of greenhouse gas emissions to global warming. *Nature*, **344**, 344-531.

Ledwell J.R., Watson A.J. and Law C.S., 1993. Evidence for slow mixing across the pycnocline from an open-ocean tracer-release experiment. *Nature*, **364**, 701-703.

Liss P.S. and Crane A.J., 1983. *Man-made Carbon Dioxide and Climate Change. A review of Scientific Problems*, University Press, London, pp 127.

Liss P.S. and Merlivat L., 1986. Air-sea gas exchange rates: Introduction and synthesis. In: *The Role of Air-Sea Gas Exchange in Geochemical Processes* (Ed: P. Buat-Menard), D. Reidal, Norwell, Mass., p113-129.

Longhurst A.R. and Harrison W.G., 1989. The biological pump: profiles of plankton production and consumption in the upper ocean. *Progr. Oceanogr.*, **22**(1), 47-123.

Maier-Reimer E. and Hasselmann K., 1987. Transport and storage of CO_2 in the ocean - an inorganic ocean-circulation carbon cycle model. *Clim. Dynamics.*, **2**(2), 63-90.

Mackey D.J., Butler E.C.V., Nichols P.D. and Higgins H.W., 1989. Continuous shipboard and *in situ* measurements of pH and fluorescence in seawater. *Mar. Chem.*, **28**, 41-60.

Martin J.H., 1990. Glacial-Interglacial CO_2 change: The iron hypothesis. *Paleoceanogr.*, **5**(1), 1-13.

Martin J.H., Gordon R.M. and Fitzwater S.E.,1990. Iron in Antarctic Waters. *Nature*, **345**, 156-158.

Mehrbach, C., Culberson, C.H., Hawley, J.E. and Pytkowicz, R.M., 1973. Measurement of the apparent dissociation constants of carbonic acid in seawater at atmospheric pressure. *Limnol. Oceanogr.*, **18**(6), 897-907.

Metzl N., Beauverger C., Brunet C., Goyet C. and Poisson A., 1991. Surface water carbon dioxide in the southwest Indian Sector of the Southern Ocean: a highly variable CO_2 source/sink region in summer. *Mar. Chem.*, **35**, 85-95.

Millero F.J., 1979. The thermodynamics of the carbonate system in seawater. *Geochim. Cosmochim. Acta*, **4**, 1651-1661.

Millero F.J., 1986. The pH of estuarine waters. *Limnol. Oceanogr.*, **31**(4), 839-847.

Millero F.J., Zhang J. -Z., Lee K. and Campbell D.M., 1993a. The use of buffers to measure the pH of seawater. *Mar. Chem.*, **44**, 143-152.

Millero F.J., Byrne R.H., Wanninkhof R., Feely R., Clayton T., Murphy P. and Lamb M.F., 1993b. The internal consistency of CO_2 measurements in the equatorial Pacific. *Mar. Chem.*, **44**, 269-280.

Monahan E.C. and Spillane M.C., 1984. The role of oceanic whitecaps in air-sea exchange. In: *Gas Transfer at Water Surfaces* (Eds: W. Brutsaert and G.H. Jirka), D. Reidal, Norwell, Mass., p495-503.

Morrison A. and Miller W., 1993. BOFS '*STERNA 92*' cruise report (Ed: D.R. Turner), Plymouth Marine Laboratory.

Murphy P.P., Feely R.A., Gammon R.H., Kelly K.C. and Waterman L.S., 1991a. Autumn air-sea disequilibrium of CO_2 in the South Pacific Ocean. *Mar. Chem.*, **35**, 77-84.

Murphy P.P., Feely R.A., Gammon R.H., Harrison D.E., Kelly K.C. and Waterman L.S., 1991b. Assessment of the air-sea exchange of CO_2 in the South Pacific during austral autumn. *J. Geophys. Res.*, **96**, C11, 20,445-20,465.

Najjar R.G., 1992. Marine Biogeochemistry. In: *Climate System Modeling*. (Ed: K.E. Trenberth) Cambridge University Press, Cambridge, p241-280.

Neftel A., Oeschger H., Staffelbach T. and Stauffer B., 1988. CO_2 record in the Byrd ice core 50,000-5,000 years BP. *Nature*, **331**, 609-611.

Nelson D.M., Smith W.O. Jr., Muench R.D., Gordon L.I., Sullivan C.W. and Husby D.M., 1989. Particulate matter and nutrient distributions in the ice-edge zone of the Weddell Sea: relationship to hydrography during late summer. *Deep-Sea Res.*, **36**(2), 191-209.

Nesbitt, H.W., 1980. A consistency test for single ion activity coefficients in electrolytic solutions, including seawater. *Chem. Geol.*, **29**, 107-116.

Nørgaard L., 1991. Determination of pH gradients and acidity constants in flow injection analysis systems by evolving factor analysis. *Anal. Chim. Acta*, **225**, 143-148.

Ohtaki E., Tsukamoto O., Iwatani Y. and Mitsuta Y., 1989. Measurements of the carbon dioxide flux over the ocean. *J. Meteor. Soc. Japan*, **67**, 4, 541-553.

Owens N.J.P., Priddle J., Turner D.R. and Williamson P., 1991. Upper ocean biogeochemistry in the south east Pacific sector of the Southern Ocean. NERC shiptime proposal, Plymouth Marine Laboratory.

Park P.K., 1966. Surface pH of the northeastern Pacific Ocean. *J. Oceanol. Soc. Korea*, **1**, 1-6.

Peng T-H., Takahashi T. and Broecker W.S., 1974. Surface measurements in the North Pacific Ocean Station PAPA. *J. Geophys. Res.*, **79**, 1772-1780.

Peng T-H., Broecker W.S., Mathieu G.G., Li Y.H. and Bainbridge A.E., 1979. Radon evasion rates in the Atlantic and Pacific oceans as determined during the GEOSECS program. *J. Geophys. Res.*, **84**, 2471-2486.

Perez, F.F. and Fraga, F., 1987. The pH measurements in seawater on the NBS scale. *Mar.Chem.*, **21**, 315-327.

Perissinotto R., Duncombe Rae C.M., Boden B.P. and Allanson B.R., 1990. Vertical stability as a controlling factor of the marine phytoplankton production at the Prince Edward Archipelago (Southern Ocean). *Mar. Ecol. Prog. Ser.*, **60**, 205-209.

Pia S.H., Waltman D.P., Hillman D.C. and Street K.W., 1990. Spectrophotometric determination of pH by flow injection. *Anal. Chim. Acta*, **231**, 21-26.

Piatkowski U., 1989. Macroplankton communities in Antarctic surface waters: spatial changes related to hydrography. *Mar. Ecol. Prog. Ser.*, **55**, 251-259,

Pickard G.L. and Emery W.J., 1982. *Descriptive Physical Oceanography*: An Introduction. 4th enlarged edition. Pergamon Press, Oxford, pp 249.

Platt T., Harrison W.G., Lewis M.R., Li W.K.W., Sathyendranath S., Smith R.E. and Vezina A.F., 1989. Biological productions of the oceans: the case for a consensus. *Mar. Ecol. Prog. Ser.*, **52**, 77-88.

Platt T. and Harrison W.G., 1985. Biogenic fluxes of carbon and oxygen in the ocean. *Nature*, **318**, 55-58.

Poisson A. and Chen C-T. A., 1987. Why is there little anthropogenic CO_2 in the Antarctic Bottom Water? *Deep-Sea Res.*, **34**(7), 1255-1275.

Poisson, A., Culkin, F. and Ridout. P., 1990. Inter-comparison of CO_2 measurements. *Deep-Sea Res.*, **37**, 1647-1650.

Ramette R.W., Culberson C.H. and Bates R.G., 1977. Acid-base properties of tris(hydroxymethyl)aminomethane (tris) buffers in seawater from 5 to 40°C. *Anal. Chem.*, **49**(6), 867-870.

Raven J.A., 1993. Carbon: a phycocentric view. In: *Global Environmental Change, Towards a Model of Ocean Biogeochemical Processes,* (Eds: G.T. Evans and M.J.R. Fasham), NATO ASI Series 1, Vol 10, p123-152.

Read J.F., Pollard R.T., Morrison A.I. and Symon C., 1994. On the southerly extent of the Antarctic Circumpolar Current in the southeast Pacific. *Journal of Geophysical Research.*, submitted.

Reibesell U., Wolf-Gladrow D.A. and Smetacek V., 1993. Carbon dioxide limitation of marine phytoplankton growth rates. *Nature*, **361**, 249-251.

Robert-Baldo G.L., Morris M.J. and Byrne R.H., 1985. Spectrophotometric determination of seawater pH using phenol red. *Anal. Chem.*, **57**, 2564-2567.

Robertson J.E. and Watson A.J., 1992. Thermal skin effect of the surface ocean and its implications for CO2 uptake. *Nature*, **358**, 738-740.

Robertson J.E. and Watson A.J., 1993. Estimation of primary production by observation of changes in the mesoscale carbon dioxide field. *ICES mar. Sci. Symp.*, **197**, 207-214.

Robertson J.E., 1993. BOFS '*STERNA 92*' cruise report (Ed: D.R. Turner), Plymouth Marine Laboratory.

Robertson J.E., Watson A.J., Langdon C., Ling R.D. and Wood J., 1993. Diurnal variations in surface pCO_2 and oxygen at 60°N, 20°W in the northeast Atlantic. *Deep-Sea Res.*, **40**, 409-422.

Robertson J.E., Robinson C., Turner D.R., Holligan P., Watson A.J., Boyd P., Fernandez E. and Finch M., 1994. The impact of a coccolithophore bloom on oceanic carbon uptake in the northeast Atlantic during summer 1994. *Deep-Sea Res.*, **41**(2), 297-314.

Robertson J.E. and Watson A.J., 1994. A summertime sink for atmospheric carbon dioxide in the Southern Ocean between 88W and 80E., In preparation.

Robinson C. and Williams P.J.leB., 1991. Development and assessment of an analytical system for the accurate and continual measurement of total dissolved inorganic carbon. *Mar. Chem.*, **34**, 157-175.

Rotty R.M., 1983. Distribution of and changes in industrial carbon dioxide production. *J.Geophys. Res.*, **88**(C2), 1301-1308.

Roy R.N., Roy L.N., Lawson M., Vogel K.M., Moore C.P., Davis W. and Millero F.J., 1993a. Thermodynamics of the dissociation of boric acid in seawater at $S = 35$ from 0 to 55 °C. *Mar. Chem.*, **44**, 243-248.

Roy R.N., Roy L.N., Vogel K.M., Moore P.C., Pearson T., Good C.E., Millero F.J. and Campbell D.M., 1993b. The dissociation constants of carbonic acid in seawater at salinities 5 to 45 and temperatures 0 to 45°C. *Mar. Chem.*, **44**, 249-267.

Sakshaug E. and Holm-Hansen O., 1984. Factors governing pelagic production in polar oceans. In *Marine Phytoplankton the Arctic*(Eds: O. Holm-Hansen, L. Bolis and R. Gilles), Springer-Verlag, Berlin, p 1-18.

Sarmiento J.L., 1991. Oceanic uptake of anthropogenic CO_2: The Major uncertainties. *Global Biogeochem. Cycles*, **5**(4), 309-313.

Sarmiento J.L. and Sundquist E.T., 1992. Revised budget for the oceanic uptake of anthropogenic carbon dioxide. *Nature*, **356**, 589-583.

Sarmiento J.L., Orr J.C. and Siegenthaler U., 1992. A perturbation simulation CO_2 uptake in an ocean general circulation model. *J. Geophys. Res.*, **97**, 3621-3645.

Schlesinger M.E. and Jiang X., 1991. Revised projection of future greenhouse warming. *Nature*, **350**, 219-221.

Serra G., Schirone A. and Boniforti R., 1990. Fibre-optic pH sensor for sea-water monitoring using a single dye. *Anal. Chim. Acta*, **232**, 337-344.

Siegenthaler U., 1983. Uptake of excess CO_2 by an outcrop-diffusion model of the ocean. *J. Geophys. Res.* **88**, 3599-3608.

Siegenthaler U. and Sarmiento J.L., 1993. Atmospheric carbon dioxide and the ocean. *Nature*, **365**, 119-125.

Sillén L.G., 1967. Master variables and activity scales. In: *Equilibrium concepts in natural water systems* (Ed: R.F. Gould), A.C.S. Advances in Chemistry Series **67**, American Chemical Society.

Skirrow G., 1975. The dissolved gases. In: *Chemical Oceanography*, (Eds: J.P. Riley and G. Skirrow), Vol 2, 2nd Edition, Academic Press, p1-181.

Smethie W.M., Takahashi T., Chipman D.W. and Ledwell J.R., 1985. Gas exchange and CO_2 flux in the tropical Atlantic Ocean determined from 222Rn and pCO2 measurements. *J. Geophys. Res.*, **90C**, 7005-7022.

Smith W.H. and Hood D.W., 1964. Recent researches in the fields of hydrosphere, atmosphere and nuclear geochemistry. (Eds: Y. Miyake and T. Koyame), Maruzen Co. Ltd., Tokyo p185-202.

Smith S.V. and Mackenzie F.T., 1991. Comments on the role of oceanic biota as a sink for anthropogenic CO_2 emissions. *Global Biogeochem. Cycles*, **5**(3), 189-190.

Smith W.O. and Nelson D.M., 1985. Phytoplankton bloom produced by a receding ice edge in the Ross Sea: spatial coherence with the density field. *Science*, **227**, 163-166.

Smith W.O. Jr., Keene N.K. and Comiso J.C., 1988. Interannual variability in estimated primary productivity of the Antarctic marginal ice zone. In: *Antarctic Ocean and Resource Variability*(Ed: D. Saarhage), Springer-Verlag, Berlin, p 131-139.

Sörenson S.P.L. and Linderström-Lang K., 1924. On the determination and value of p_π in electrometric determinations of hydrogen ion concentrations. *C. R. Trav. Lab. Carlsberg*, **15**(6).

Stumm W. and Morgan J.J., 1981. *Aquatic Chemistry*. Wiley, New York.

Sullivan C.W., McClain C.R., Comiso J.C. and Smith W.O. Jr., 1988. Phytoplankton standing crops within an Antarctic ice edge assessed by satellite remote sensing. *J. Geophys. Res.*, **93C**, 12487-12498.

Sullivan C.W., Arrigo K.R., McClain C.R., Comiso J.C. and Firestone J., 1994. Distributions of phytoplankton blooms in the Southern Ocean. *Science*, **262**, 1832-1837.

Sverdrup M.U., 1953. On conditions for the vernal blooming of phytoplankton. *J. Cons. int. Explor. Mer.*, **18**, 287-295.

Takahashi T. and Chipman D., 1982. Carbon dioxide partial pressure in the surface waters of the Southern Ocean. *Ant. J. U.S.*, **17**(5), 103-104.

Takahashi T., Olafsson J., Goddard J.G., Chipman D.W. and Sutherland S.C., 1993. Seasonal variations of CO_2 and nutrients in the high-latitude surface oceans: a comparative study. *Global Biogeochemical Cycles.*, **7**(4), 843-878.

Tans P.P., Fung I.Y. and Takahashi T., 1990. Observational constraints on the global atmospheric CO_2 budget. *Science*, **247**, 1431-1438.

Taylor A.H., Watson A.J., Ainsworth M., Robertson J.E. and Turner D.R., 1991. A modelling investigation of the role of phytoplankton in the balance of carbon at the surface of the North Atlantic. *Global Biogeochem. Cycles*, **5**(2), 151-171.

Turner D.R., 1993. BOFS '*STERNA 92*' cruise report (Ed: D.R. Turner), Plymouth Marine Laboratory.

UNEP, 1988. *Interaction of the oceans with greenhouse gases and atmospheric aerosols.* UNEP Regional Seas Reports and Studies No. 94., UNEP, 24 pp.

UNESCO, 1987. Thermodynamics of the carbon dioxide system in seawater. *Report by the carbon dioxide sub-panel of the joint panel on oceanographical tables and standards. UNESCO Technical Papers in Marine Science* **51**, UNESCO press, Paris, 55 pp.

UNESCO, 1990. Intercomparison of total alkalinity and total inorganic carbon determinations in seawater (Eds: A. Poisson, F. Culkin and P.Ridout). *UNESCO Technical Papers in Marine Science* 59, UNESCO press, Paris, 69 pp.

Upstill-Goddard R.C., Watson A.J., Liss P.S. and Liddicoat M.I., 1990. Gas transfer in lakes measured with SF_6. *Tellus*, **42B**, 364-377.

Vithanage R.S. and Dasgupta P.K., 1986. Quantative study of chemical equilibria by flow injection analysis with diode array detection. *Anal. Chem.*, **58**, 326-330.

Vives S.S., Hernandez M.J.M., Herrera J.L.M. and Ramos G.R., 1992. Spectrophotometric measurements of pH gradients in continuous-flow systems. *Anal. Chim. Acta*, **269**, 29-38.

Wanninkhof R., Ledwell J.R and Broecker W.S., 1985. Gas exchange-wind speed relation measured with sulfur hexafluoride on a lake. *Science*, **227**, 1224-1226.

Wanninkhof R., 1992. Relationship between windspeed and gas exchange over the ocean. *J. Geophys. Res.*, **97**, C25, 7373-7382.

Wanninkhof R., Asher W., Weppernig R., Chen H., Schlosser P., Langdon C. and Sambrotto R., Gas transfer experiment on Georges Bank using two volatile deliberate tracers. *J. Geophys. Res.*, **98**, C11, 20,237-20248.

Watson A.J., Upstill-Goddard R.C. and Liss P.S., 1991a. Air-sea gas exchange in rough and stormy seas measured by a dual-tracer technique. *Nature*, **349**, 145-147.

Watson A.J., Robinson C., Robertson J.E., Williams P.J. le B. and Fasham M.J.R., 1991b. Spatial variability in th sink for atmospheric carbon dioxide in the North Atlantic. *Nature*, **350**, 50-53.

Wefer G., Fischer G., Füetterer D. and Gersonde R., 1988. Seasonal particle flux in the Bransfield Strait, Antarctica. *Deep-Sea Res.*, **35**(5), 891-898.

Weiss R., 1974. CO_2 in water and seawater: the solubility of a non ideal gas. *Mar. Chem.*, **2**, 203-215.

Wesley M.L., Cook., Hart R.L. and Williams R.M., 1982. Air-sea exchange of CO_2 and evidence for upward fluxes. *J. Geophys. Res.*, **87C**, 8827-8832.

Whitfield M., 1971. Ion selective electrodes for the analysis of natural waters. *AMSA Handbook*, No.2, Australian Marine Sciences Association, Sydney, 130pp.

Whitfield M., 1975. The electroanalytical chemistry of seawater. In: *Chemical Oceanography*, Vol. 4., (Ed: J.P. Riley and G. Skirrow), Academic Press, London, p 1-154.

Whitfield, 1979. Activity coefficients in natural waters. In: *Activity Coefficients in Electrolyte Solutions*, Vol. 2., (Ed: R.M. Pytkowitz), CRC Press, Boca Raton, Florida, p 153-299.

Whitfield M., Butler R.A. and Covington A.K., 1985. The determination of pH in estuarine waters 1. Definition of pH scales and the selection of buffers. *Oceanol. Acta*, **8**(4), 423-432.

Whitfield M. and Turner D.R., 1986. The carbon dioxide system in estuaries - an inorganic perspective. *Sci. Total Environ.*, **49**, 235-255.

Whitworth T., 1988. The Antarctic Circumpolar Current. *Oceanus*, **31**, 2, 53-58.

Wigley T.M.L. and Raper S.C.B., 1992. Implications for the climate and sea level of revised IPCC emissions scenarios. *Nature*, **357**, 293-300.

Yamazaki H., Sperline R.P. and Freiser H., Spectrophotometric determination of pH and its application to determination of thermodynamic equilibrium constants. *Anal. Chem.*, **64**, 2720-2725.

Zirino A, 1975. Measurement of the apparent pH of seawater with a combination microelectrode. *Limnol. Oceanogr.*, **20**, 654-657.

Zirino A., Clavell C., Seligmann P.F. and Barber R.T., 1983. Copper and pH in the surface waters of the eastern tropical Pacific Ocean and the Peruvian upwelling system. *Mar. Chem.*, **12**, 25-42.

Zirino A., Fuhrmann R.A., Oksanen-Gooden D., Lieberman S.H., Clavell C. and Seligman P.F., 1986. pH-temperature-nutrient relationships in the eastern tropical Pacific Ocean. *Sci. Total Environ.*, **58**, 117-137.

APPENDIX 1. Specifications of the Spectrophotometer (Cecil CE2020) used during this study.

Wavelength range	190 - 1000nm
Wavelength resolution	0.1nm
Wavelength reproducibility	Better than 0.1nm
Wavelength accuracy	Within 1nm
Stray light	Less than 0.01% at 220nm and 340nm
Optical bandwidth	4nm
Photometric range	-0.3-3.0A/0-200%T/0-9999C
Photometric accuracy	± 1% or 0.005A whichever is the greater
Photometric noise	Less than ±0.0002A at 500nm
Absorbance zero stability	Better than $\pm 0.001 A.h^{-1}$
Absorbance zero setting	0A and 100%T
Peak seek	Automatic search programme
Computer interface	Bi-directional RS232C
Analogue output	$100mV.AE^{-1}$
Sample temperature	Displayed or set from keyboard
Sample compartment dimensions	196 x 96 x 107mm
Size	480 x 340 x 205mm
Weight	19kg
Power requirement	110/250V, 50/60Hz, 120W

PAGE/PAGES
EXCLUDED
UNDER
INSTRUCTION
FROM
UNIVERSITY